INVESTIGATION OF CORROSION AND CORROSION INHIBTION OF DIFFERENT METAL SURFACES

A THESIS PRESENTED BY

RATHIGA SENTHOORAN

to the Board of Study in Chemical Sciences of the

POSTGRADUATE INSTITUTE OF SCIENCE

in partial fulfillment of the requirement

for the award of the degree of

MASTER OF PHILOSOPHY

of the

UNIVERSITY OF PERADENIYA

SRI LANKA

2013

DECLARATION

I do hereby declare that the work reported in this thesis was exclusively carried out by me under the supervision of Prof. H.M.D.N.Priyantha. It describes the results of my own independent research except where due reference has been made in the text. No part of this thesis has been submitted earlier or concurrently for the same or any other degree.

Date: 07.10.2013 ..... S. Rathiga .....

Signature of the Candidate

Certified by:

1. Supervisor (Name): Prof. Namal Priyantha Date: 07/10/2013

(Signature): .....

PGIS Stamp:

INVESTIGATION OF CORROSION AND CORROSION INHIBTION OF DIFFERENT METAL SURFACES

Rathiga Senthooran

Postgraduate Institute of Science, University of Peradeniya, Peradeniya

Sri Lanka

In the present study, attempts were made to mitigate the corrosion of mild steel in HCl, galvanized steel in NaCl and copper in both HCl and NaCl media using natural products. A multi-technique approach, including mass loss measurements, pH measurements, open circuit potential measurements, potentiodynamic polarization studies and electrochemical impedance spectroscopic analysis, was employed to obtain corrosion measurements before and after introduction of mitigation attempts.

The effect of acidic extracts of cinnamon (*Cinnamomum zeylanicumm*) leaves on the corrosion behavior of mild steel in HCl solutions of different concentrations has been investigated using the above techniques. These measurements conclusively demonstrate that the cinnamon leaf extract has a strong ability of controlling the corrosion of mild steel in HCl solutions of different concentrations ranging from 0.1 mol dm^{-3} to 2.0 mol dm^{-3}.

Effect of tea (*Camellia sinensis*) leaf extracts on the corrosion behavior of copper in HCl solutions of different concentrations ranging from 0.05 mol dm^{-3} to 1.0 mol dm^{-3} has been investigated using the above techniques. All experimental techniques indicate that tea leaf extracts show strong inhibition on the corrosion of copper at low acid concentrations (0.05 mol dm^{-3}). However, tea leaf extracts in high acid concentrations show high inhibition effect for short immersion periods (2 h). Corrosion inhibition effect is due to selective adsorption of certain compounds such as plant pigments on metal surfaces. Polyphenolic compounds in tea leaves also contribute to the inhibition effect at low acid concentrations.

Tea leaf extracts in 0.1 mol dm^{-3} NaCl solution show higher inhibition effect on corrosion of galvanized steel at pH = 2 and 3 as compared to other pH values. Electrochemical techniques also support the inhibition potential of tea leaf extracts.

Results of electrochemical studies reveal that methanol extracts of tea leaves show inhibition on copper corrosion in 0.1 mol dm^{-3} NaCl solutions. UV-Vis spectroscopic studies suggest adsorption of tea leaf components on copper surface contributes to the corrosion inhibition effect. According to mass loss measurements, percentage inhibition efficiency is the highest at pH = 3.

To My Loving Husband,

Parents and Teachers

ACKNOWLEDGMENTS

I am very grateful to my supervisor Prof. Namal Priyantha for giving me a great opportunity to be a postgraduate student of the Analytical Chemistry Research Group, University of Peradeniya. This thesis would not have been made possible without his excellent guidance and valuable suggestions. Since the time I initiated the research project (September 2010), he has provided immense supervision and assisted in the proper direction.

I am greateful to Head, Department of Chemistry, University of Peradeniya, giving me unrestricted laboratory facilities. I extend my thanks to Head, Department of Physics for allowing me to use workshop facilities and other resources in the Department of Physics. I also extend my sincere thanks to Prof. R.M.G. Rajapakse for allowing me to use the instruments in the Physical Chemistry Research Laboratory.

I would like to extend my thanks to all technical staff members of Department of Chemistry, University of Peradeniya, for their great assistance.

I would like to thank my colleagues, Anushka Bandaranayaka, Damitha, Sanjeewani, Chandima, Anushka Liyandeniya, Sugath, Shameemah, Sampath, Piyal, Malavipathirana, Thanuja and Sarathy for making the laboratory a home away from my home and supporting at all times.

Finally, above all, to my family, without whom this work wouldn't have been made possible. Their unwavering love, support and encouragement have been my biggest companion and asset. I am indebted to all of you.

TABLE OF CONTENTS

LIST OF TABLES

LIST OF FIGURES

CHAPTER 1

INTRODUCTION

1.1 Introduction to Corrosion

1.1.1 Metal corrosion and its chemistry in aqueous environments

Metal corrosion is the deterioration of a metal's physical and chemical properties due to the interaction with its aggressive environment [1]. Any corrosion reaction in aqueous solution must involve oxidation of the metal and reduction of a species in solution with consequent electron transfer between the two reactants. Metals can react with many liquids or gaseous environments spontaneously in which they are placed. Based on the type of the environment, corrosion of metals can be broadly divided into dry corrosion and wet corrosion. In dry corrosion, metal is oxidized due to the interaction with gas or vapour, where nonmetals such as oxygen, halogens, hydrogen sulphide and sulphur vapour are interacted with the metal. Corrosion products due to oxidation of metals and reduction of non-metals are formed on the site at which the interaction of metal and oxidizing agent take place. Wet corrosion occurs in an aqueous environment, which ranges from very thin condensed films of moisture to bulk solutions. Aqueous environments include natural environments, such as the atmosphere, natural waters, soils, body fluids chemicals and food products. In wet corrosion, corrosion products formed at the metal/solution interface are thermodynamically stable and they may be transported away from the interface by migration, diffusion and convection. If reaction products are continuously removed from the metal surface by any process mentioned above, reactants and the metal are not separated by a barrier [1].

The present study is confined to corrosion of mild steel, galvanized steel and copper in aqueous solutions. When a metal is exposed to a solution, positively charged metal ions tend to pass from the metal into the solution, leaving electrons behind on the metal, as shown below

$$M(s) \longrightarrow M^{n+}(aq) + ne^{-}(M) \qquad (1.1)$$

During the corrosion of a metal in aqueous medium, anodic reaction is the dissolution of the metal. A potential difference between the metal surface and the solution is thus developed due to the accumulation of negative charges on the metal. This process tends to retard the dissolution of metal ions, but to promote the deposition of dissolved metal ions from the solution onto the metal. Due to the continuous dissolution and deposition of metal ions, the system reaches equilibrium having a stable potential, called the reversible potential (E_r) [2]. At equilibrium, the rate of dissolution becomes equal to the rate of deposition. The reversible potential depends on the activity of dissolved metal ions and the standard reversible potential, according to the Nernst equation as shown in Equation (1.2).

$$E_{r,M^{n+}/M} = E^{\theta}{}_{M^{n+}/M} + \frac{RT}{nF} \ln a_{M^{n+}} \tag{1.2}$$

where R is the universal gas constant, T is the absolute temperature, F is the Faraday constant and n is the number of electrons transferred in the half-reaction.

The potential of a metal in a solution does not usually reach the reversible potential and remains more positive because electrons can be removed from the metal by cathodic reactions. Cathodic reaction is either the reduction of oxygen or evolution of hydrogen, as shown below. The Nernst equation for each reduction reaction is also given with the reaction.

In basic or neutral medium,

$$O_2(g) + 4e^- + 2H_2O(l) \longrightarrow 4OH^-(aq) \tag{1.3}$$

$$E_{r,O_2/OH^-} = E^{\theta}_{O_2/OH^-} - \frac{RT}{4F} \ln \frac{(a_{OH^-})^4}{P_{O_2}/p^{\theta}} \tag{1.4}$$

OR

In acidic medium,

$$O_2(g) + 4H^+(aq) + 4e^- \longrightarrow 2H_2O(l) \tag{1.5}$$

$$E_{r,O_2/H_2O} = E^{\theta}_{O_2/H_2O} - \frac{RT}{4F} \ln \frac{1}{\left(\frac{P_{O_2}}{p^{\theta}}\right)(a_{H^+})^4} \tag{1.6}$$

OR

$$2H^+(aq) + 2e^- \longrightarrow H_2(g) \tag{1.7}$$

$$E_{r,H^+/H_2} = E^{\theta}_{H^+/H_2} - \frac{RT}{2F} \ln \frac{(P_{H_2}/p^{\theta})}{(a_{H^+})^2} \quad (1.8)$$

Therefore, metal corrosion continues due to the occurrence of reactions 1.3, 1.5 or 1.7. The formation of a thin oxide film or films of other corrosion products influences the rate of corrosion of metals in aqueous medium. These products may be formed either naturally by reaction with their environments or as a result of some deliberate pretreatment processes. These films form a barrier that isolates the metal from its environments and thus control the rate of corrosion. Processes, such as the rate of diffusion of species to and from the metal surface also control the rate of corrosion of metals in aqueous solutions [1].

1.1.2 Types of corrosion

Corrosion occurs in two forms based on the type of attack, such as uniform corrosion and localized corrosion. In uniform corrosion, all area of the metal surface corrodes at more or less equal rate. Uniform corrosion includes atmospheric corrosion, galvanic corrosion, liquid-metal corrosion and biological corrosion. Oxidation and tarnishing of metals and active dissolution of metals in acids are also examples for uniform corrosion. On the other hand, localized corrosion can be divided into several forms, such as pitting corrosion, crevice corrosion, intergranular corrosion, filiform corrosion, biological corrosion due to fouling organisms non-uniformly adhered on metal surfaces and selective leaching corrosion [3]. Details of some common types of corrosion are given in the following sections.

1.1.2.1 Galvanic corrosion

The electrochemical degradation derived from joining two or more dissimilar metals or alloys is termed galvanic corrosion. The coupling of two different metals or alloys together either directly or through an external path increases the corrosion rate of a metal or alloy. The substance which has a more electronegative potential undergoes corrosion and reduces the corrosion rate of the other substance which has a more electropositive potential. The magnitude of the potential difference between dissimilar materials cannot necessarily be used to predict the extent of galvanic corrosion because electrochemical potentials are a function of thermodynamics, not of the kinetics of reactions. It is the surface kinetics that determines the rate of galvanic corrosion [4].

1.1.2.2 Pitting corrosion

Localized corrosion is the selective corrosion of a metal at small areas on a metal surface in contact with a corrosive environment, usually a liquid. Highly localized attack is called pitting corrosion, in which passivity is lost or ruptured through a chemical or an electrochemical action of a specific component of the environment [5]. It usually takes place when small local sites are attacked at a much higher rate than the rest of the original surface. It is believed that two main steps are involved in the localized corrosion process: initiation and propagation. Any localized damage to the protective layer of a metal surface may be one of the ways to initiate localized corrosion [6].

The most commonly encountered pitting agent in aqueous environments is chloride. However, sulphide ions and sulphur oxy-anions, such as thiosulphate, would also cause pitting corrosion in ferrous materials and nickel-based materials. Many metals, such as steels and stainless steels, nickel, copper and aluminium, and their alloys, undergo pitting corrosion in chloride solutions of sufficient concentration. Several possible mechanisms of initiation have been put forward in this regard. Complexing of metal cations on the surface of the film has been proposed to lead to local dissolution of the oxide layer, the site then receding to the metal surface. Alternatively, chloride migration through the oxide film may lead to its accumulation as a metal chloride at the metal-film interface.

Pitting factor is the ratio between the depth of the deepest pit resulting from corrosion and the average penetration. A low value of pitting factor, closer to zero, represents general corrosion while a high value, closer to 1, indicates localized corrosion.

1.1.2.3 Inter-granular corrosion

A form of localized corrosion associated with a defective micro-structure. For example, presence of iron as a residual impurity in the grain boundaries causes inter-granular corrosion of aluminium in alkali, and precipitation of chromium carbide due to heat treatment of stainless steel depletes the surrounding chromium and hence reduces its corrosion resistance [7-8].

1.1.2.4 Crevice corrosion

Intense localized corrosion occurs within narrow crevices, where mass transfer is limited. It may be formed by:

1. The geometry of the structure, e.g. riveted plates, welded fabrications, threaded joints.
2. Contact of the metal with non-metallic solids, e.g. plastics, rubber, glass.
3. Deposits of sand, dirt or permeable corrosion products on the metal surface.

Crevice corrosion can occur with a variety of metals and alloys ranging from noble metals, silver and copper, to the very electronegative metals, such as aluminium and titanium. It is particularly prone to occur with metals and alloys that rely on passivity for their corrosion resistance. Implant alloys, such as stainless steel (316L) and titanium based alloys (Ti–6Al–4V, Ti–6Al–7Nb), are susceptible to crevice corrosion [9]. Crevice widths are usually of the order of about 0.025 to 0.10 mm [1]. The crevice must be wide enough to permit entry of the solution, but sufficiently narrow to maintain a stagnant zone of solution within the crevice so that entry of the cathode reactant and removal of reaction products is very slow and occurs only by diffusion and migration (if the species are charged). Crevice corrosion takes place mostly in near-neutral solutions in which dissolved oxygen is the cathodic reactant, while H_3O^+ is the cathodic reactant in acid solutions. Although crevice corrosion occurs in any type of environment, solutions containing chloride ions are the most favorable to crevice corrosion.

In crevice corrosion, the metal outside the crevice is predominantly cathodic whilst the metal within the crevice is predominantly anodic. As the oxidant in the crevice is consumed at cathodic sites, a very long current path is developed between anodic sites in the crevice and cathodic sites on the external surface. These processes result in a voltage drop, called the IR drop, which leads to an electrode potential on the crevice wall which is less noble than the surface. Therefore, metal undergoes intense attack [10].

1.1.2.5 Filiform corrosion

This is a special type of crevice corrosion which occurs under a protective film. It is common on food and beverage cans being exposed to the atmosphere.

1.1.2.6 Erosion corrosion

This type of corrosion is resulted from the movement of corrosive media, in which protective films, and even the metal surface itself, are removed by the abrasive action of movement of a gas or a liquid at high velocity. The most significant effect of erosion-

corrosion is the constant removal of protective films which may range from thick visible films of corrosion products to thin invisible passivating films from the metal's surface, thus resulting in localized attack at the areas at which the film is removed [11]. This can be caused by movement at high velocities, and is particularly prone to occur if the solution contains solid particles (e.g., insoluble salts, sand and silt) that have an abrasive action. In addition to the mechanical damage of the protective film, velocity or movement will also bring the cathode reactants more rapidly to the metal surface, thus decreasing cathodic polarization. In general, the higher the velocity, the more abrasive the solution is. In most cases, the rate of attack increases with velocity of the solution. Metals and alloys which have a moderate corrosion rate in static solutions may corrode rapidly when the corrosive environment is moving at higher velocity. For example, severity of corrosion of copper condenser tubing and piping in sea water and carbon steel boiler tubes in water and water/steam increases when velocity of water increases.

1.1.2.7 Stress corrosion

Stress corrosion of metal occurs in the presence of tensile stress in corrosive environment. The composition and structure of metals and alloys are also important in determining stress corrosion. Low-carbon and chromium-nickel steels, certain copper alloys, nickel and aluminium alloys are prone to exhibit stress-corrosion cracking in specific environments. Chlorides and moist air promote stress corrosion of aluminium. Ammonia, moist air and moist sulphur dioxide promote stress corrosion of certain copper alloys. Nitrates, hydroxides, carbonate and anhydrous ammonia also promote stress corrosion of different metals [12].

1.1.2.8 Selective leaching corrosion

This is a selective removal of a particular metal (more active) from an alloy matrix; for instance, zinc removal from a Cu-Zn alloy [13]. Dezincification factor (Z) for this process can be calculated using the following relationship,

$$Z = (Zn/Cu)_{sol}/(Zn/Cu)_{alloy} \tag{1.9}$$

where $(Zn/Cu)_{sol}$ is the ratio of the mass percentage between Zn and Cu in solution and $(Zn/Cu)_{alloy}$ is the ratio of the mass percentage between Zn and Cu in the alloy.

Dezincification factor of brass (chemical composition: Cu; 60.3%, Zn; 34.6%, Se; 4.3% and Bi; 0.8%) in sea water in the absence and presence of 5.0×10^{-2} mol dm^{-3} benzotriazole are 23 and 16, respectively [14].

1.1.3 Factors influencing metal corrosion in aqueous environments

There are several environmental factors that affect the corrosion rate of a metal. These factors include the presence of electrolyte, availability of oxygen, presence of CO_2 and H_2S, microbes, acidity, pH, temperature, pressures, velocity of the movement of aqueous environment, solid particles and abrasion, metallurgical structure (crystal defects), length of exposure and mechanical stress.

Presence of electrolyte and its concentration contributes to the conduction of charge in aqueous environments. Sea water, being a chloride source, is an excellent electrolyte, which acts as a pitting corrosion agent [15-16]. Oxygen is the key corrosion element. For instance, dissolution of copper in de-aerated mineral acids is very low. However, the solubility increases significantly in the presence of O_2. Corrosion of metals caused by CO_2 is called sweet corrosion. CO_2 dissolved in water to form carbonic acid, which is corrosive to carbon steel. CO_2 causes severe corrosion damage to oil, gas production and transport industries [17]. Corrosion caused by H_2S is called sour corrosion, which occurs in gas production wells having a certain concentration of H_2S [18].

Presence of bacteria forms bio-films, such as microbial cells, extracellular polymeric materials and adsorbed organics. Metabolic products of micro-organisms, such as enzymes, exopolysaccharides which are extracellular polysaccharides secreted by microorganisms into the surrounding environment, organic and inorganic acids, and volatile compounds, such as ammonia or hydrogen sulfide, can alter electrochemical processes at the biofilm–metal interface through co-operative effects [19-20]. The accumulation of metabolic products is aggressive to the metal. Sulphate reducing bacteria produces hydrogen sulphide, which accelerates the corrosion of metals [21].

In acidic environments, some metals and alloys, such as steel, are vulnerable to corrosion. However, susceptibility for corrosion of mild steel and high-carbon steel differ significantly with the type of acid. HNO_3 is generally found to be more corrosive than $HClO_4$ and HCl, as it is a strong oxidizing agent [22]. The medium pH plays an important role in corrosion, where the reduction of H_3O^+ ions is the cathodic reaction, especially in

CO_2 corrosion. The corrosion rate of carbon steel at room temperature changes considerably with the change in electrolyte pH.

As temperature plays a significant role in the formation of protective films on metallic surfaces, it affects the corrosion rate of metals. Temperature also influences the transport of chemical species towards and from the metal surface such as diffusion of oxygen. Generally, increase in temperature increases the corrosion rate [23].

1.1.4 Consequences of metal corrosion

Corrosion of metals leads to several problems as environmental effects and industrial settings provide necessary conditions for corrosion to initiate and continue. Some common problems are listed below [24].

- Failure of metallic structures: Corrosion promotes the reduction of the thickness of metallic objects leading to the loss of mechanical strength and structural failure. E.g., breakdown of bridges.
- Loss of efficiency: A common example is the decrease in heat transfer rate in heat exchangers due to the deposition of corrosion products.
- Loss of products: Contamination due to corrosion of containers.
- Environmental pollution: Perforation of metal pipes due to localized corrosion leads to the leakage of fluids to the environment.
- Safety problems: Release of toxic material occurs due to the sudden failure in the equipment.
- Blockage of pipes due to solid corrosion products.
- Reduction of the value of goods due to the deterioration of appearance.

Therefore, prevention of corrosion is important. In this context, determination of corrosion rate is important before measures are to be taken to prevent corrosion, followed by the determination of corrosion rate after introducing preventive measures.

1.2 Corrosion Monitoring Techniques

Several corrosion monitoring techniques have been developed and detection methods fall into two major categories, such as electrochemical techniques and non-electrochemical techniques. Given below are common laboratory techniques that can be employed to measure the rate of corrosion in aqueous environments.

1.2.1 Mass loss measurements

Mass loss measurement is a basic corrosion monitoring technique. For this measurement, a cleaned metal specimen of known mass and area is suspended in the corrosive media. Metal specimens are retrieved from the corrosive media after predetermined immersion time, and mass of the metal specimen is recorded after proper cleaning. Mass loss is calculated by subtracting the final mass of the metal specimen from the initial mass, and the corrosion rate is calculated using the following equation:

$$\text{Corrosion rate of metal (mpy)}, R = \frac{87.6\,\Delta W}{DAt} \qquad (1.10)$$

where R is the corrosion rate (mpy), ΔW is the mass loss of metal specimen (mg), D is the density of metal (g cm^{-3}), A is the area of the metal exposed to corrosive media (cm^2) and t is the immersion time (h) [25-26]. The unit, millimeters per year (or mpy) is a common unit used to express the rate of corrosion in the field of corrosion science.

1.2.2 Potentiodynamic polarization analysis

Potentiodynamic polarization analysis is an electrochemical technique used to monitor the corrosion of metals. In this technique, the potential of the working electrode is varied at a selected scan rate over a potential range about ± (250-200) mV from the open circuit potential (V_{oc}) [27]. Potentiodynamic polarization curve is the plot of log (i) vs. the potential of the working electrode. Figure 1.1 shows a sample polarization curve of a mild steel specimen in 0.5 mol dm^{-3} H_2SO_4. The anodic and cathodic branches of the polarization curve are extrapolated towards their corrosion potential (E_{corr}) and corrosion current density (i_{corr}) is calculated from the intersection as shown in Figure 1.1. The potentiodynamic polarization parameters, such as E_{corr}, i_{corr} and anodic and cathodic Tafel slopes (b_a, b_c) for the above system are -502 mV, 3.288 μA cm^{-2}, 190 mV dec^{-1} and 130 mV dec^{-1}, respectively.

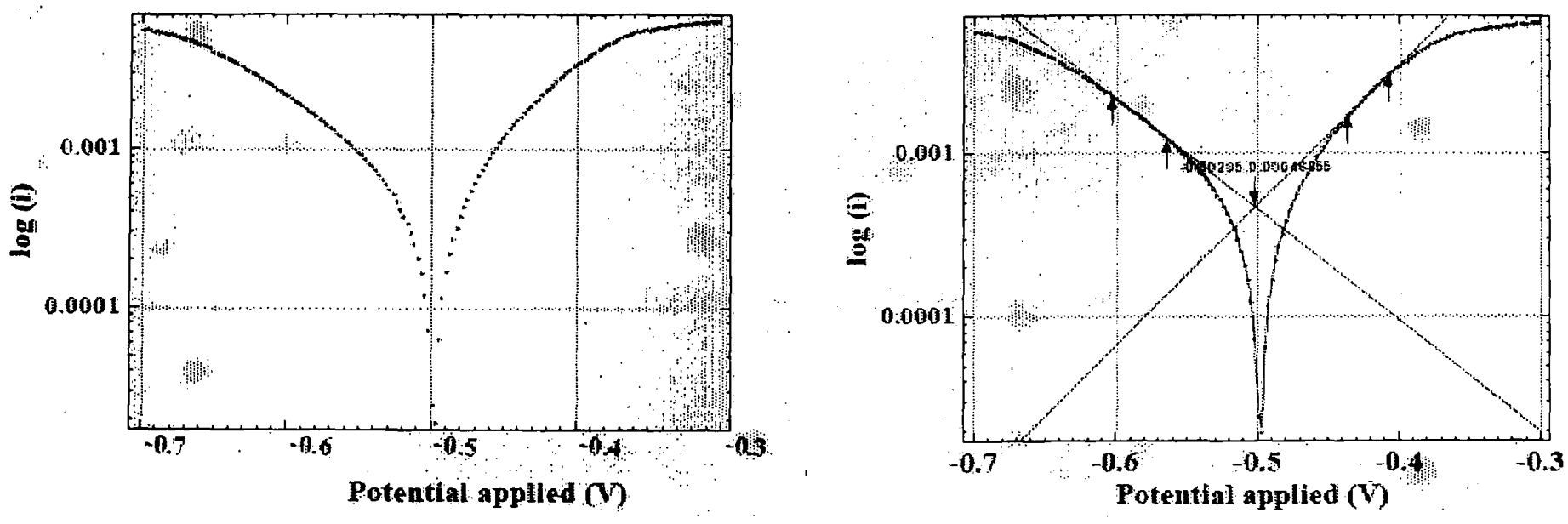

Figure 1.1: (a) Polarization curves for a mild steel specimen in 0.5 mol dm^{-3} H_2SO_4 and (b) extrapolation of anodic and cathodic branches.

Corrosion rate of the metal can be calculated from the polarization curve using the following equation [28].

$$\text{Corrosion rate of metal (milli-inch per year)}, R = \frac{0.129 \times i_{corr} \times eq.weight}{density \times area} \qquad (1.11)$$

where i_{corr} is the corrosion current (μA) and *eq. weight* is the equivalent weight of the metal, which is equal to the atomic weight of the metal divided by the valence.

1.2.3 Hydrogen evolution method

This method is commonly used to determine the corrosion rate of metals in acidic medium. In this method, a weighed metal specimen is introduced to the test solution and the volume of hydrogen gas evolved is recorded with time. The corrosion rate is then expressed in terms of $H_2(g)$ evolved per unit area [29], which could be converted to standard units.

1.2.4 Electrochemical impedance spectroscopy (EIS)

In this technique, a certain area (usually small) of the metal of interest is exposed to the corrosive medium and its impedance is measured using a three electrode system, which includes a metal working electrode, a counter electrode and a reference electrode, by applying a small amplitude alternating potential to the working electrode in a predetermined frequency range. Interpretation of impedance spectra is usually done by

fitting the experimental data with an equivalent circuit. The higher the impedance, the lower the corrosion rate is [30]. EIS gives information on the corrosion mechanism as well [31].

Figure 1.2 shows a sample electrochemical impedance spectra (also called the Nyquist plot) of a mild steel specimen in 0.5 mol dm^{-3} H_2SO_4 and the equivalent circuit used to extract electrochemical parameters. The values of electroctrochemical impedance parameters, such as solution resistance (R_s), charge transfer resistance (R_{ct}) and constant phase element (CPE), which is not an ideal capacitor, are also shown in the figure.

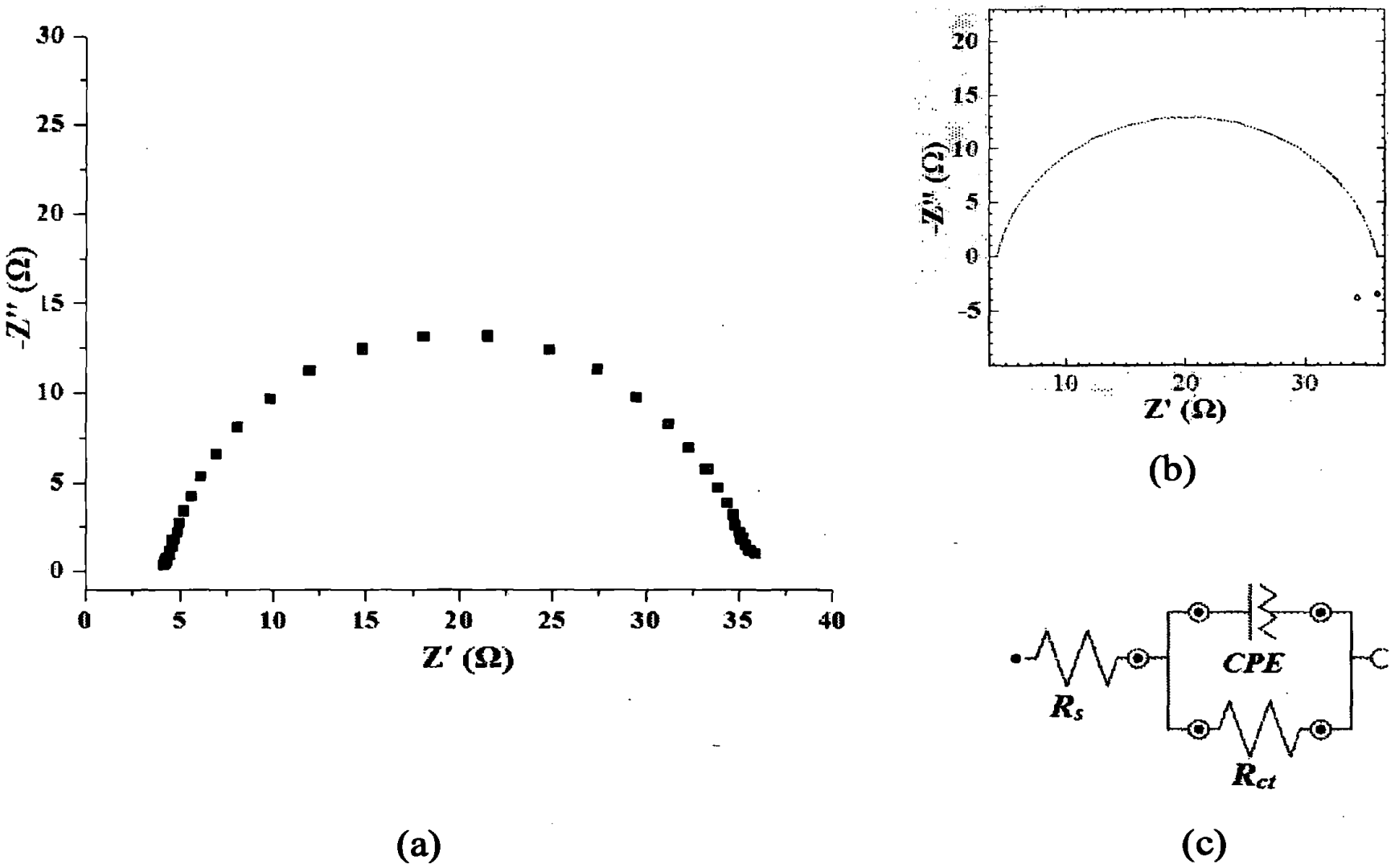

Figure 1.2: (a) Nyquist plots of mild steel in 1.0 mol dm^{-3} H_2SO_4, (b) experimental data fitted with equivalent circuit and (c) equivalent circuit used to represent the system.

1.2.5 Open circuit potential (V_{oc}) measurements

Open circuit potential indicates the tendency of a metal to electrochemical oxidation in a corrosive medium which stabilizes around a stable value after a certain period of immersion. This value may vary with immersion time due to the changes in the nature of the electrode's surface as corrosion occurs. Open circuit potential of a metal in a particular corrosive medium is measured with respect to a stable reference electrode, such as the saturated calomel electrode (SCE), the copper/copper sulfate electrode (CSE) and

the silver/ silver chloride electrode. Therefore, any change in the measured potential can be attributed to the metal/solution interface. V_{oc} measurements are important in corrosion monitoring of concrete rebars. Table 1.1 shows the relationship between the open circuit potential and the corrosion condition of reinforcement reported by Song and Saraswathy [32].

Table 1.1: Corrosion conditions of reinforcement related to the open circuit potential.

Open circuit potential value		**Corrosion condition**
(mV vs. SCE)	**(mV vs. CSE)**	
< -426	< -500	Severe corrosion
< -276	< -350	High (< 90% risk of corrosion)
-126 to -275	-350 to -200	Intermediate corrosion risk
> -125	> -200	Low (10% risk of corrosion)

V_{oc} measurements are useful in determining the inhibition mechanism. For example, open circuit potential of 304 stainless steel in ground water is -171 mV which shifts to a more positive value (-6 mV) in the presence of 30 ppm aminotrimethylidene phosphonic acid (ATMP) indicating that the ATMP controls the anodic reaction predominantly [33].

1.3 Prevention of Corrosion of Metals in Aqueous Environments

Corrosion of metals can be mitigated by several ways, such as application of coatings, use of inhibitors, cathodic protection and proper designing of equipment. Metals can be coated with metals or nonmetals, such as galvanization of mild steel and coating with plastic, in order to protect the metal from corrosive environments. For example, zinc surface treated with 4% benzaldehyde thiosemicarbazone in ethanol for 1-3 h at room temperature shows good corrosion resistance in aqueous chloride-sulphate solution (87% inhibition efficiency) at 25 °C [34]. Corrosion inhibitors are used to mitigate the corrosion of metals which are in contact with bulk solutions. In cathodic protection, additional electrons are introduced on the metal surface either by an external power supply or by the use of a sacrificial anode. When a certain metallic object is connected with a more negative metal in the galvanic series (sacrificial anode), electrons are transferred to the cathode form the anode, decreasing the dissolution of the metal. Proper designing of parts of the

equipment reduces the possibility of corrosion. For example, when designing a metal condenser, a heat exchanger and a process cooler, the inlet water box should be designed to facilitate the smooth flow of water.

1.3.1 Corrosion inhibitors

Corrosion inhibitors, which are chemical substances, can retard or prevent the corrosion of metals when added in small concentrations to the fluids in contact with the metal. They play a vital role in the prevention of corrosion of metals, especially low grade metals, and hence improve the extended performance of equipment in a wide range of corrosive media.

Inhibitors are usually organic compounds having N, S or O atoms with free (donor) electron pairs. Some quaternary ammonium compounds with no donor atoms also show inhibitive properties in acidic solutions. Simple diols and triols function as corrosion inhibitors in concentrated organic and inorganic acids without any neutralization of the acid. These corrosion inhibitors are cheap and readily available in large quantities. Diols and triols also reduce evaporation of the acid and thus improve the working environment. Majority of the inhibitors are applied to the following group of systems [35]:

- Natural waters, supply waters in the near neutral pH range (5-9);
- Aqueous solutions of acids as used in pickling for the removal of rust or rolling scale during the production or fabrication of metals or in the post-service cleaning of the metal surface;
- Primary and secondary production of gas and subsequent refining and transport process.

1.3.2 Application of inhibitors in different fields

The application of corrosion inhibitors depends on the field in which metals are in use and the type of the metal. Inorganic inhibitors, such as silicates, phosphates, molybdates and tungstates, are important species in the prevention of corrosion of metals in open cooling water systems. Corrosion inhibitors are used with certain additives in cooling water systems in order to prevent mineral and scale formation, solid deposition and microbial fouling. Biocides and anti-scaling agents, such as sodium metaphosphate and phosphonates, are used for this purpose [36]. Alkali metal borates, silicates, benzoates, nitrates, nitrites and molybdates and hydrocarbyl thioazole are the conventional inhibitors

for the corrosion of aluminium in closed cooling water systems (engine coolant). Thiol based inhibitors are in use to prevent the white corrosion of galvanized surfaces. Azole based compounds continue to be in the frontline as corrosion inhibitors for copper.

In the field of oil and gas production, water soluble and oil soluble inhibitors, especially adsorption type inhibitors are used for the prevention of internal corrosion of pipelines carrying refined petroleum products. Dimers and trimers of oleic and linoleic acids are neutralized with an appropriate amine and used as oil-soluble inhibitors for oil well piping. Metal salts of $CH_3SCH_2CH_2CH(NHCOR)COOH$ containing anionic and cationic surfactants have been reported as less-toxic, water soluble and biodegradable inhibitors [37].

Corrosion inhibitors are also added to lubricants in order to prevent corrosion of metal surface of internal combustion engines. Na^+ or Ca^{2+} salts of dinonylnaphthalene-sulfonic acid have been used as corrosion inhibitors for vegetable oil based lubricants. Inorganic inhibiting pigments, such as strontium chromate, are widely used as anti-corrosive modifiers for lacquer coatings [37-38].

In acidic conditions, oxide films are not usually present on the metal surface and the cathodic reaction is primarily that of hydrogen discharge rather than oxygen reduction. Thus, inhibitors that would adsorb or bond directly onto the bare metal surfaces and/or raise the over-potential for hydrogen ion discharge.

1.3.3 Mechanism of corrosion inhibition

Some inhibitors inhibit the corrosion of metals by passivating the metal surface. For instance, in the corrosion inhibition of aluminium in chloride solutions by chromate, the chromate anion is involved in an oxidation-reduction reaction producing a stable hydrated oxide film as shown below:

$$2Al + 2CrO_4^{2-} + 10H^+ \longrightarrow Al_2O_3.3H_2O + 2Cr^{3+} + 2H_2O \qquad (1.12)$$

Chromate ions exhibit large passivating ability due to greater oxidizing power. This layer protects the base metal from corrosion [6].

Some corrosion inhibitors may adsorb on the metal surface and create a barrier between the aggressive environment and the metal surface. For example, commercial inhibitors for CO_2 corrosion of carbon steel in oil and gas production industry consist of at

least one of the following: fatty acids; amines; fatty amines/diamines; fatty amido-amines; imidazolines; other amine derivatives and oxygen, sulphur or phosphorus containing compounds. These compounds are adsorbed on the steel surface forming a protective hydrophobic film thereby protecting the metal from corrosion [39]. Inhibitor molecules are adsorbed on the metal surface either by donating lone pair electrons of heteroatoms to vacant metal orbitals or by forming complexes with the metal ion. For example, benzotriazole (BTA) is the best inhibitor for copper corrosion as it forms a complex with Cu(I) as shown in Figure 1.3 forming a protective polymeric film on the metal surface [40]. Adsorption behavior of inhibitor molecules on the metal surface can be theoretically explained by fitting the experimental data to different adsorption isotherm models [41].

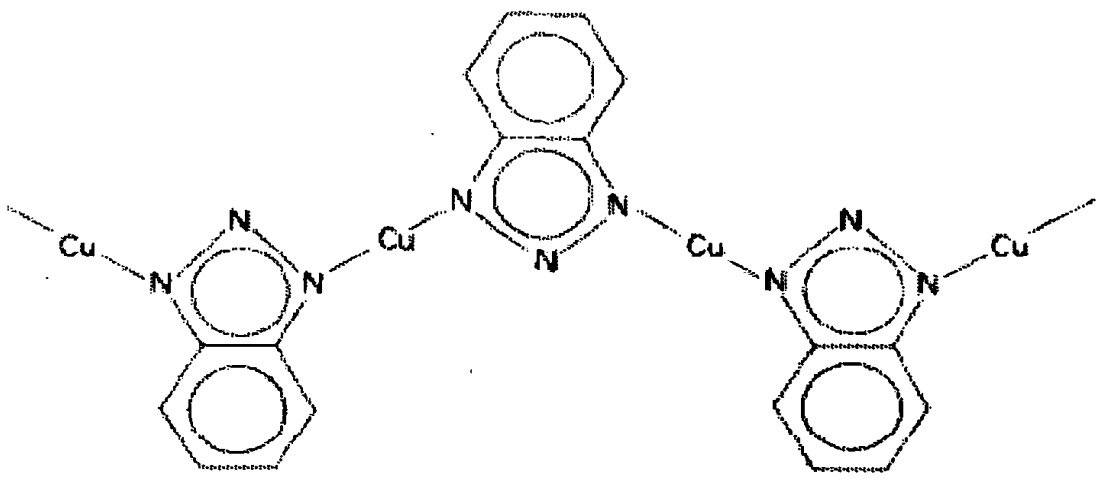

Figure 1.3: Structure of Cu(I)BTA polymer complex.

Some inhibitors function by reducing the aggressiveness of the environment, such as scavenging of oxygen. For instance, sodium sulfite, sodium nitrite or hydrazine can be used to scavenge the oxygen from the corrosive media as the presence of oxygen is necessary to sustain the corrosion process [35]. The chemical reactions of scavenging are given below.

$$2Na_2SO_3 + O_2 \longrightarrow 2Na_2SO_4 \quad (1.13)$$

$$N_2H_4 + O_2 \longrightarrow N_2 + 2H_2O \quad (1.14)$$

Based on the inhibitive mechanism, inhibitors are classified as cathodic inhibitors which slow down cathodic reaction only, anodic inhibitors which slow down anodic reaction only and mixed inhibitors which slow down both anodic and cathodic reactions [35]

1.3.4 Anodic inhibitors

Anodic inhibitors cause a large anodic shift in the corrosion potential, forcing the metallic surface into the passivation range. There are two types of passivating inhibitors: oxidizing anions, such as chromate, nitrite, and nitrate, that can passivate steel in the absence of oxygen and nonoxidizing ions, such as phosphate, tungstate, and molybdate, that require the presence of oxygen to passivate steel. In general, passivation inhibitors can actually cause pitting and accelerate corrosion when concentrations fall below minimum limits. For this reason, it is essential that monitoring of the inhibitor concentration be performed.

1.3.5 Cathodic inhibitors

Cathodic inhibitors either slow down the cathodic reaction or selectively precipitate on cathodic areas to increase the surface impedance, which would limit the diffusion of reducible species to these areas. Cathodic inhibitors can provide inhibition by three different mechanisms: (1) as cathodic poisons, (2) as cathodic precipitates, and (3) as oxygen scavengers. Some cathodic inhibitors, such as compounds of arsenic and antimony, make the discharge of hydrogen more difficult. Other cathodic inhibitors, such as ions of calcium, or magnesium, would be precipitated as phosphate to form a protective layer on the galvanized steel in the presence of orthophosphate [42]. In the third mechanism, oxygen scavengers assist to inhibit corrosion by preventing the cathodic depolarization caused by oxygen. The most commonly used oxygen scavenger at ambient temperature is probably sodium sulfite (Na_2SO_3).

1.3.6 Synthetic inhibitors

Due to the higher demand for corrosion inhibitors, several synthetic compounds, especially organic compounds, have been investigated for the inhibition action on corrosion of different metals in different corrosive media. Table A.1 (Annexure) summarizes the synthetic compounds which exhibit inhibition properties against corrosion of different steel and copper surfaces [43-64].

1.4 Green Inhibitors

The majority of metal corrosion inhibitors that have been used are toxic for the human being and the environment. Economical factors associated with the production of

synthetic inhibitors and their toxic effects necessitate the search for green inhibitors. Therefore, green inhibitors, which are environmental friendly, are being increasingly investigated. Organic green inhibitors include natural products and synthetic compounds with less toxicity. Inorganic green inhibitors include $CeCl_3$, $CeCl_3.7H_2O$, $La(NO_3)_3$, $LaCl_3$, $Sm(NO_3)_3$ and $SmCl_3$. Natural polymers, such as, mimosa tannin, guar gum, gum Arabic, exudate gum, carboxymethyl cellulose and starch, have also been reported as green inhibitors [65].

Table 1.2 shows the inhibition efficiency of some synthetic and natural green inhibitors based on mass loss measurements [66-68].

Table 1.2: Inhibition efficiencies of some green inhibitors on corrosion of mild steel in different corrosive media.

Corrosive medium	Green inhibitor	Optimum inhibitor concentration	% Inhibition efficiency	Ref. No
0.5 mol dm^{-3} H_2SO_4	2-Nonyl-1, 3-imidazoline	500 ppm	95.2	[66]
	2-Undecyl-1, 3-imidazoline		97.4	
	2-Pentadecyl-1, 3-imidazoline		91.9	
	2-Heptadecyl-1, 3-imidazoline		87.2	
1.0 mol dm^{-3} HCl	Green tea (Malaysia)	200 ppm	81.54	[67]
	Green tea (UK)		84.73	
0.5 mol dm^{-3} H_2SO_4	1-methionine	5×10^{-2} mol dm^{-3}	93.2	[68]
	1-methionine sulfoxide		94.0	
	1-methionine sulfone		98.2	

1.4.1 Natural products

As natural products are economical, eco-friendly, readily available and renewable, they have been investigated for the inhibition of corrosion of different metals in a wide variety of corrosive environments in recent years [70]. Therefore, a large number of natural products have been reported to have inhibition ability against steel and copper corrosion in acidic media [70- 89].

1.5 Objectives

In the present study, attempts were made to mitigate the corrosion of mild steel in HCl, galvanized steel (GS) in NaCl and copper in both HCl and NaCl media using natural products. A multi-technique approach, including mass loss measurements, pH measurements, open circuit potential measurements, potentiodynamic polarization studies and electrochemical impedance spectroscopic analysis, was employed to obtain corrosion measurements before and after introduction of mitigation attempts.

1.5.1 Corrosion of mild steel in HCl solutions

Carbon steels are iron-carbon alloys. They are subdivided further based on the carbon content into mild or low carbon steel (0.08 – 0.30% carbon), medium carbon steel (0.3 – 0.5% carbon) and high carbon steel (0.55 – 1.40% carbon) [90].

As mild steels are relatively inexpensive construction materials, they are extensively used in many applications. However, they usually have poor corrosion resistance properties even in ordinary environmental conditions, and hence mild steels are protected by some forms of coatings, such as galvanization. Surface preparation is very important as optimum performance of protection coatings can be achieved by satisfactory treatment of the surface of steel.

Acid pickling is an industrial process for the removal of rust and scales from mild steel objects prior to galvanization, in which steel is immersed in hot acid in closed tanks or cold acid in open tanks. This process is important in the production of hot dip galvanized steel [91].

1.5.2 Corrosion of galvanized steel in NaCl solutions

Galvanized steel (GS) is widely used in structural applications, such as buildings and bridges due to corrosion resistance and low-cost. Although GS attains corrosion protection in normal environmental conditions by its zinc coating, it is subjected to corrosion in harsh conditions, such as industrial and marine environments. Another problem of GS is the formation of white rust. In the fully immersed situation, the corrosion product is produced by a secondary reaction such as,

$$Zn^{2+}(aq) + 2H_2O(l) \rightleftharpoons Zn(OH)_2(s) + 2H^+(aq) \qquad (1.15)$$

In dilute aerated chloride solutions, the anodic and cathodic sites are separated. Therefore, OH^- ions are formed at the cathode and Zn^{2+} ions at the anode, giving rise to dispersed $Zn(OH)_2$ where they meet and react and the corrosion product cannot influence the kinetics under these circumstances. In the presence of chloride, a basic compound Zn(OH)(Cl), may form, whose range of stability would depend upon the concentration of chloride and the pH of the solution [1]. White rust is not a protective layer and hence destruction of GS continues and leads to failure in equipment. This leads to deterioration of appearance and properties of galvanized steel.

1.5.3 Corrosion of copper in HCl and NaCl solutions

Copper is a common constructing material for industrial and domestic tools due to its high thermal and electrical conductivities, appearance and workability [92]. A main application of copper is its use in the manufacture of cooling devices, such as condensers in nuclear industries. Interaction of copper surfaces with coolant liquids, such as sea water, a commonly used coolant liquid, leads to the formation of scale on copper devices. This decreases the performance of such devices. Frequent cleaning of copper devices is thus necessary to recover the performance, and use of acid pickling baths is a common practice. Although copper shows high resistance to corrosion under normal conditions, considerable metal dissolution occurs when exposed to harsh environments [93]. Pipeline failures usually occur not as a result of uniform corrosion but from localized attack, generally as pitting or galvanic corrosion of welds. These forms of attack are much more damaging and difficult to predict.

The corrosion rate of copper in acid solutions is low, but significantly increases in the presence of oxygen (Table 1.3). This can be explained by the following thermodynamic parameters at $a_{H^+} = 1$ and $pO_2 = 1$ atm, [1]. In the presence of oxygen, copper dissolution is favored as the magnitude of the Gibb's free energy and equilibrium constant increase significantly.

Table 1.3: Thermodynamic parameters of dissolution of copper in the absence and presence of O_2 [1].

Thermodynamic parameters	Reaction			
	$Cu^{2+}(aq) + H_2(g)$	$\longrightarrow 2H^+(aq) + Cu(s)$	$2Cu(s) + ½O_2(g) + 2H^+(aq)$	$\longrightarrow 2Cu^+(aq) + H_2O(l)$
$E^{\theta}_{M^{z+}/M}$ (V)	0.337		0.521	
$E^{\theta}_{reaction}$ (V)	0.337		0.71	
$(-)\Delta G^{\theta}$ (kJ mol^{-1})	65		137	
K	2.6×10^{11}		1.1×10^{20}	

1.5.4 Cinnamon leaf extract as green inhibitor

The aim of the present study is to investigate the possibility of using plant materials for the prevention of wet corrosion of different types of metals in different types of corrosive media as an economical and low-cost approach. Cinnamon (*Cinnamomum zeylanicum*) is an endemic plant in Sri Lanka, and its leaves contain more than 75% euginol and several other compounds, including benzyl benzoate, cinnamaldehyde, cinnamyl acetate, α-terpinene, linalool, α-pinene and p-cymene as minor components [94]. Although, cinnamon bark has a high consumer demand as a spices, cinnamon leaves have low consumer demand, and hence, it was selected in our study as a green inhibitor. Acidic extracts of cinnamon leaves were tested for the inhibition potential on corrosion of mild steel in HCl.

1.5.5 Tea leaf extract as green inhibitor

Methanol extracts of tea (*Camellia sinensis*) leaves were tested for the mitigation of corrosion of copper in HCl and corrosion of copper and GS in NaCl. Based on the chemical composition of tea leaves, such as polysaccharides, volatile oils, vitamins, minerals, purines, alkaloids (e.g., caffeine) and polyphenols (catechins and flavonoids) [83] and less economical demand of matured tea leaves, it was selected for the extraction of the inhibitor.

In this research, corrosion inhibition effect of plant extracts was investigated using a multi-technique approach, including electrochemical impedance spectroscopic (EIS)

analysis, potentiodynamic polarization technique and mass loss measurements. EIS analysis provides information about the mechanism of corrosion and surface homogeneities in the presence of the extract, while potentiodynamic polarization measurements provide information about inhibition mechanism. The majority of the experiments were carried out at ambient temperature except adsorption experiments. The choice of the present inhibitors is based on the following considerations:

- Economical factors
- Toxicity
- Environmental friendliness
- Availability

CHAPTER 2

EXPERIMENTAL DETAILS

2.1 Materials

2.1.1. Preparation of corrosive media and standard solutions

Hydrochloric acid solution (2.0 mol dm^{-3}) was prepared by diluting analytical grade grade HCl (assay 34.5%) using distilled water. Hydrochloric acid solutions of different concentrations lower than 2.0 mol dm^{-3} were prepared by diluting 2.0 mol dm^{-3} HCl solution using distilled water. Sodium chloride solutions of different concentrations were prepared by using NaCl (LOBA Chemie, minimum assay 99.5%). Sodium chloride solutions of different pHs were prepared to investigate the inhibition ability of tea leaf extract and hence the pH of NaCl solutions with and without tea leaf extract were adjusted by using concentrated HCl. Standard solutions of copper were prepared from the 1000 ppm standard solution of copper (Buck Scientific, single element AAS standards for Cu). Standard solutions of Zn(II) were prepared from the 1001 ppm standard solution of zinc (Buck Scientific Graphic^{tm} Standards atomic absorption standards) for solution analysis. Analytical grade KI (Research-Lab Fine Chem. Industries, minimum assay of 99.8% after drying) was used to study the effect of iodide ions on the inhibition effect of cinnamon leaf extract.

2.1.2 Preparation of plant extracts

2.1.2.1 Acidic extracts of cinnamon leaves

Raw plant materials were collected from Gampola, Sri Lanka. Stock solutions of acidic extracts of cinnamon leaves were prepared by refluxing 15.0 g of fresh matured leaves with 250.0 cm^3 of 0.1 mol dm^{-3} HCl solution for 6 h in Soxhlet apparatus. The resulting solution was allowed to cool, filtered and the volume of the filtrate was made up to 250.00 cm^3 in a volumetric flask using 0.1 mol dm^{-3} HCl solution. The concentration of the extract in this solution was considered as of 60.0 g dm^{-3} as the exact composition of the extract was not known. In order to prepare cinnamon leaf extracts in HCl solutions of different concentrations, the same procedure was followed with relevant acid concentrations (0.5 mol dm^{-3} – 2.0 mol dm^{-3}). Cinnamon leaf extracts of different

concentrations were prepared from each stock solution of the acidic extract by diluting the stock solution with the acid of the same concentration. Iodide solutions of different concentrations were prepared in 3.0 g dm^{-3} and 0.1 g dm^{-3} extract (in 0.5 mol dm^{-3} HCl) by dissolving appropriate amounts of KI in the extract.

2.1.2.2 Methanol extracts of tea leaves

A representative sample of powdered dry matured tea leaves (1.00 g) was stirred with 50.0 cm^3 of methanol at room temperature for 2 h using a magnetic stirrer. The resulting solution was filtered and the final volume was made up to 50.00 cm^3 using methanol.

2.1.3 Preparation of metal specimens

Rectangular mild steel specimens with dimensions of 4.0 cm (L) × 2.0 cm (W) × 0.6 cm (thickness) were cut from a mild steel sheet having percentage composition (w/w) of C: 0.18, Mn: 0.78, Si: 0.16, P: 0.023, S: 0.022, Al: 0.042 and the remainder is iron for mass loss measurements. Mild steel rod specimens with diameter of 0.5 cm were cut from the same sheet for electrochemical experiments. Working electrodes were prepared by mounting the above rods on a rectangular Teflon block leaving a surface area of 0.2 cm^2 at the bottom of the Teflon block exposed to the corrosive medium. Both rods and rectangular mild steel specimens were polished prior to each experiment with emery papers of different grades (P40 – P800), followed by alumina (200 mesh size) and acetone (Figure 2.1).

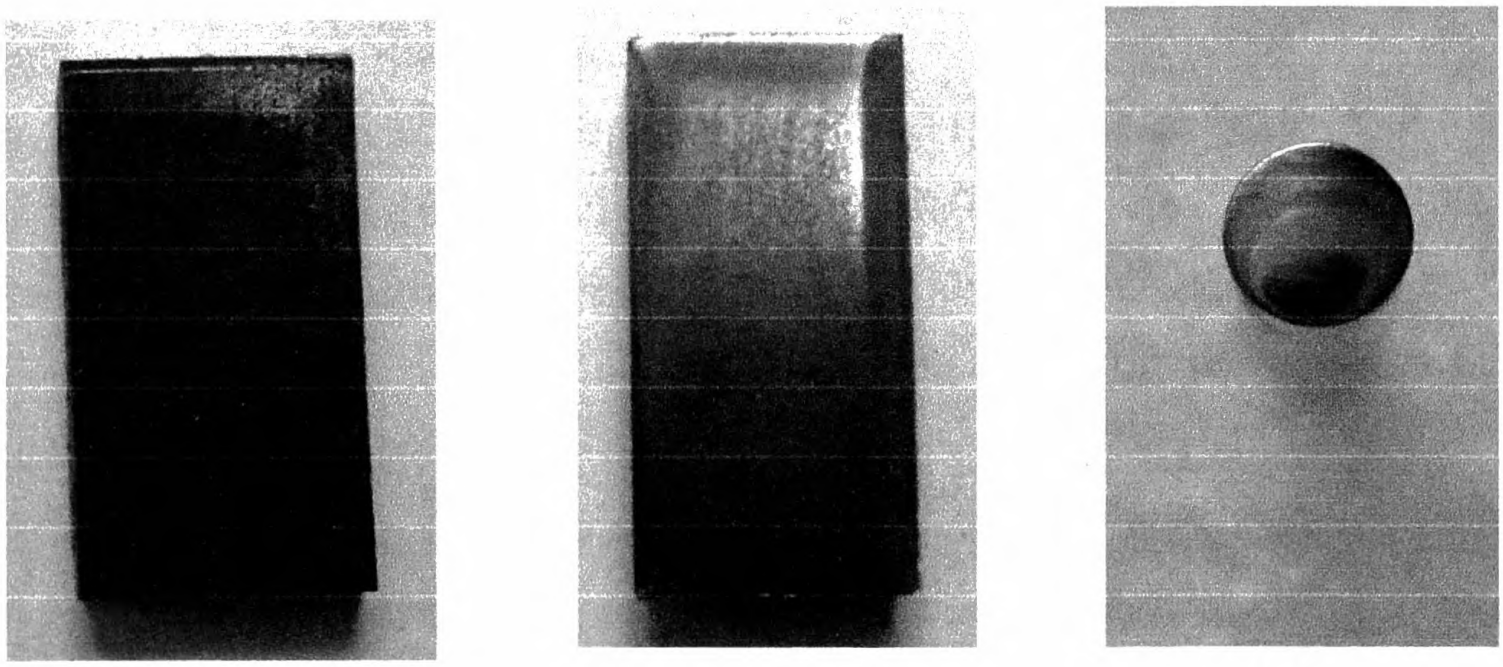

Figure 2.1: (a) Mild steel specimen as received, (b) mild steel specimen after cleaning, and (c) cross-section of mild steel rod specimen.

Rectangular-shaped galvanized steel specimens were cut from a sheet (18 μm coating thickness). The galvanized steel specimens were not polished since the polishing would remove the outer zinc layer on steel and hence unpolished galvanized steel specimens were used. However, galvanized steel specimens were cleaned using acetone. The specific surface area of specimens used for each experiment is provided under respective section.

Rectangular-shaped copper specimens were cut from a copper sheet having the metallic composition of 98.98% Cu and 0.02% Fe according to XRF analysis. Copper specimens were polished well using alumina (200 mesh size) followed by acetone prior to each experiment.

2.2 Instrumentation

Open circuit potentials (V_{oc}) were measured using an electronic multi-meter with respect to a saturated calomel electrode (SCE). Electrochemical experiments were performed using a potentiostat-galvanostat (PGSTAT 12/30/302) and results were interpreted using NOVA software. A simple three electrode system consisting of the selected metal specimen (plate or rod), a Pt foil and SCE as working, counter and reference electrodes, respectively, was used for EIS and potentiodynamic studies (Tafel slope analysis). All EIS were recorded over a frequency range from 100 kHz to 10 mHz with a signal amplitude perturbation of 10 mV at the open circuit potential (V_{oc}). All potentials were measured with respect to SCE.

UV-Vis spectrophometer (Shimadzu UV-1800) was used to record the spectrum of natural products used. Quartz cells were used to record all UV-Vis spectra and the path length was 1.0 cm. Methanol was used as the blank to record UV-Vis spectra of methanol extracts of tea leaves. UV-Vis spectrum of 10% (v/v) tea leaf extract in 0.05 mol dm^{-3} HCl was recorded using 10% (v/v) methanol in 0.05 mol dm^{-3} HCl as the blank. BUCK Scientific 200 A atomic absorption spectrophotometer (AAS) was used to determine the concentration of zinc released into NaCl solution due to the corrosion of galvanized steel in NaCl. Buck Scientific, hollow cathode lamp (elements Ca, Mg, Zn) was used at a λ_{max} of 213.9 nm for this determination. Spectro-Electronic M Series atomic absorption spectrophotometer was used to measure the concentration of Cu released into HCl solutions due to the corrosion of copper in HCl solution. Thermo Scientific, Cu hollow cathode lamp was used for this determination. XRF studies were conducted using the

X-ray flurorescence spectrophotometer (Fischerscope Model-DF500FG-456). Mass loss measurements were recorded using an analytical balance (Denver TP-214). The pH measurements were recorded on a digital pH meter (Thermo scientific, Orion 2 star).

2.3 Research Design

2.3.1 Corrosion of mild steel in HCl solutions and its prevention

2.3.1.1 Effect of the concentration of hydrochloric acid on corrosion of mild steel

The effect of the concentration of HCl on the extent of corrosion of mild steel was investigated using mass loss and pH measurements. EIS measurements were conducted to study the corrosion mechanism.

Mild steel specimens with of 4.0 cm (L) × 2.0 cm (W) × 0.6 cm (thickness) were immersed in 125.0 cm^3 HCl solutions of different concentrations ranging from 0.1 mol dm^{-3} to 2.0 mol dm^{-3} in duplicate at ambient temperature after recording its initial mass. Metal specimens were then retrieved from HCl solution in pre-determined time intervals, washed well with distilled water, dried and re-weighed. The same experimental set-up was used to monitor the variation of pH of the corrosive medium.

A mild steel specimen (rod) with an exposed surface area of 0.2 cm^2 was dipped in 50.0 cm^3 of 0.1 mol dm^{-3} HCl solution and EIS was recorded at V_{oc} after 2 h immersion. The same experiment was repeated for HCl solutions of different concentrations (0.5 mol dm^{-3} – 2.0 mol dm^{-3}).

2.3.1.2 Inhibition effect of acidic extracts of cinnamon leaves on corrosion of mild steel in HCl

Rectangular mild steel specimens with of 4.0 cm (L) × 2.0 cm (W) × 0.6 cm (thickness) were immersed in 125.0 cm^3 of HCl of different concentrations without and with 60.0 g dm^{-3} extract prepared in acid of different concentrations (0.1 mol dm^{-3}-2.0 mol dm^{-3}) at ambient temperature after recording its initial mass. Each experiment was conducted in duplicate. Mass loss of mild steel specimens was recorded as mentioned in section 2.3.1.1 at pre-determined time intervals. The same experimental set-up was used to measure the pH of corrosive media with time.

2.3.1.3 Effect of concentration of acidic extracts on corrosion inhibition

Mild steel specimens (rods) with the exposed surface area of 0.2 cm^2 were dipped in 50.0 cm^3 of 0.1 mol dm^{-3} HCl solutions with and without the extracts of different concentrations (0.1 g dm^{-3} – 0.6 g dm^{-3}). Different concentrations of the extract in 0.1 mol dm^{-3} HCl were prepared in 0.1 mol dm^{-3} HCl by diluting 60.0 g dm^{-3} extract prepared in 0.1 mol dm^{-3} HCl using 0.1 mol dm^{-3} HCl. EIS were recorded after 2 h immersion. The same experimental set-up was used to record potentiodynamic polarization curves in the potential range from -0.7 V to -0.3 V at the ambient temperature. Each experiment was performed in duplicate. The same procedure was repeated with HCl solutions of different concentrations (0.5 mol dm^{-3} – 2.0 mol dm^{-3}).

2.3.1.4 Adsorption consideration

Mild steel specimens with of 4.0 cm (L) × 2.0 cm (W) × 0.6 cm (thickness) were immersed in 125.0 cm^3 of 0.5 mol dm^{-3} HCl solution and in acidic extracts of different concentrations ranging from 3.0 to 60.0 g dm^{-3} extract prepared in 0.5 mol dm^{-3} HCl at ambient temperature and at 50 °C. Acidic extracts of cinnamon leaves of different concentrations lower than 60.0 g dm^{-3} were prepared by diluting 60.0 g dm^{-3} cinnamon leaf extract prepared in 0.5 mol dm^{-3} HCl using 0.5 mol dm^{-3} HCl. Each experiment was performed in duplicate. Mass loss of mild steel specimens was recorded as mentioned in Section 2.3.1.1 at pre-determined time intervals. Surface coverage of extract components on mild steel surfaces was calculated based on mass losses obtained for mild steel specimen in 0.5 mol dm^{-3} HCl and in cinnamon leaf extracts of different concentrations prepared in 0.5 mol dm^{-3} HCl. These data were used to fit adsorption isotherm models.

2.3.1.5 Enhancement of inhibition effect of cinnamon leaf extracts by KI

Mild steel specimens with of 4.0 cm (L) × 2.0 cm (W) × 0.6 cm (thickness) were dipped in 125.0 cm^3 of 0.5 mol dm^{-3} HCl and 3.0 g dm^{-3} acidic extracts prepared in 0.5 mol dm^{-3} HCl without and with KI of different concentrations ranging from 0.5 mmol dm^{-3} to 2.5 mmol dm^{-3} at ambient temperature after recording its initial mass. Mass loss of mild steel specimens in each medium was recorded at a pre-determined time intervals as mentioned in Section 2.3.1.1.

EIS (at V_{oc}) and potentiodynamic polarization curves (-0.7 V to -0.3 V) were recorded for mild steel rod specimens with an exposed surface area of 0.2 cm^2 in each of the following solutions at ambient temperature after 2 h immersion.

- 50.0 cm^3 of HCl,
- 50.0 cm^3 of 0.1 g dm^{-3} extract prepared in 0.5 mol dm^{-3} HCl,
- 50.0 cm^3 of 0.1 g dm^{-3} extract prepared in 0.5 mol dm^{-3} HCl with 0.5 mmol dm^{-3} and 2.5 mmol dm^{-3} KI.

2.3.1.6 Morphological study

Surface pictures of cleaned mild steel specimens were examined under a polarizing microscope (× 100) before and after immersion in 0.5 mol dm^{-3} HCl and in 3.0 g dm^{-3} cinnamon leaf extracts prepared in 0.5 mol dm^{-3} HCl after 2 h and 24 h.

2.3.1.7 Effect of acidic extracts of cinnamon leaves on removal of rust from mild steel

Mild steel specimens with an exposed surface area of 32.0 cm^2 were immersed in 150.0 cm^3 of 0.5 mol dm^{-3} HCl and 3.0 g dm^{-3} acidic extracts prepared in 0.5 mol dm^{-3} HCl. Mild steel specimens were used as received and edges of the mild steel specimens were painted to expose the flat surface area only, which covered with rust and scales, to the corrosion medium. Specimens were cleaned by using acetone. Mass loss of mild steel specimens in each medium was recorded at a pre-determined time intervals as mentioned in Section 2.3.1.1.

2.3.2 Corrosion of copper in HCl and its preventions

2.3.2.1 Effect of acid concentration on corrosion of copper in HCl

2.3.2.1.1 Mass loss measurements, pH measurements and solution analysis: In order to estimate the corrosion rate with respect to HCl concentration, mass loss of Cu specimens with an exposed surface area of 6.35 cm^2 to test solutions suspended in 125.0 cm^3 HCl solutions of different concentrations (0.05 mol dm^{-3} – 1.0 mol dm^{-3}) was recorded after 6, 12, 18 and 24 days of immersion. The same experimental set-up was used to monitor the pH of each corrosive medium. Aliquots of 2.0 cm^3 of each test solution were withdrawn after 6, 12, 18 and 24 days of immersion for analyzing the concentration of Cu in corrosive medium by atomic absorption spectroscopy. Each experiment was conducted in duplicate.

2.3.2.1.2 Open circuit potential measurements: V_{oc} of each system in a completely open environment at ambient temperature was measured in duplicate in regular time intervals using copper specimens with an exposed surface area of 6.35 cm^2 in 125.0 cm^3 of HCl solutions of different concentrations (0.05 mol dm^{-3} – 1.0 mol dm^{-3}).

2.3.2.2 Inhibition of copper corrosion in HCl using methanol extract of tea leaves

In order to study the inhibition effect of methanol extract of tea leaves, 10% (v/v) methanol extract in 0.05 mol dm^{-3} HCl was prepared by mixing 25.0 cm^3 methanol extract of tea leaves with 225.0 cm^3 HCl solution which was prepared by diluting 2.0 mol dm^{-3} HCl solution. Required volume of 2.0 mol dm^{-3} HCl was calculated to prepare 225.0 cm^3 HCl solution in order to maintain the final concentration of HCl as 0.05 mol dm^{-3}. The same amount of methanol was added to the blank solution. The same procedure was repeated to prepare 10% (v/v) extract in HCl solutions of different concentrations (0.1 mol dm^{-3} – 1.0 mol dm^{-3}). Mass loss of copper specimens with an exposed surface area of 6.35 cm^2 to test solutions suspended in 125.0 cm^3 HCl solutions with and without 10% (v/v) tea leaf extract in one day intervals for up to 5 days was measured in duplicate as stated in Section 2.3.1.1.

2.3.2.3 Effect of inhibitor concentration on corrosion inhibition of copper corrosion in HCl

A copper specimen with an exposed surface area of 2.15 cm^2 was dipped in 50.0 cm^3 of 0.05 mol dm^{-3} and 1.0 mol dm^{-3} HCl solutions with 2%, 4%, 6%, 8% and 10% (v/v) tea leaf extract. EIS were then recorded in duplicate at V_{oc} after 2 h and 24 h immersion. Potentiodynamic polarization curves were recorded using the same experimental set-up by scanning the potentials from -0.4 V to 0 V for 0.05 mol dm^{-3} HCl and from -0.5 V to -0.1 V for 1.0 mol dm^{-3} HCl, both at a scan rate of 0.01 V s^{-1}.

2.3.2.4 Adsorption consideration

Mass loss of copper specimens with an exposed surface area of 6.35 cm^2 to test solutions, suspended in 125.0 cm^3 of 0.05 mol dm^{-3} HCl solutions without and with 4%, 6%, 8%, 10% and 15% tea leaf extract, was recorded in duplicate in one day intervals for up to 7 days as mentioned in Section 2.3.1.1. Surface coverage of tea leaf extract on copper specimens in 0.05 mol dm^{-3} HCl was calculated based on the results obtained from mass loss experiments and these data were then used to fit adsorption isotherm models. Further,

results obtained from potentiodynamic polarization measurements after 2 h of immersion were also fitted with the adsorption isotherm models.

2.3.2.5 UV-Vis spectroscopic studies

UV-Vis spectrum of each of the following solutions was recorded in the wavelength range of 190-800 nm.

- Methanol extract of tea leaves,
- Methanolic solution obtained by immersing the copper specimen completely, which was dipped in 25.0 cm^3 10% (v/v) extract in 0.05 mol dm^{-3} HCl and removed after 2 h and 24 h, in methanol (7.0 cm^3),
- 10% (v/v) tea leaf extract in 0.05 mol dm^{-3} HCl before placing copper specimen.
- 10% (v/v) tea leaf extract in 0.05 mol dm^{-3} HCl after placing copper specimen for 24 h.

The same experiment was repeated for 1.0 mol dm^{-3} HCl.

2.3.2.6 Active components in tea leaf extract responsible for corrosion inhibition

2.3.2.6.1. Antioxidant ability of the tea leaf extract: 2,2'-azinobis(3-ethylbenzothiazoline-6-sulfonic acid) diammonium salt (ABTS) (7 mmol dm^{-3}) and $Na_2S_2O_8$ (2.45 mmol dm^{-3}) were mixed in 2:1 ratio to prepare the reagent to check the antioxidant ability. The colourless ABTS molecules is converted into the blue-green coloured radical cation, $ABTS^{\cdot+}$, by sodium persulphate. In this method tea leaves extract in HCl solutions of different concentrations (0.05 mol dm^{-3} – 1.0 mol dm^{-3}) was added to $ABTS^{\cdot+}$ and the absorbance of $ABTS^{\cdot+}$ was recorded at 734 nm after one minute. An aliquot of 3.0 cm^3 of reagent and 100 µl of demonized water were mixed for the control and 3.0 cm^3 of reagent and100 µl of 10% (v/v) tea leaf extracts were mixed to prepare the test solution while the blank solution was prepared in the absence of tea leaf extract. Absorbance of both solutions at 734 nm was then recorded.

2.3.2.6.2. Effect of caffeine: Mass losses of copper specimens in 0.05 mol dm^{-3} HCl, methanol extract of tea leaves in 0.05 mol dm^{-3} HCl and synthetic caffeine of different concentrations prepared in 0.05 mol dm^{-3} HCl (10, 50, 100 and 1000 ppm) were recorded in duplicate as stated in Section 2.3.1.1.

2.3.2.7 Surface pictures

Surface pictures of cleaned copper specimens were examined under a polarizing microscope (×100) after immersion in 0.05 mol dm^{-3} HCl for 48 h without and with 10% (v/v) tea leaf extract. Concentration of HCl solutions without and with extract was maintained as 0.05 mol dm^{-3}.

2.3.3 Corrosion of galvanized steel in NaCl solutions and its prevention

2.3.3.1 Effect of NaCl on corrosion behavior of galvanized steel in NaCl environments

Galvanized steel (GS) specimens with 4.00 cm (L) × 1.00 cm (W) × 0.03 cm (thickness) were exposed to 125.0 cm^3 of 0.1 mol dm^{-3}, 1.0 mol dm^{-3} and 4.0 mol dm^{-3} NaCl solutions in duplicate for a period of 60 days, and V_{oc} of each electrode was measured at a predetermined time interval at ambient temperature. The same procedure was repeated with 1.0 mol dm^{-3} NaCl solution at 50 °C. V_{oc} of GS in 0.1 mol dm^{-3} at pH = 1 were also monitored at ambient temperature.

GS specimens with 1.00 cm (L) × 1.00 cm (W) × 0.03 cm were exposed to 50.0 cm^3 of 0.1 mol dm^{-3}, 1.0 mol dm^{-3} and 4.0 mol dm^{-3} NaCl solutions in duplicate. After 24 h immersion, EIS were recorded at V_{oc}. The same experimental set-up was used to record the polarization curves in the potential range of -1.4 V to -0.6 V at a scan rate of 0.01 V s^{-1}.

GS specimens with 4.00 cm (L) × 1.00 cm (W) × 0.03 cm (thickness) were exposed to 125.0 cm^3 of 0.1 mol dm^{-3} and 1.0 mol dm^{-3} NaCl solutions after weighing in duplicate. After 1 week and 2 weeks, GS specimens were withdrawn, corrosion products on the surface were removed by using a brush and reweighed. Each solution was filtered and the white coloured precipitate was weighed, while the solution was analyzed for total concentration of Zn using AAS.

2.3.3.2 Corrosion inhibition of GS in NaCl using tea leaf extracts

GS specimens with 4.00 cm (L) × 1.00 cm (W) × 0.03 cm (thickness) were exposed to 125.0 cm^3 0.1 mol dm^{-3} NaCl at pH = 1, 2, 3, 4 and 5 with and without 5% (v/v) tea leaf extract. Mass loss of GS specimens and change in pH of corrosive media were recorded in one day intervals. The pH of NaCl solutions in the presence and absence of the extract was adjusted by adding concentrated HCl solution.

2.3.3.3 Effect of concentration of tea leaf extract on corrosion inhibition of GS in NaCl

Rectangular GS specimens with 4.00 cm (L) × 1.00 cm (W) × 0.03 cm (thickness) were exposed to 125.0 cm^3 of 0.1 mol dm^{-3} NaCl solutions and 2.5%, 5.0%, 7.5% and 10% (v/v) tea leaf extracts in 0.1 mol dm^{-3} NaCl at pH = 2. Mass loss of GS specimens and change in pH of corrosive media were recorded in one day intervals.

Electrochemical experiments were conducted using GS specimens with 1.00 cm (L) × 1.00 cm (W) × 0.03 cm (thickness) as the working electrode and 0.1 mol dm^{-3} NaCl with and without methanol extracts of tea leaves at pH = 2 as the electrolyte. EIS of each solution was recorded at the V_{oc} while potentiodynamic polarization curves were recorded in the potential range of $V_{oc} \pm 100$ mV.

The concentration of NaCl was maintained as 0.1 mol dm^{-3} in all test and blank solutions. Required amount of NaCl was calculated to maintain the NaCl concentrations as 0.1 mol dm^{-3} by considering the change in volume after adding methanol extract and methanol to the blank. For the blank, the same amount of methanol was added to check the effect of the background medium on corrosion prevention. All the experiments were carried out in duplicate under air-saturated conditions at ambient temperature.

2.3.4 Corrosion of copper in NaCl solutions and its prevention

2.3.4.1 Effect of NaCl on corrosion behavior of copper in NaCl environments

Copper specimens with an exposed surface area of 2.15 cm^2 were suspended in 50.0 cm^3 of 0.1, 0.5 and 1.0 mol dm^{-3} NaCl solutions in duplicate. After 24 h immersion, potentiodynamic polarization curves were recorded using copper specimen, SCE and Pt foil as working, reference and counter electrodes, respectively. All experiments were conducted in open environment.

2.3.4.2 Corrosion inhibition of copper in NaCl

EIS and potentiodynamic polarization curves of copper specimens with an exposed surface area of 2.15 cm^2 were recorded in 50.0 cm^3 of 0.1 mol dm^{-3} NaCl solutions without and with tea leaf extracts of different concentrations of 10%, 15% and 20% (v/v) after 24 h immersion. EIS were recorded at the V_{oc} using a three electrode system as stated in Section 2.3.4.1. For potentiodynamic polarization experiments, the potential was scanned at a scan rate of 0.01 V s^{-1} from -0.4 V to 0 V in open environment.

Mass loss measurements of copper specimens were not accurate in near neutral medium due to the deposition of corrosion products on the surface. As corrosion products dissolved and removed from the copper surface at low pH levels, pH of 0.1 mol dm^{-3} NaCl with and without 20% (v/v) tea leaf extract were adjusted to 1, 2, 3 and 4 using concentrated HCl. Rectangular Cu specimens of known mass with dimension of 3.00 cm (L) × 1.00 cm (W) × 0.05 cm (thickness) were dipped in 0.1 mol dm^{-3} of NaCl with and without 20% tea leaves extracts at ambient temperature in duplicate and mass losses were recorded at pre-determined time intervals. The change in pH of the test solution was also monitored with time using the same experimental set-up.

2.3.4.3UV-Vis spectrascopic studies

Copper specimens with with 4.00 cm (L) × 1.00 cm (W) × 0.05 cm (thickness) were dipped in 25.0 cm^3 of 20% (v/v) extract in 0.1 mol dm^{-3} NaCl solution and copper specimen was removed after removed 24 h. It was washed well with distilled water, dipped in 7.0 cm^3 methanol for 10 min and UV-Vis spectrum was recorded using this methanolic solution. UV-Vis spectrum of 20% (v/v) tea leaf extract in 0.1 mol dm^{-3} NaCl were also recorded before and after immersion of copper specimens for comparison purposes.

CHAPTER 3

RESULTS AND DISCUSSION

3.1 Corrosion of Mild Steel in HCl Solutions and Its Prevention

3.1.1 Effect of the concentration of hydrochloric acid on corrosion of mild steel

Mild steel objects are immersed in a series of acid pickling baths in the order of decreasing acid concentrations prior to galvanization in industrial scale. This process removes rust and scales on the surface as it is important to obtain a clean and a smooth surface for coating with zinc. Use of hydrochloric acid is preferable to sulphuric acid in pickling baths as the former is more active at normal concentrations and temperatures, probably due to higher rate of diffusion of H^+ towards the steel surface and ferrous ions out of the steel surface. Therefore, hydrochloric acid can be used at low temperature for pickling of mild steel objects in open tanks. However, high speed pickling of mild steel specimens can be achieved at high temperatures in closed tanks in order to prevent the loss of acid by volatilization. Further, it is more suitable than sulphuric acid for pickling of mild steel objects which are to be galvanized since it gives less smut on the steel. In addition, any residual iron chloride left on the steel can be rinsed off more readily than residual iron sulphate deposits if sulphuric acid is used. Hydrochloric acid, however, readily dissolves detached iron oxides, and consequently, the ferric ion produced increases the rate of attack on the steel thus increasing the acid consumption.

Interaction of mild steel with components in acidic environments is inevitable as bare metal surfaces are exposed to acidic environment during the removal of rust and scales. This reaction causes over pickling of mild steel objects and hence decreases the life time of the pickling bath. Addition of corrosion inhibitors to pickling baths is a common practice in industries to mitigate over pickling of mild steel objects.

As the pickling process is carried out using a series of acid baths with different acid concentrations, the investigation of corrosion behavior of mild steel in acids of different concentrations is the preliminary step in the study of inhibition. Therefore, the corrosion behavior of mild steel in HCl solutions of different concentrations was studied using mass loss measurements, and the results are shown in Figure 3.1. In order to simulate the conditions in acid pickling baths, the edges of mild steel specimens were not smoothened. As shown in Figure 3.1, the rate of dissolution of mild steel specimens increases with

increasing the concentration of hydrochloric acid. Initial rate of corrosion of mild steel specimens dipped in 2.0 mol dm^{-3} HCl is closer to the rate of corrosion of mild steel specimens dipped in 1.5 mol dm^{-3} HCl. However, dissolution of mild steel dipped in 2.0 mol dm^{-3} HCl continues after the dissolution of mild steel dipped in 1.5 mol dm^{-3} HCl attains the steady state.

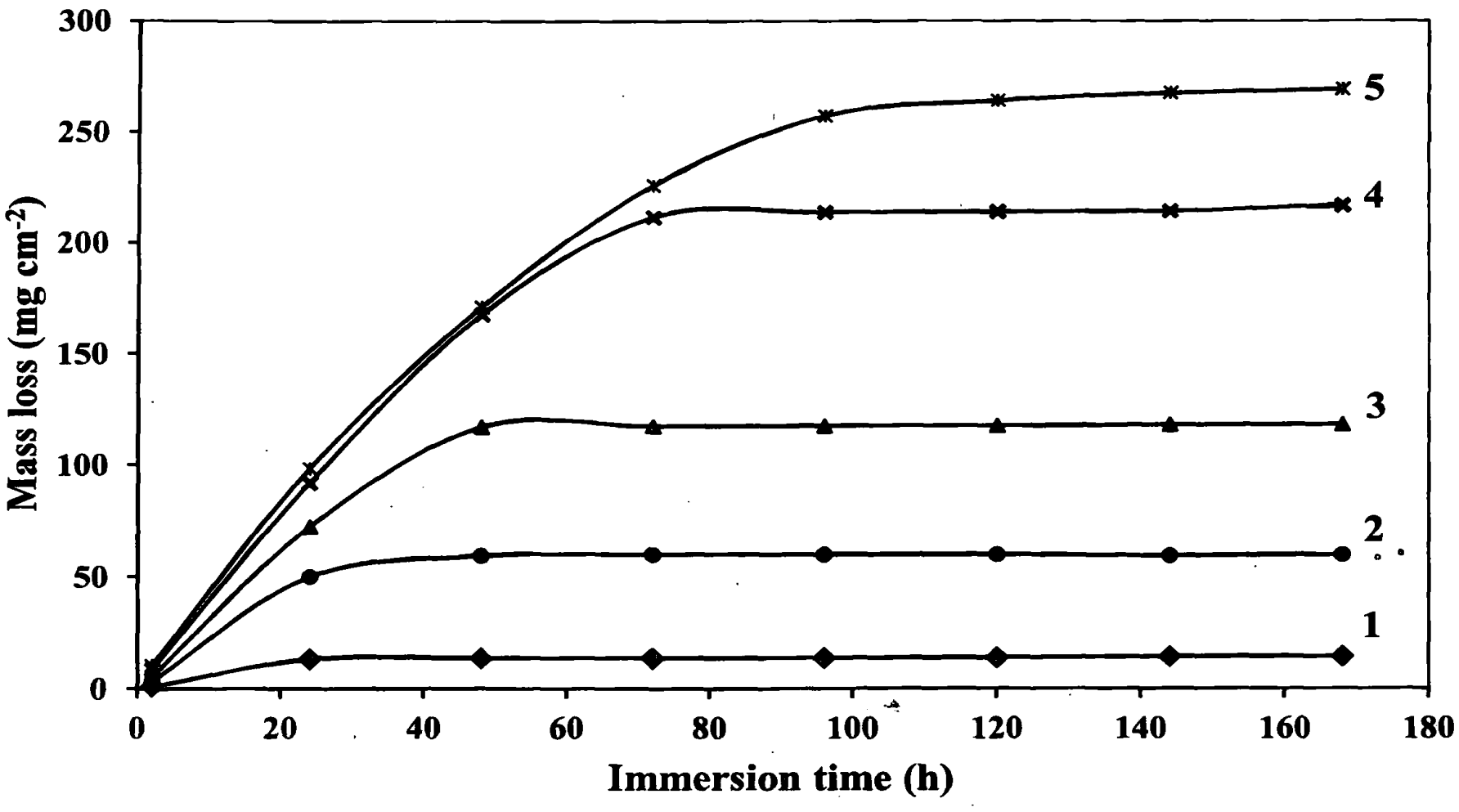

Figure 3.1: Mass loss of mild steel specimens in HCl solutions of different concentrations (1) 0.1, (2) 0.5, (3) 1.0, (4) 1.5 and (5) 2.0 mol dm^{-3}.

Corrosion rates of mild steel specimens in millimeters per year (mpy) in HCl solutions of different concentrations were calculated using the mass loss results according to Equation (3.1),

$$R = \frac{87.6\,\Delta W}{DAt} \tag{3.1}$$

where R is the corrosion rate (mpy), ΔW is the mass loss of the metal specimen (mg), D is the density of the metal (g cm^{-3}), A is the area of the metal exposed to corrosive media (cm^2) and t is the immersion time (h). Derivation of Equation 3.1 is given below,

Mass loss of metal specimen $= \Delta w$

Reduction in volume of metal specimen $= mass\ loss/density$

$$= \Delta w/d \ \text{cm}^3$$

Penetration rate $$= Reduction\ in\ volume/area$$

$$= \frac{\Delta w/d \ \text{cm}^3}{A \ \text{cm}^2}$$

$$= \Delta w/dA \ \text{cm}$$

If the mass loss is in mg, density is in g cm^{-3}, surface area is in cm^2 and time is in h,

Corrosion rate (mpy) $$= \frac{24\times365}{100}\frac{\Delta w}{dAt}$$

$$= \frac{87.6\ \Delta w}{dAt}$$

The results of the calculations of rate of corrosion are shown in Table 3.1.

Table 3.1: Time dependence of average corrosion rate of mild steel specimens in HCl solutions of different concentrations.

Concentration of HCl (mol dm^{-3})	Average corrosion rate (mpy) at different immersion time (h)							
	2	24	48	72	96	120	144	168
0.1	5.95	6.01	3.12	2.08	1.58	1.26	1.09	0.93
0.5	18.32	22.95	13.64	9.17	6.88	5.51	4.56	3.93
1.0	29.61	33.21	26.89	17.98	13.50	10.80	9.04	7.75
1.5	47.13	42.16	38.47	32.39	24.54	19.64	16.41	14.23
2.0	56.83	45.15	39.26	34.59	29.54	24.27	20.49	17.67

The effect of acid concentration on the rate of corrosion can be correlated by the following kinetics equation [73]:

$$\log R = \log k + n \log C \qquad (3.2)$$

where R is the rate of corrosion (mpy), k is the rate constant of corrosion, n is the order of the reaction with respect to HCl and C is the molar concentration of HCl.

The plot log R vs. log C gives a straight line (Regression coefficient = 0.993) based on mass loss measurements recorded after 24 h of immersion as shown in Figure 3.2 with a slope close to unity. This indicates that the dissolution of mild steel specimen in HCl is of first order with respect to HCl. Corrosion rate of the mild steel specimen placed in 2.0 mol dm^{-3} HCl was not used to plot the graph due to the similar corrosion rate as in 1.5 mol dm^{-3} HCl during early immersion time periods. It has been reported that corrosion of mild steel in H_2SO_4 is of first order with respect to H_2SO_4 to support the results

obtained [73]. It is thus evident that iron dissolution in HCl depends on the concentration of H^+. Further, the slope of the graph obtained in this study is not exactly 1, which may be due to localized corrosion during the pickling processes [1].

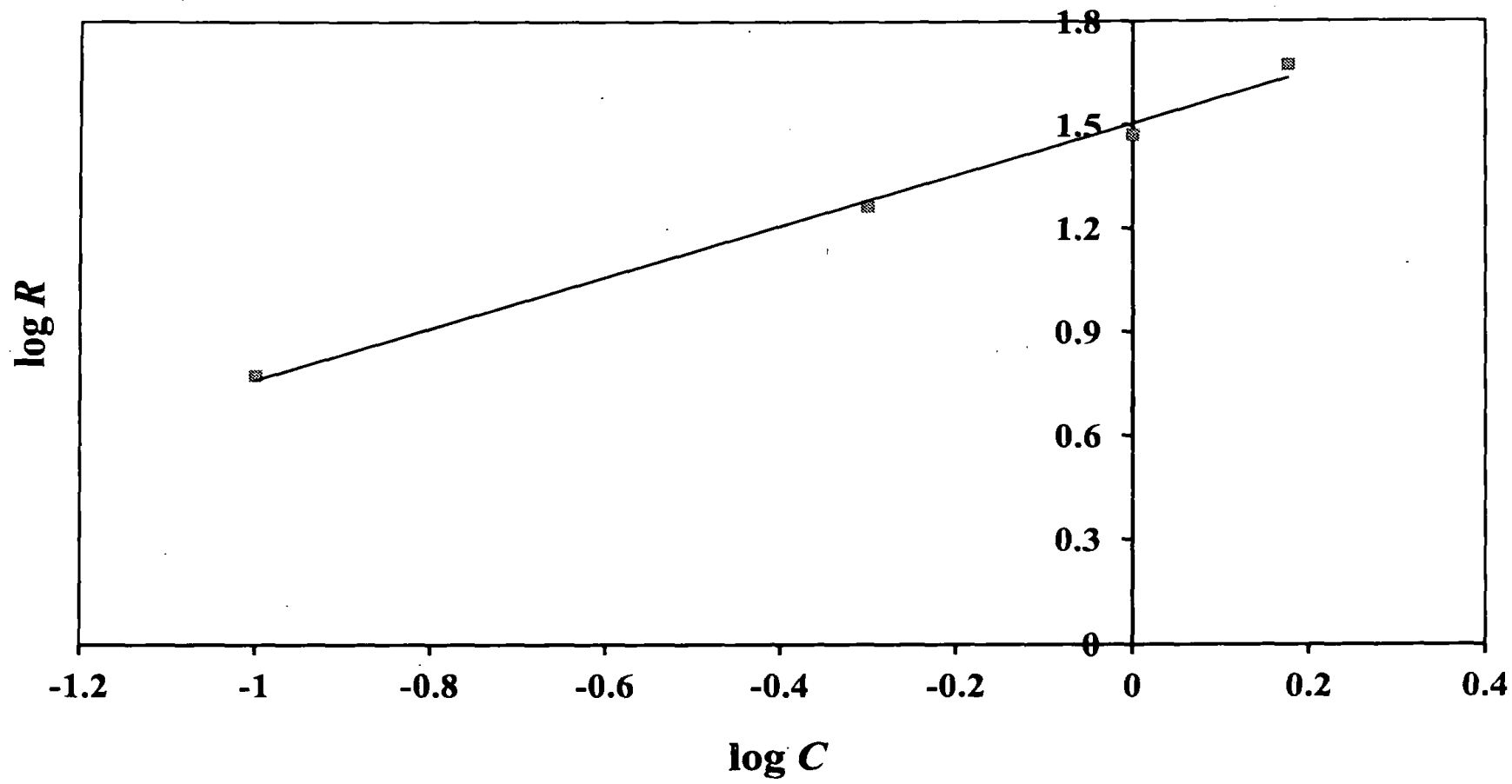

Figure 3.2: The relationship between log *R* of mild steel specimen and log *C* after 24 h immersion.

Figure 3.3 shows the change in pH of HCl solutions of different concentrations in which mild steel specimens were placed. As the cathodic reaction is the consumption of H_3O^+ to produce $H_2(g)$, the pH of the corrosive media increases with time as observed. Further, the corrosion system in low concentrated acid solutions attains steady pH value within a shorter time period. For instance, 0.1 mol dm^{-3} medium and 2.0 mol dm^{-3} medium attained steady pH values after 48 h and 120 h immersion, respectively.

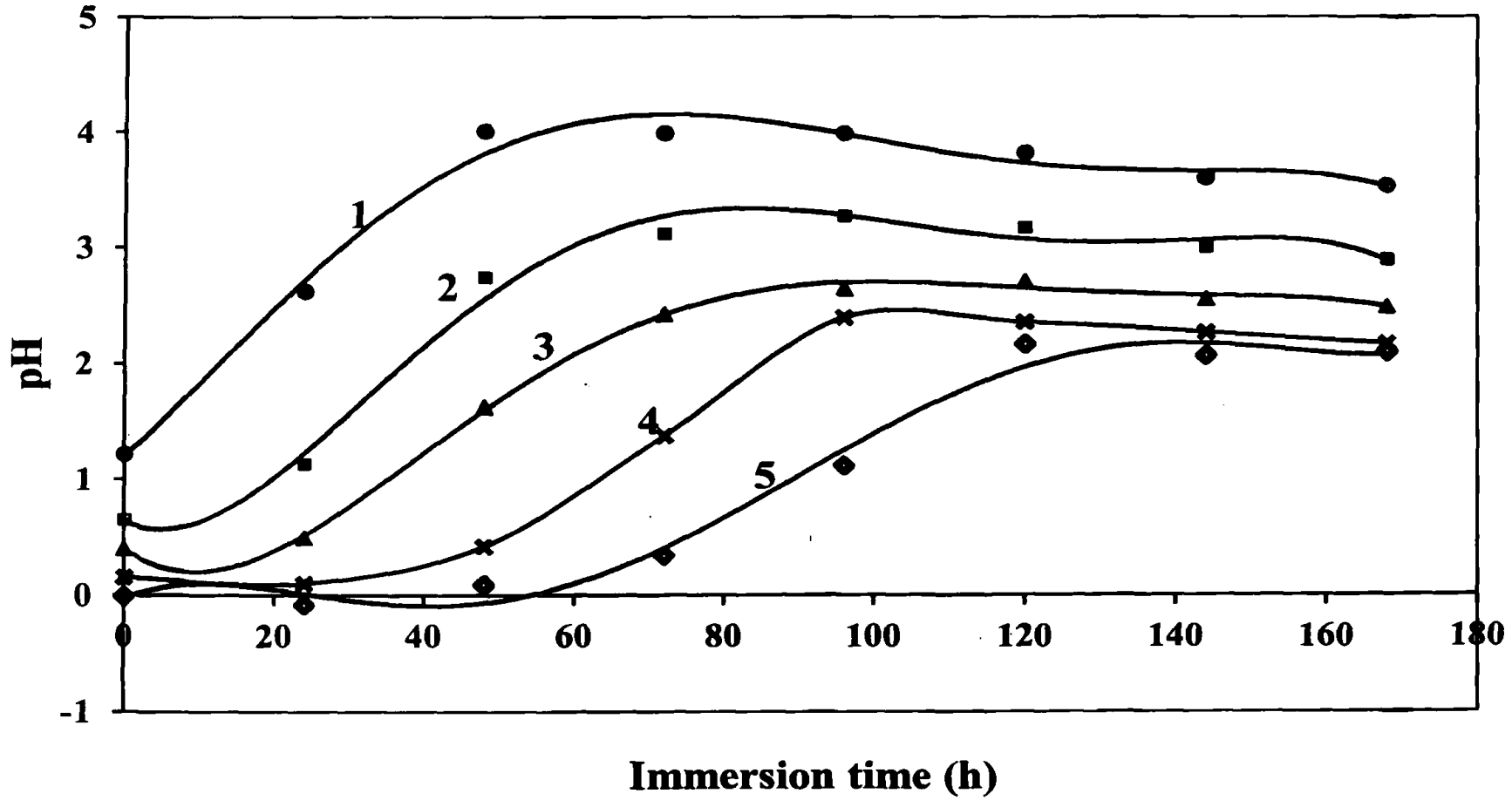

Figure 3.3: Variation of pH of HCl solutions in which mild steel specimens were placed. The concentrations (in mol dm^{-3}) of HCl solutions are (1) 0.1, (2) 0.5, (3) 1.0, (4) 1.5 and (5) 2.0.

In addition to mass loss measurements, electrochemical impedance spectroscopic studies were conducted in order to investigate the corrosion mechanism. Figure 3.4 shows the Nyquist plots of mild steel specimens placed in HCl solutions of different concentrations. All Nyquist plots obtained contain only a single depressed semicircle, indicating that the electrode reaction is mainly controlled by charge transfer [95]. Depressed semicircles with the center below the real axis indicate the inhomogeneous nature of the metal surface [96]. It can be noticed that the solution resistance, which is determined from the intersection of the semicircle at high frequency region, is small (20 Ω for 0.1 mol dm^{-3} HCl and 2 Ω to 10 Ω for higher concentrations of HCl solutions) due to the high conductivity of the solution. The charge transfer resistance (R_{ct}), which can be calculated from the difference between the intersection at low frequency region and high frequency region, decreases with increase in the concentration of acid, indicating that corrosion rate of mild steel increases with increase in the concentration of the acid.

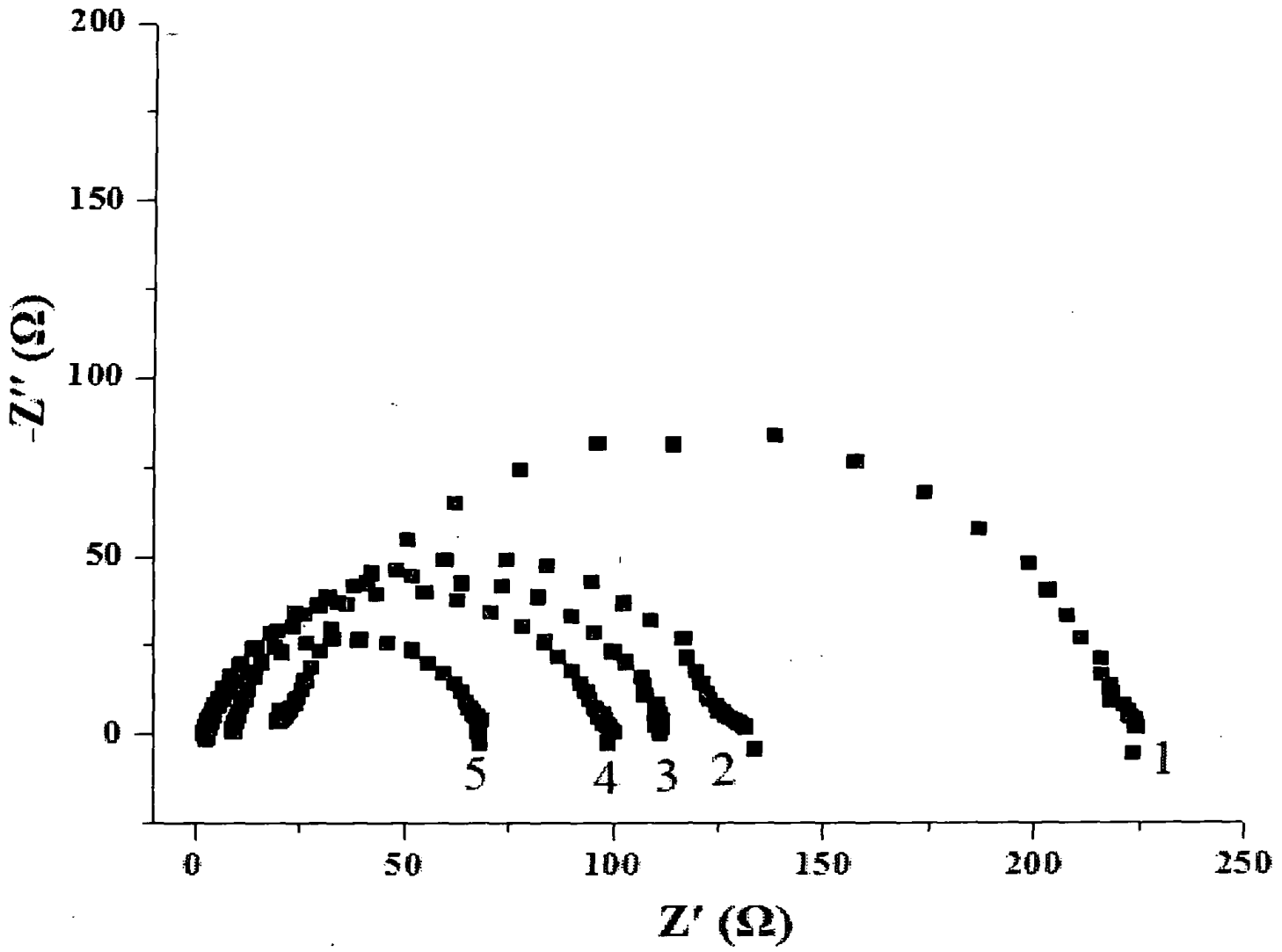

Figure 3.4: Nyquist plots of mild steel specimens in HCl solutions of different concentrations in mol dm^{-3} (1) 0.1, (2) 0.5, (3) 1.0, (4) 1.5 and (5) 2.0.

3.1.2 Inhibition effect of acidic extracts of cinnamon leaves on corrosion of mild steel in HCl

A preliminary experiment was carried out to investigate the inhibition ability of acidic extracts of cinnamon leaves on the corrosion of mild steel specimens in HCl solutions of different concentrations ranging from 0.1 mol dm^{-3} to 2.0 mol dm^{-3} using mass loss measurements in the presence and absence of 60.0 g dm^{-3} extract. Interestingly, acidic extracts of cinnamon leaves show inhibition effect on mild steel corrosion in all tested concentrations. Corrosion rates of mild steel specimens in the presence and absence of extracts were calculated using Equation (3.1) are shown in Table 3.2.

Table 3.2: Corrosion rates of mild steel specimens in different concentrations of HCl solutions with and without 60.0 g dm^{-3} acidic extracts of cinnamon leaves with time.

[HCl] (mol dm^{-3})	[Extract] (g dm^{-3})	Average corrosion rate (mpy)							
		2 h	24 h	48 h	72 h	96 h	120 h	144 h	168 h
0.1	0	5.95	6.01	3.12	2.08	1.58	1.26	1.09	0.93
0.1	60.0	1.38	0.56	0.45	0.41	0.38	0.36	0.36	0.35
0.5	0	18.32	22.95	13.64	9.17	6.88	5.51	4.56	3.93
0.5	60.0	1.27	0.96	1.20	1.33	1.32	1.33	1.3	1.31
1.0	0	29.61	33.21	26.89	17.98	13.50	10.8	9.04	7.75
1.0	60.0	3.14	1.62	2.20	2.46	2.54	2.57	2.64	2.62
1.5	0	47.13	42.16	38.47	32.39	24.54	19.64	16.41	14.23
1.5	60.0	3.75	2.03	2.80	3.39	3.68	3.93	4.28	4.47
2.0	0	56.83	45.15	39.26	34.59	29.54	24.27	20.49	17.67
2.0	60.0	3.64	2.96	3.96	4.76	4.83	4.83	4.97	5.02

According to Figure 3.3, the pH of 0.1 mol dm^{-3} HCl solution which contains a mild steel specimen increased by almost 1.5 units after 24 h and the corresponding pH increase in 2.0 mol dm^{-3} HCl solution was about 1 unit after 4 days. However, the pH of the above systems in the presence of cinnamon leaf extract does not change significantly even after 7 days. It can be clearly seen in Figure 3.5. Therefore, the rates of corrosion of mild steel specimens decrease to a great extent in the presence of extracts supporting the results obtained from mass loss measurements. Therefore, addition of extracts increases the life time of the medium. The life-time of pickling baths used in industries is determined by monitoring the pH of the pickling bath.

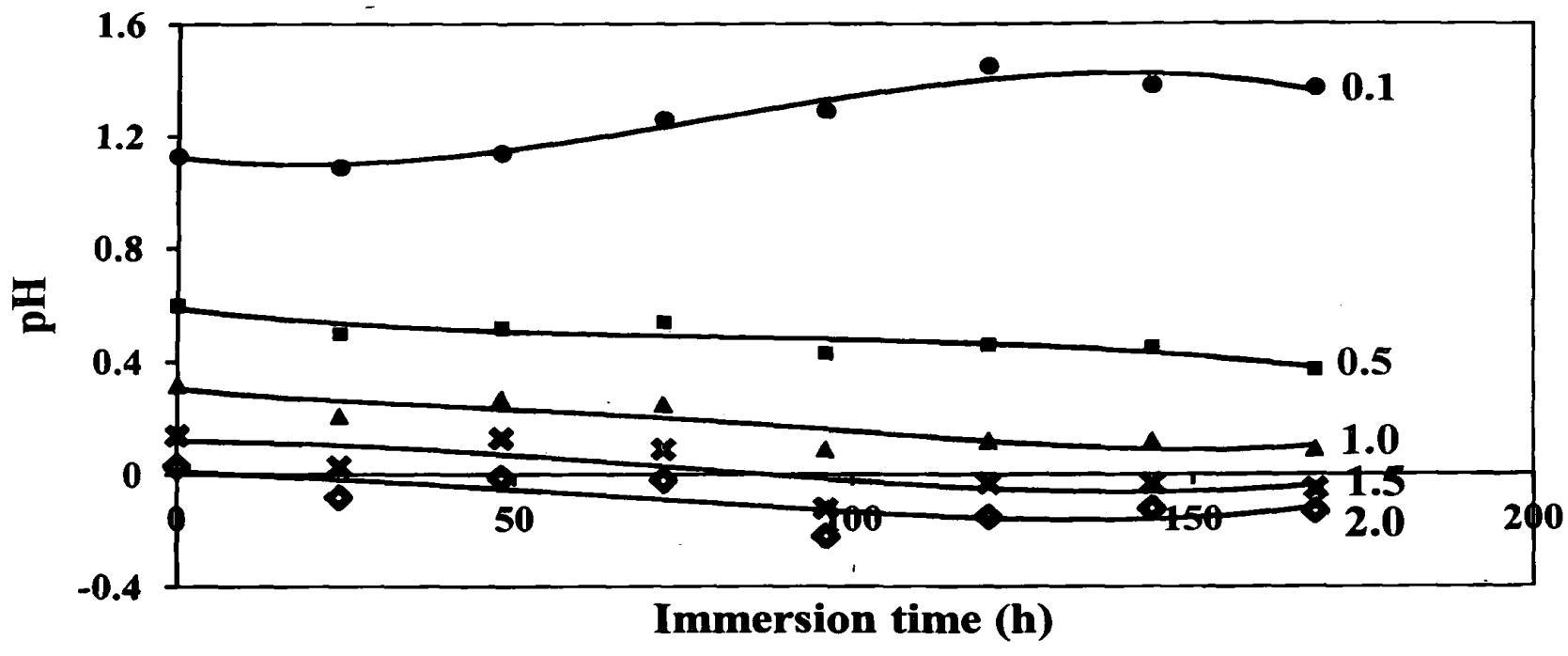

Figure 3.5: Variation of solution pH of HCl solutions of different concentrations (in mol dm^{-3}) containing mild steel specimens in the presence of 60.0 g dm^{-3} cinnamon leaf extracts.

3.1.3 Effect of concentration of acidic extracts on corrosion inhibition

As acidic extracts of cinnamon leaves have a corrosion inhibition effect, electrochemical impedance spectroscopic analysis and potentiodynamic polarization studies were carried out using different concentrations of cinnamon leaf extracts prepared in different concentrations of HCl ranging from 0.1 mol dm^{-3} to 2.0 mol dm^{-3} to study the effect of inhibitor concentration. As only a small surface area of mild steel specimens was exposed to corrosive media for electrochemical studies, the concentration of inhibitor which used for the electrochemical experiments were lower than that of mass loss measurements. Figures 3.6 to 3.10 show Nyquist plots of mild steel specimens in HCl solutions of different concentrations ranging from 0.1 mol dm^{-3} to 2.0 mol dm^{-3} in the absence and presence of different concentrations of acidic extracts of cinnamon leaves after 2 h immersion. Nyquist plots of mild steel specimens in HCl show the same trend of EIS spectra with and without extracts indicating the same mechanism for corrosion in the absence and presence of cinnamon leaf extract [54, 82]. Further, the presence of the extract increases the charge transfer resistance (R_{ct}), which is a measure of the resistance of a metal surface towards corrosion. The value of R_{ct} increases with increasing the concentration of extracts in all acid concentrations. Increase in R_{ct}, which may be due to the change in the double layer capacitance as a result of adsorption of inhibitor molecule on the metal surface [72], demonstrates the corrosion inhibition ability of acidic extracts of cinnamon leaves.

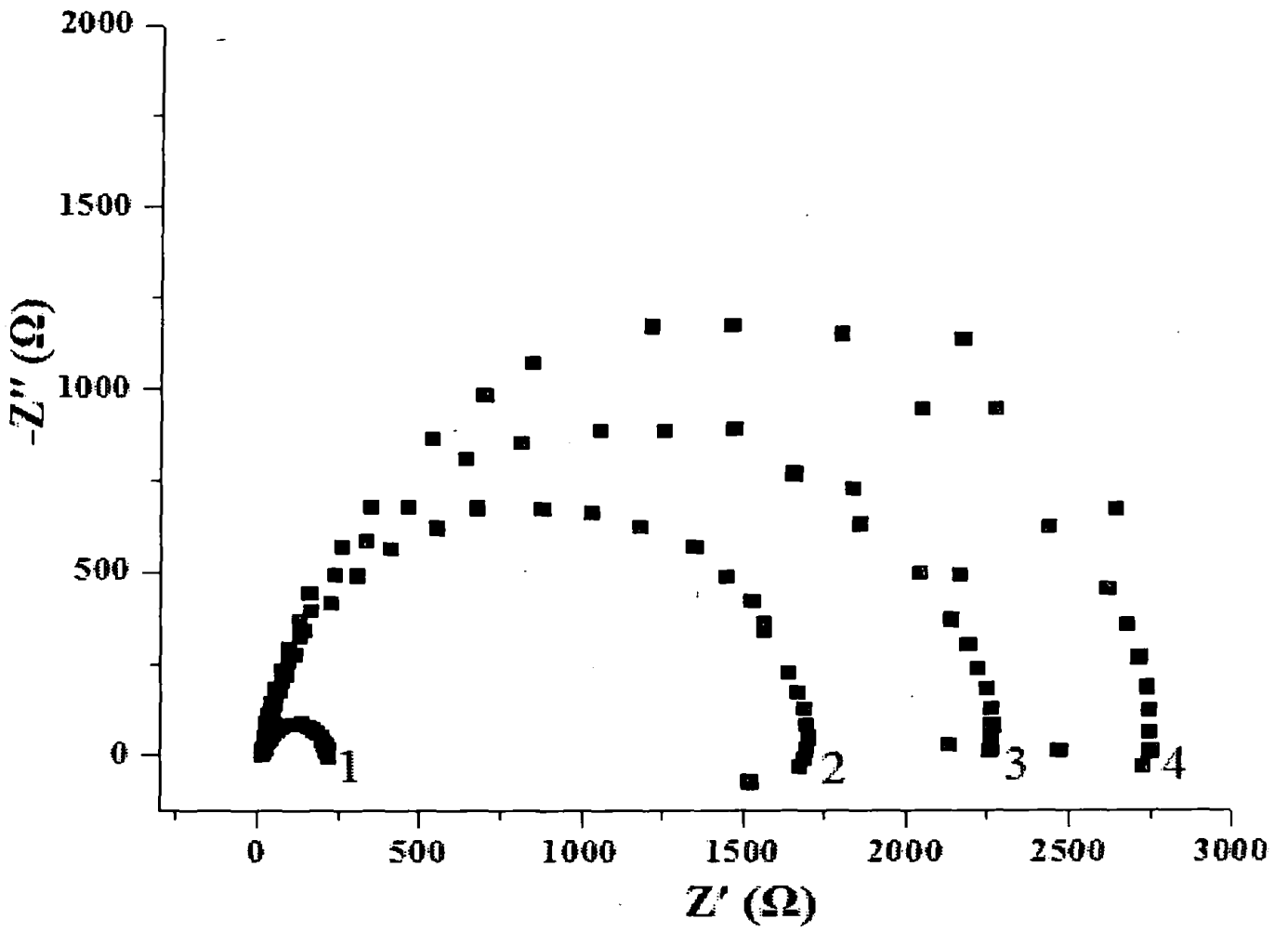

Figure 3.6: Nyquist plots of mild steel specimens in 0.1 mol dm^{-3} HCl with acidic extracts of cinnamon leaves of different compositions (1) 0, (2) 0.1, (3) 0.3 and (4) 0.6 g dm^{-3}.

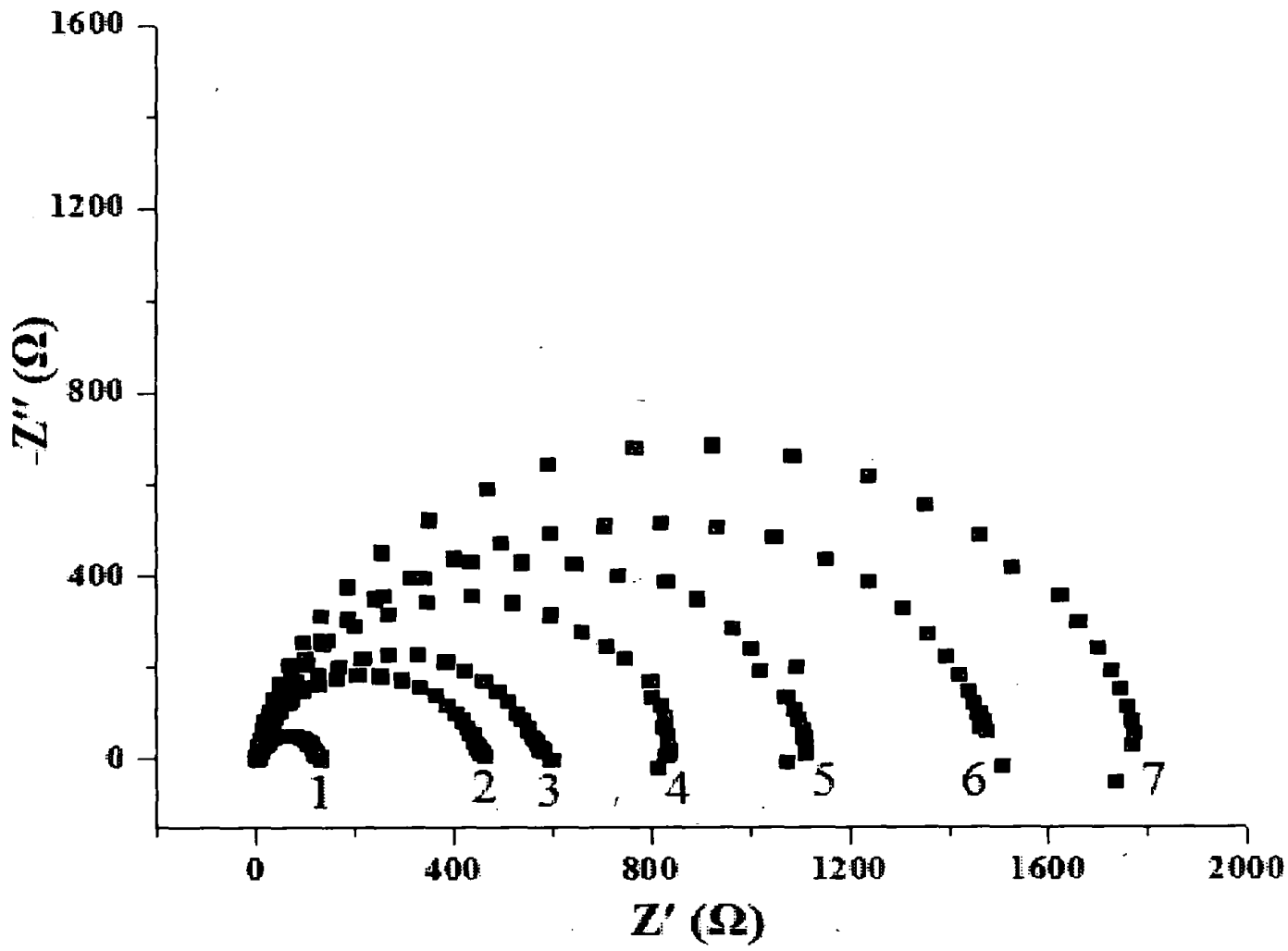

Figure 3.7: Nyquist plots of mild steel specimens in 0.5 mol dm^{-3} HCl with acidic extracts of cinnamon leaves of different compositions (1) 0, (2) 0.1, (3) 0.2, (4) 0.3, (5) 0.4, (6) 0.5 and (7) 0.6 g dm^{-3}

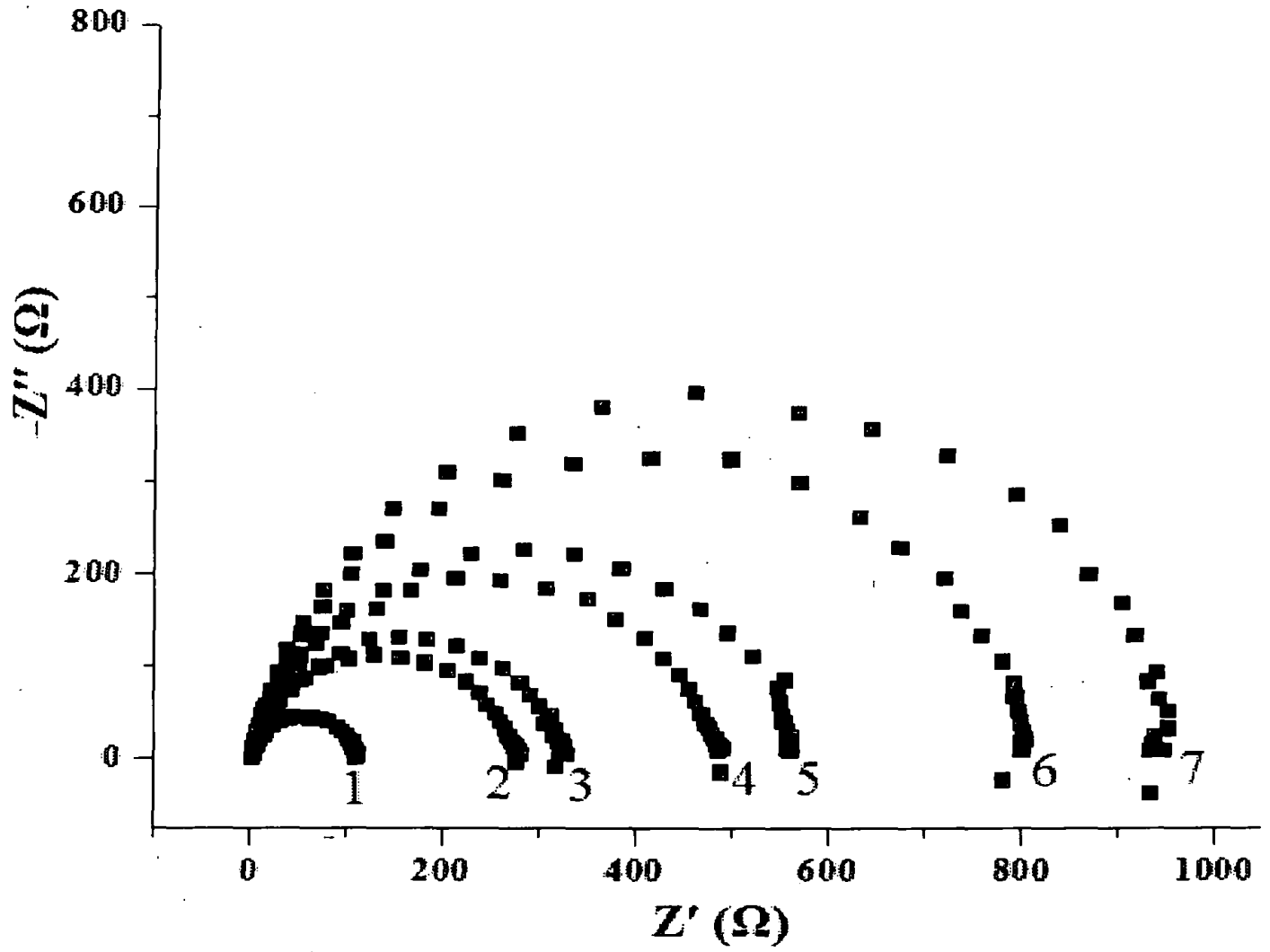

Figure 3.8: Nyquist plots of mild steel specimens in 1.0 mol dm^{-3} HCl with acidic extracts of cinnamon leaves of different compositions (1) 0, (2) 0.1, (3) 0.2, (4) 0.3, (5) 0.4, (6) 0.5 and (7) 0.6 g dm^{-3}.

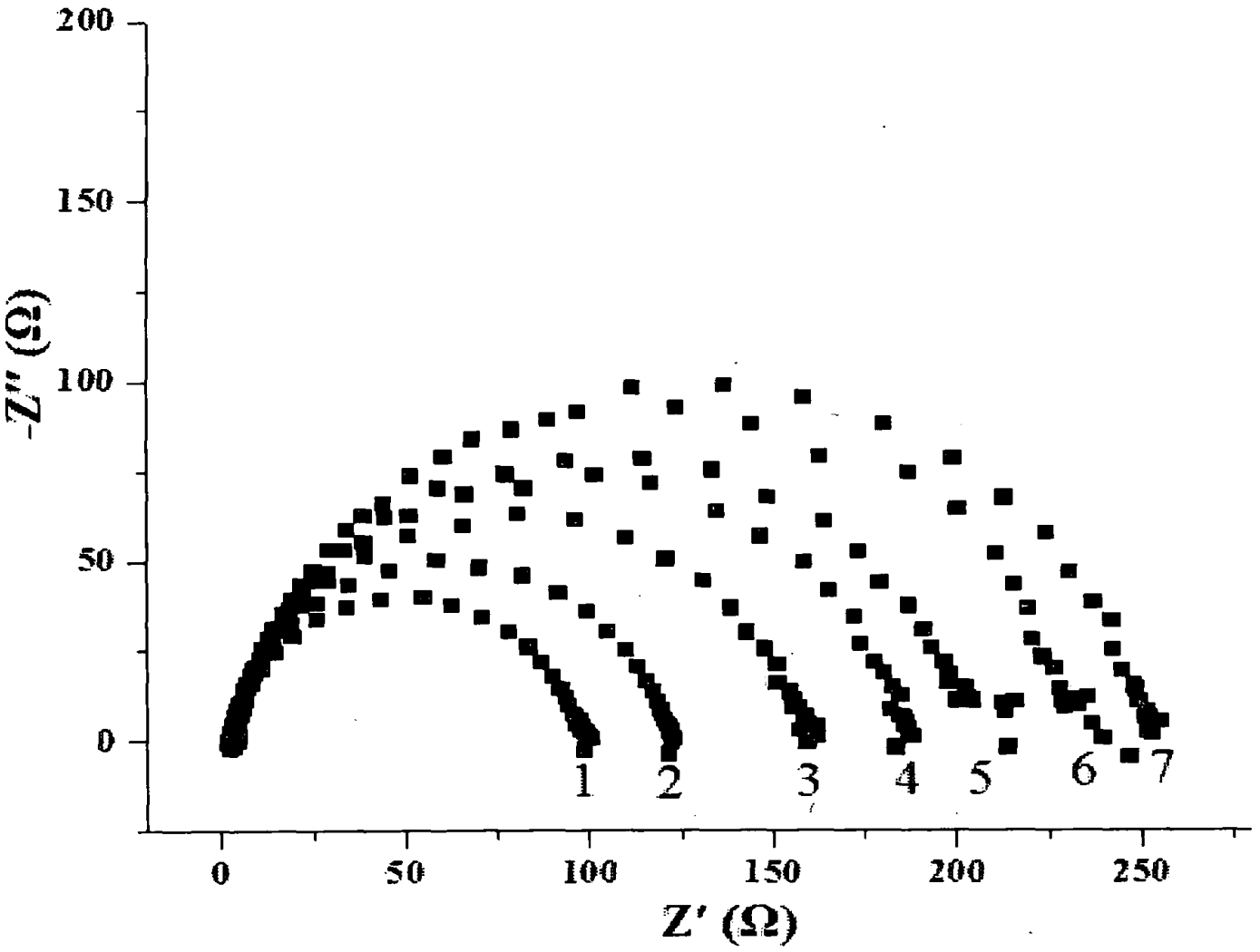

Figure 3.9: Nyquist plots of mild steel specimens in 1.5 mol dm^{-3} HCl with acidic extracts of cinnamon leaves of different compositions (1) 0, (2) 0.1, (3) 0.2, (4) 0.3, (5) 0.4, (6) 0.5 and (7) 0.6 g dm^{-3}

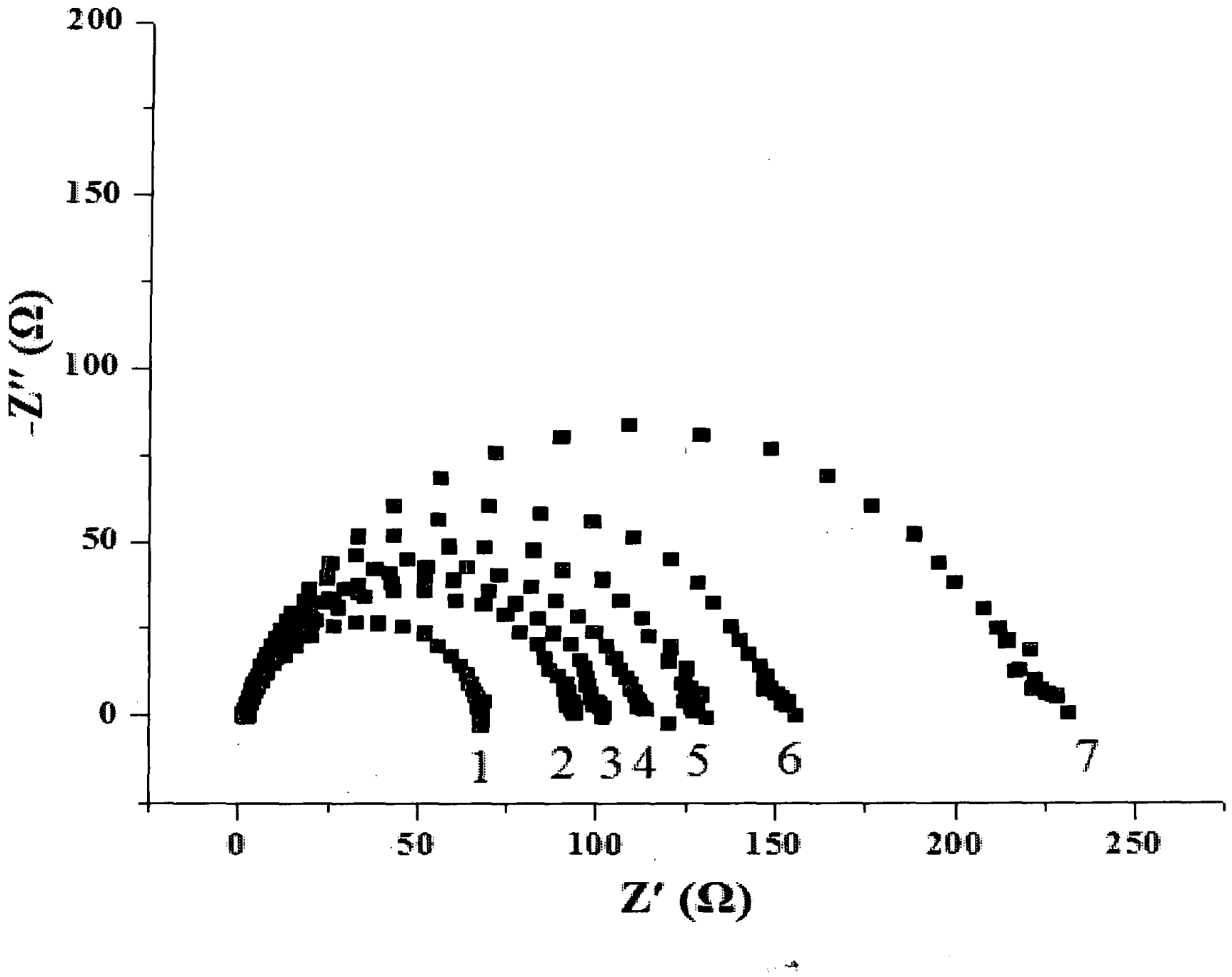

Figure 3.10: Nyquist plots of mild steel specimens in 2.0 mol dm^{-3} HCl with acidic extracts of cinnamon leaves of different compositions (1) 0, (2) 0.1, (3) 0.2, (4) 0.3, (5) 0.4, (6) 0.5 and (7) 0.6 g dm^{-3}.

The equivalent circuit, which is representative of the physical processes taking place in the system under investigation, is commonly used to calculate the parameters of interest. As the electrochemical system of mild steel in hydrochloric acid with and without cinnamon leaf extract shows only a single semi-circle, it can be represented by the simple Randles equivalent circuit, including the charge-transfer resistance (R_{ct}) parallel with the constant phase element (*CPE*) in series with solution resistance (R_s), as shown in Figure 3.11 [97-98]

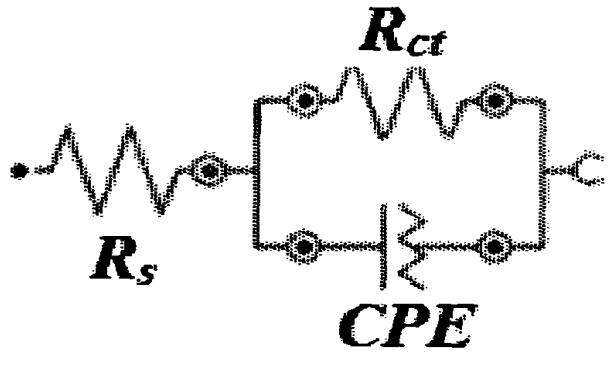

Figure 3.11: Equivalent circuit used to represent the mild steel/HCl system.

Table 3.3 shows electrochemical impedance parameters, such as R_s, R_{ct} and double layer capacitance (C_{dl}) for mild steel in HCl solutions of different concentrations without and with different concentrations of cinnamon leaf extract. The double layer between the charged metal surface and the solution is considered as an electrical capacitor. Hence, C_{dl} was calculated using Equation (3.3) [99].

$$C_{dl} = \frac{1}{2\pi R_{ct} f_{max}} \tag{3.3}$$

where f_{max} is the frequency at which imaginary component of the impedance ($-Z''$) is maximum and R_{ct} is the charge transfer resistance.

According to Table 3.3, R_{ct} of mild steel specimens in HCl solutions of 0.1, 0.5, 1.0, 1.5 and 2.0 mol dm^{-3} in the presence of 0.6 g dm^{-3} cinnamon leaf extract increases by a factor of about 13, 14, 9, 3 and 3, respectively, demonstrating that the corrosion rate of mild steel in HCl solutions of different concentrations decreases in the presence of extract and confirming the excellent corrosion inhibition effect of the cinnamon leaf extract. Decrease in the double layer capacitance in the presence of extracts also demonstrates the corrosion inhibition ability of cinnamon leaf extracts. Percentage inhibition efficiency (%IE) of acidic extracts of cinnamon leaves was calculated using Equation (3.4) and reported in Table 3.3.

$$\%\ \mathrm{IE} = \frac{R_{in} - R_{un}}{R_{in}} \times 100 \tag{3.4}$$

where R_{un} and R_{in} are the charge transfer resistances of mild steel in HCl in the absence and presence of extract, respectively [100].

Table 3.3: Electrochemical impedance parameters of mild steel specimens in HCl solutions of different concentrations in the presence and absence of cinnamon leaf extracts.

Concentration of HCl (mol dm^{-3})	Concentration of extract (g dm^{-3})	R_s (Ω)	R_{ct} (Ω)	C_{dl} (F cm^{-2}) × 10^5	% IE
0.1	0	20.5	205	10.4	
	0.1	18.0	1680	3.9	88
	0.3	18.5	2300	3.8	91
	0.6	17.3	2750	4.2	92
0.5	0	9.9	119	13.5	
	0.1	4.6	454	11.0	74
	0.2	5.2	571	11.5	79
	0.3	4.4	841	7.8	86
	0.4	4.5	1100	7.9	89
	0.5	6.7	1480	7.8	92
	0.6	5.6	1730	6.7	93
1.0	0	3.0	109	14.8	
	0.1	3.0	273	13.5	60
	0.2	2.8	323	13.9	66
	0.3	2.9	483	11.6	77
	0.4	3.0	563	14.1	81
	0.5	2.9	800	9.4	86
	0.6	3.1	946	8.7	88
1.5	0	2.6	95	16.9	
	0.1	2.6	119	13.5	20
	0.2	3.4	154	13.9	38
	0.3	2.7	184	11.6	48
	0.4	4.0	200	14.1	52
	0.5	3.0	228	9.4	58
	0.6	3.3	246	8.8	61
2.0	0	2.5	66	18.3	
	0.1	2.2	92	13.2	28
	0.2	2.3	99	12.3	33
	0.3	2.0	111	10.9	40
	0.4	2.2	126	9.6	47
	0.5	2.2	148	10.9	55
	0.6	2.0	218	7.4	70

Figures 3.12 to 3.16 show potentiodynamic polarization curves (Tafel plots) of mild steel specimens in HCl solutions of different concentrations ranging from 0.1 mol dm^{-3} to 2.0 mol dm^{-3} in the absence and presence of acidic extracts of cinnamon leaves of different concentrations after 2 h immersion. According to potentiodynamic polarization studies, the presence of cinnamon leaf extract reduces both anodic and cathodic current densities. Therefore, the extract acts as a mixed type inhibitor, and it is suggested that this is due to the adsroption of the extract on the mild steel surface. This results supports the results obtained from EIS analysis as the addition of extract decreases the double layer capacitance. This may be due to the decrease in the dielectric constant and increase in the thickness of the electrical double layer due to the adsorption of inhibitor molecules on the surface [72]. Although the extract inhibits both oxidation and reduction reactions, inhibition of the cathodic reaction is more prominent as the corrosion potential shifts slightly toward negative direction in all acidic concentrations except in 0.1 mol dm^{-3} HCl solution. Also, the reduction in cathodic current density is higher than that of the anodic current density in the presence of extracts, further supporting that cathodic inhibition is prominent. However, shift in the corrosion potential to more possitive direction in the presence of cinnamon leaf extracts in 0.1 mol dm^{-3} HCl indicates that the retardation of the anodic reaction is more prominent at this concentration. Further, the extract decreases the cathodic curent density without any significant change in the cathodic Tafel slope, indicating that the components in the extract block the active sites without changing the mechanism.

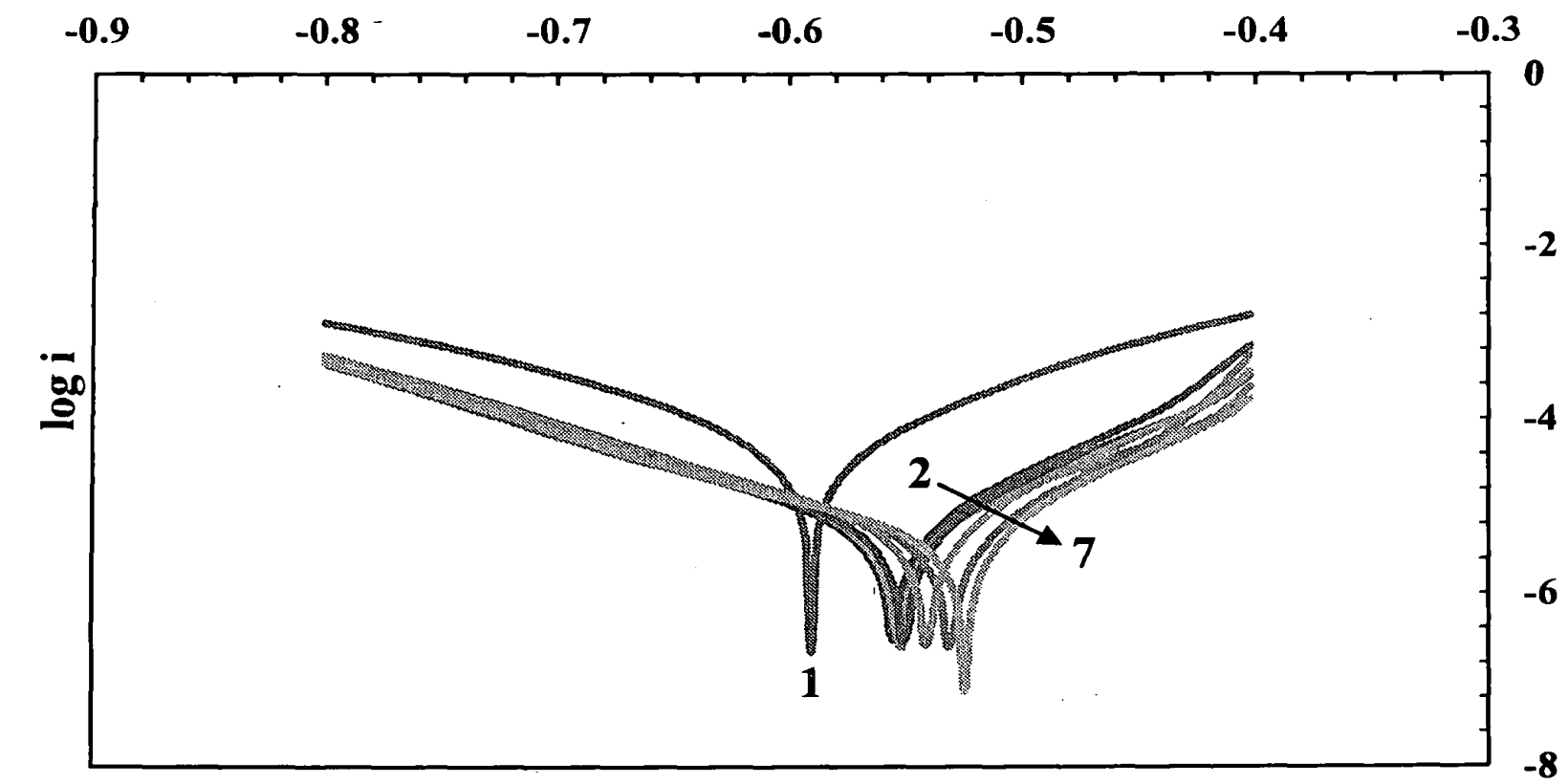

Figure 3.12: Potentiodynamic polarization curves of mild steel specimens in 0.1 mol dm^{-3} HCl with acidic extracts of cinnamon leaves of different compositions (1) 0, (2) 0.1, (3) 0.2, (4) 0.3, (5) 0.4, (6) 0.5 and (7) 0.6 g dm^{-3}.

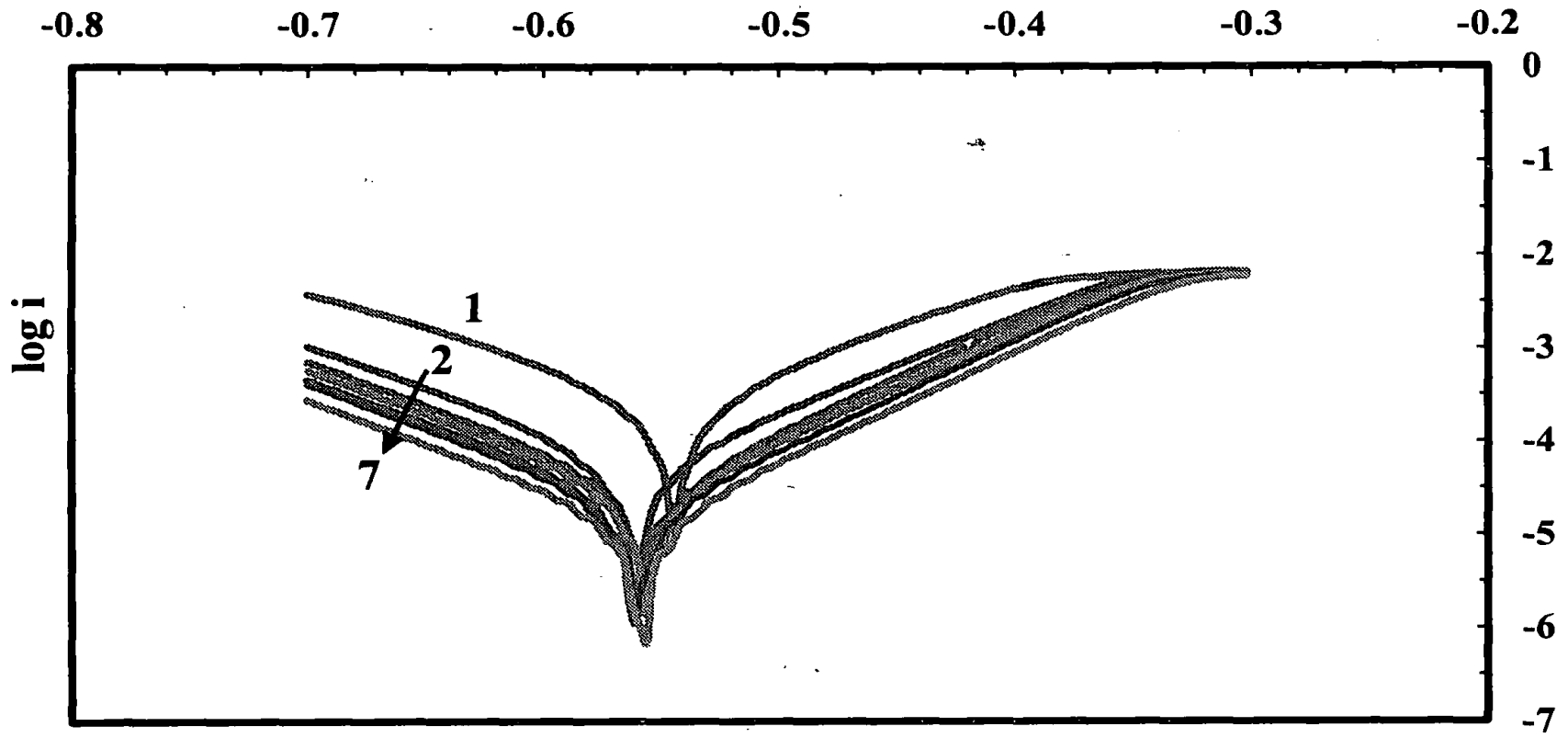

Figure 3.13: Potentiodynamic polarization curves of mild steel specimens in 0.5 mol dm^{-3} HCl with acidic extracts of cinnamon leaves of different compositions (1) 0, (2) 0.1, (3) 0.2, (4) 0.3, (5) 0.4, (6) 0.5 and (7) 0.6 g dm^{-3}.

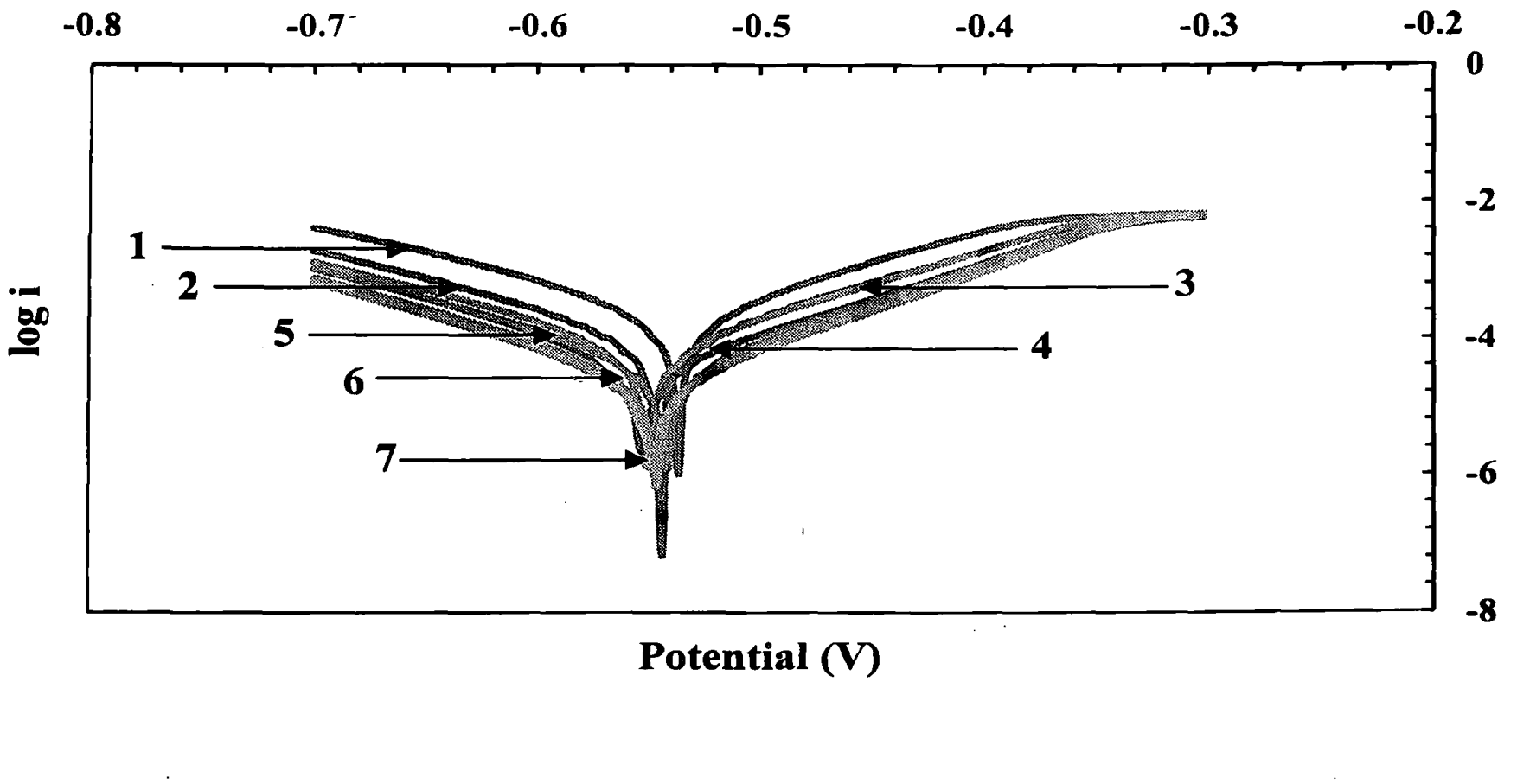

Figure 3.14: Potentiodynamic polarization curves of mild steel specimens in 1.0 mol dm^{-3} HCl with acidic extracts of cinnamon leaves of different compositions (1) 0, (2) 0.1, (3) 0.2, (4) 0.3, (5) 0.4, (6) 0.5 and (7) 0.6 g dm^{-3}

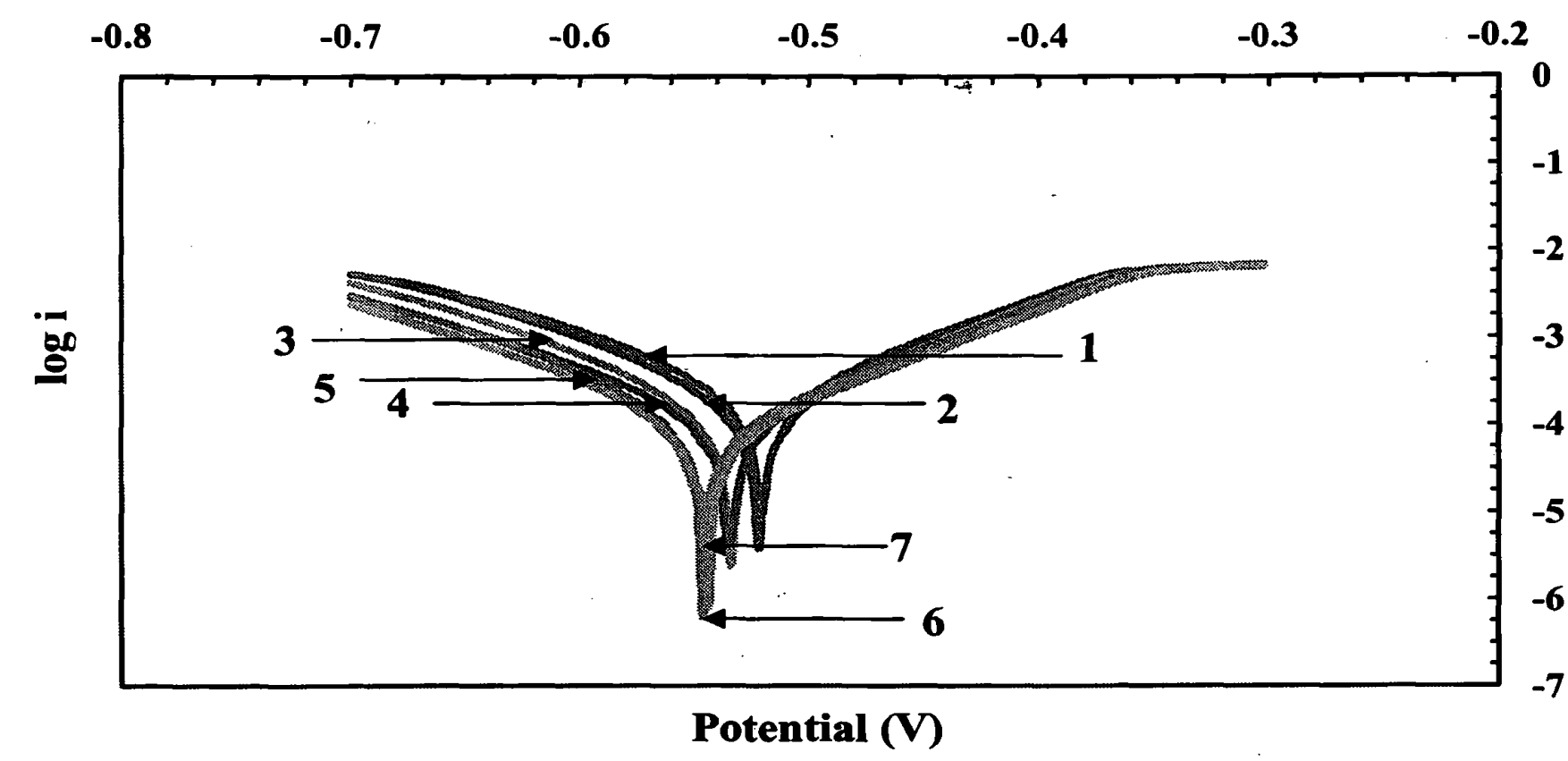

Figure 3.15: Potentiodynamic polarization curves of mild steel specimens in 1.5 mol dm^{-3} HCl with acidic extracts of cinnamon leaves of different compositions (1) 0, (2) 0.1, (3) 0.2, (4) 0.3, (5) 0.4, (6) 0.5 and (7) 0.6 g dm^{-3}.

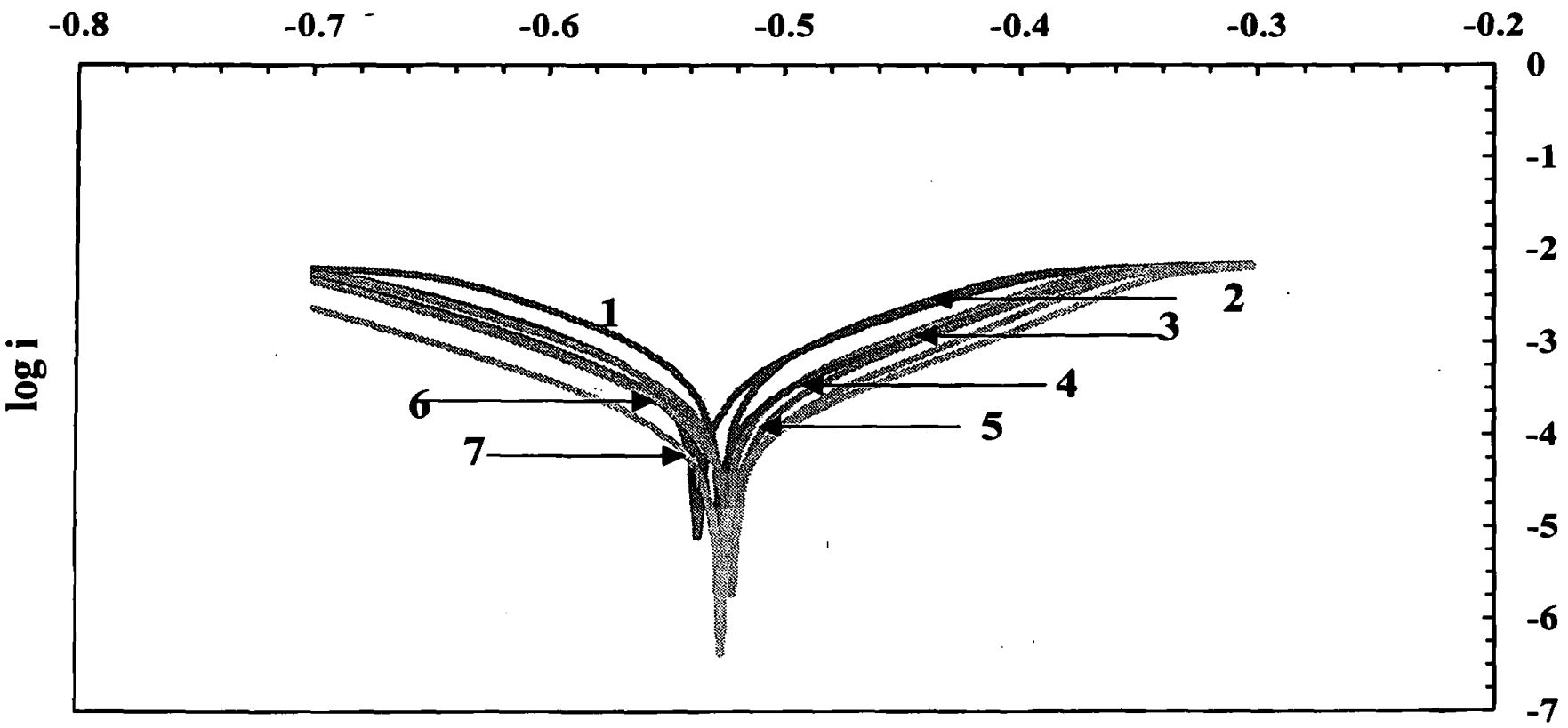

Figure 3.16: Potentiodynamic polarization curves of mild steel specimens in 2.0 mol dm^{-3} HCl with acidic extracts of cinnamon leaves of different compositions (1) 0, (2) 0.1, (3) 0.2, (4) 0.3, (5) 0.4, (6) 0.5 and (7) 0.6 g dm^{-3}.

Table 3.4 shows the potentiodynamic polarization parameters, such as anodic and cathodic Tafel slopes (b_a and b_c, respectively), corrosion current densities (i_{corr}) and corrosion potential (E_{corr}) values of mild steel specimens under different conditions. Corrosion current density and Tafel slopes of cathodic and anodic branches were deermined by extrapolating the linear portions of respective branches of corresponding polarization curves to the zero over voltage with the help of the NOVA software. Percentage inhibition efficiency was calculated using Equation (3.5) and reported in Table 3.4.

$$\% \text{ IE} = \frac{i'_{corr} - i_{corr}}{i'_{corr}} \times 100 \qquad (3.5)$$

where i'_{corr} and i_{corr} are the corrosion current densities of mild steel in HCl without and with cinnamon leaf extract, respectively [44-45].

Table 3.4: Potentiodynamic polarization parameters of mild steel specimens in HCl solutions of different concentrations in the presence and absence of cinnamon leaf extarcts.

Concentration of HCl (mol dm^{-3})	Concentration of inhibitor (g dm^{-3})	Potentiodynamic polarization parameters				
		b_a (mV dec^{-1})	b_c (mV dec^{-1})	- E_{corr} (mV)	I_{corr} (µA cm^{-2})	% IE
0.1	0	69.1	74.4	589	106.0	
	0.1	66.0	82.4	556	16.7	84.2
	0.2	77.1	77.4	554	16.6	84.3
	0.3	66.0	77.8	552	16.1	84.8
	0.4	65.1	79.1	543	15.4	85.5
	0.5	64.2	83.8	532	14.3	86.5
	0.6	68.1	81.3	531	13.8	87.0
0.5	0	75.6	80.9	545	535.8	
	0.1	71.0	76.9	550	148.6	72.3
	0.2	67.9	74.6	556	92.4	82.8
	0.3	73.0	73.5	558	77.9	85.5
	0.4	72.2	74.7	562	71.9	86.6
	0.5	80.3	70.2	564	61.1	88.6
	0.6	76.9	77.4	561	45.8	91.5
1.0	0	81.4	91.3	535	701.1	
	0.1	82.7	80.6	545	289.0	58.8
	0.2	81.9	78.4	552	222.0	68.3
	0.3	77.7	74.7	551	131.5	81.2
	0.4	74.0	74.7	543	119.4	83.0
	0.5	72.7	72.1	548	84.8	87.9
	0.6	76.2	75.1	549	73.9	89.5
1.5	0	81.3	84.0	519	715.7	
	0.1	75.4	74.8	521	515.0	28.0
	0.2	81.1	80.0	531	440.4	38.5
	0.3	75.0	79.0	534	350.4	51.0
	0.4	84.0	69.0	545	321.8	55.0
	0.5	86.3	74.8	547	311.3	56.5
	0.6	82.2	71.0	544	264.1	63.1
2.0	0	76.2	72.5	527	1456.0	
	0.1	80.2	75.0	538	1119.0	23.1
	0.2	77.9	74.0	525	750.9	48.4
	0.3	82.9	77.3	530	651.7	55.2
	0.4	73.0	79.5	521	548.6	62.3
	0.5	73.3	71.6	520	388.0	73.4
	0.6	76.4	80.8	526	274.8	81.1

3.1.4 Adsorption consideration

The inhibition effect may be due to the adsorption of some constituents of the extract on the mild steel surface. In order to study this behavior, mass losses of mild steel specimens were monitored in 0.5 mol dm^{-3} HCl in the absence and presence of acidic extracts of cinnamon leaves of different concentrations. As the corrosion rate is high at highly acidic concentrations, 0.5 mol dm^{-3} HCl was selected for this study. Figure 3.17 shows the change in the mass of mild steel specimens placed in 0.5 mol dm^{-3} HCl solution and acidic extracts of cinnamon leaves of different concentrations prepared in 0.5 mol dm^{-3} HCl with time at ambient temperature. The figure clearly illustrates the higher corrosion susceptibility of mild steel in the blank solution which attains the steady state after 48 h of immersion. Further, the rate of dissolution of metal decreases with increasing concentration of cinnamon leaf extracts which gradually increases with increase in exposure time. Percentage inhibition efficiencies were calculated based on mass loss measurements using Equation (3.6),

$$\% \text{ IE} = \frac{W_{un} - W_{in}}{W_{un}} \times 100 \qquad (3.6)$$

where W_{un} and W_{in} are the mass loss of mild steel specimens in uninhibited and inhibited solutions, respectively [45]. The inhibition efficiency of 93% is observed after immersion for 2 h, which increases up to 96% after 24 h at higher concentration (60.0 g dm^{-3}) of the cinnamon leaf extract at ambient temperature.

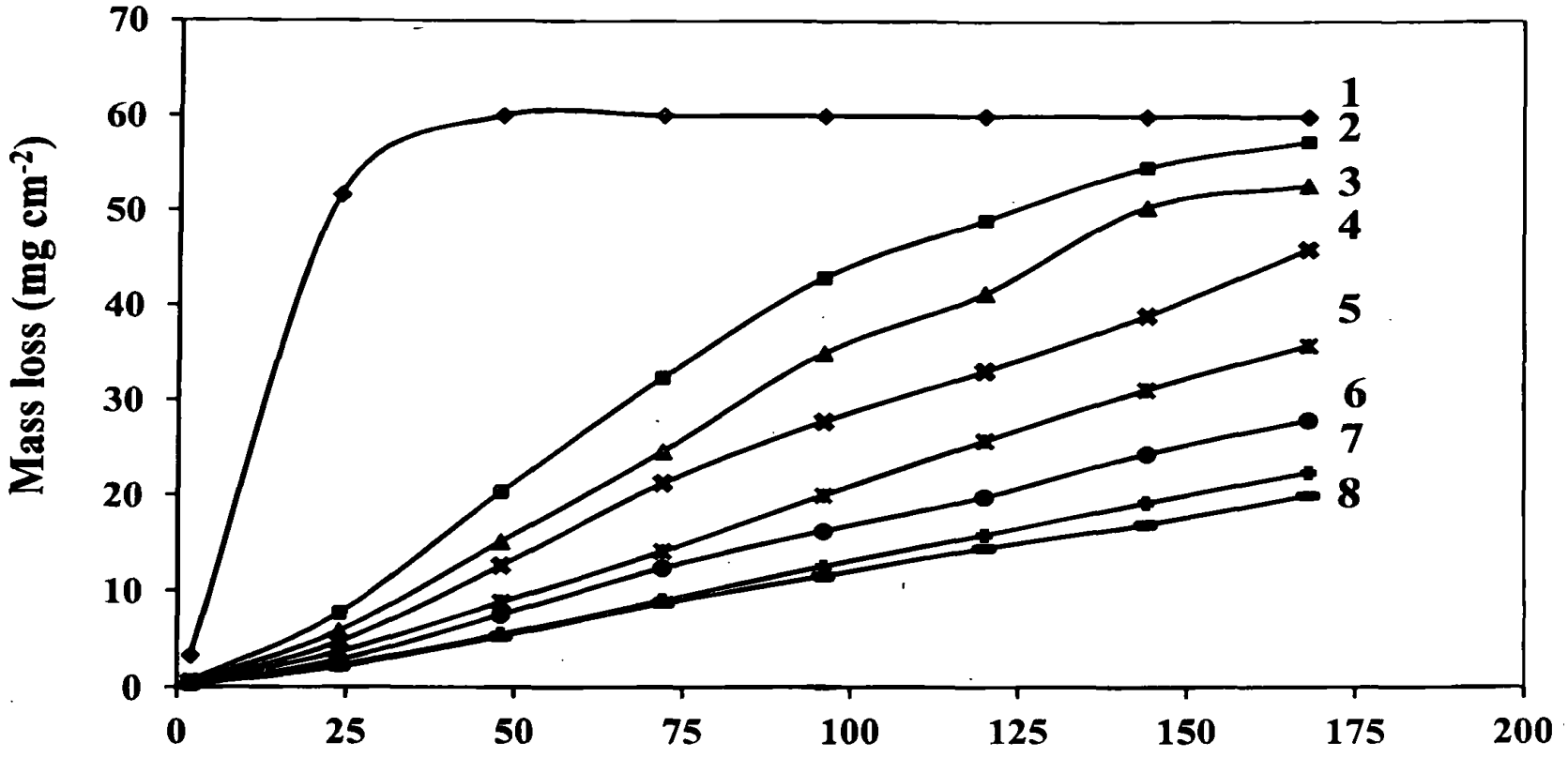

Figure 3.17: Mass loss of mild steel specimens in 0.5 mol dm^{-3} HCl with acidic extracts of cinnamon leaves of different compositions (1) 0, (2) 3.0, (3) 6.0, (4) 12.0, (5) 24.0, (6) 36.0, (7) 48.0 and (8) 60.0 g dm^{-3}.

Adsorption isotherm models are widely used in order to explain the nature of adsorption of inhibitor molecules on the metal surface and hence the mechanism of corrosion inhibition. Table 3.5 summarizes some adsorption isotherms used in corrosion studies.

Table 3.5: Adsorption isotherm models proposed for inhibition mechanism of some inhibitors for different metals in different corrosive media.

Metal	Medium	Inhibitor	Type of isotherm	Ref. No
Low-carbon steel	H_2SO_4 pH = 1, 2	Mimosa tanin	Temkin Frumkin	101
	pH = 3	Mimosa tanin	Freundlich	
Iron	HCl	Piperidine	Temkin	102
Aluminium	HCl	Substituted N-aryl pyrrole	Langmuir	103

To obtain basic information about the interaction between the inhibitor and mild steel surfaces, data obtained from mass loss measurements of mild steel specimens carried out in 0.5 mol dm^{-3} HCl in the absence and presence of the extracts of different concentrations at the ambient temperature and at 50 °C were used. Surface coverage was calculated using Equation 3.7 [104],

$$\theta = \frac{W_{un} - W_{in}}{W_{un}} \tag{3.7}$$

where W_{un} and W_{in} are the mass loss of mild steel specimens in uninhibited and inhibited solutions, respectively. Table 3.6 shows the surface coverage of cinnamon leaf extract on mild steel surface at the ambient temperature and 50 °C after 2 h and 24 h immersion. At 50 °C, higher surface coverage was observed as the corrosion rate of mild steel is much higher in HCl solutions and the adsorbed inhibitor on mild steel slows down the corrosion rate. However, after 24 h immersion, surface coverage is decreased, probably due to desorption of the inhibitor from mild steel surface.

Table 3.6: Surface coverage of cinnamon leaf extracts on mild steel surface at different temperatures.

Concentration of inhibitor (g dm^{-3})	Surface coverage at ambient temperature		Surface coverage at 50 °C	
	2 h	24 h	2 h	24 h
3.0	0.80	0.85	0.86	0.27
6.0	0.83	0.89	0.86	0.34
12.0	0.84	0.91	0.88	0.50
24.0	0.84	0.93	0.91	0.63
36.0	0.86	0.95	0.92	0.70
48.0	0.88	0.96	0.95	0.74
60.0	0.93	0.96	0.95	0.76

The variation of the ratio between the concentration and the surface coverage with the concentration of the extract is shown in Figure 3.18 at ambient temperature and at 50 °C. The best fit is obtained for the Langmuir adsorption isotherm, which is given by the Equation 3.8 [105],

$$\theta = \frac{K\,C_{inh}}{(1+KC_{inh})} \tag{3.8}$$

where C_{inh} represents the concentration of extract, θ is the degree of surface coverage and K is the equilibrium constant of adsorption which is related to free energy of adsorption by the Equation (3.10).

Equation (3.8) can be rearranged to the following format:

$$\frac{C_{inh}}{\theta} = \frac{1}{K} + C_{inh} \tag{3.9}$$

The validity of the Langmuir isotherm supports the monolayer adsorption. The free energy values associated with the adsorption of the extract were calculated using Equation 3.10 [105],

$$K = \frac{1}{C'} e^{\left(-\Delta G_{ads}/RT\right)} \tag{3.10}$$

where c' is the molar concentration of water (55.5), R is the universal gas constant and T is the absolute temperature. The free energy values, calculated assuming that room temperature is 25 °C, are reported in Table 3.7. The negative value of ΔG_{ads} indicates that the adsorption of extracts on the mild steel surface is a spontaneous process.

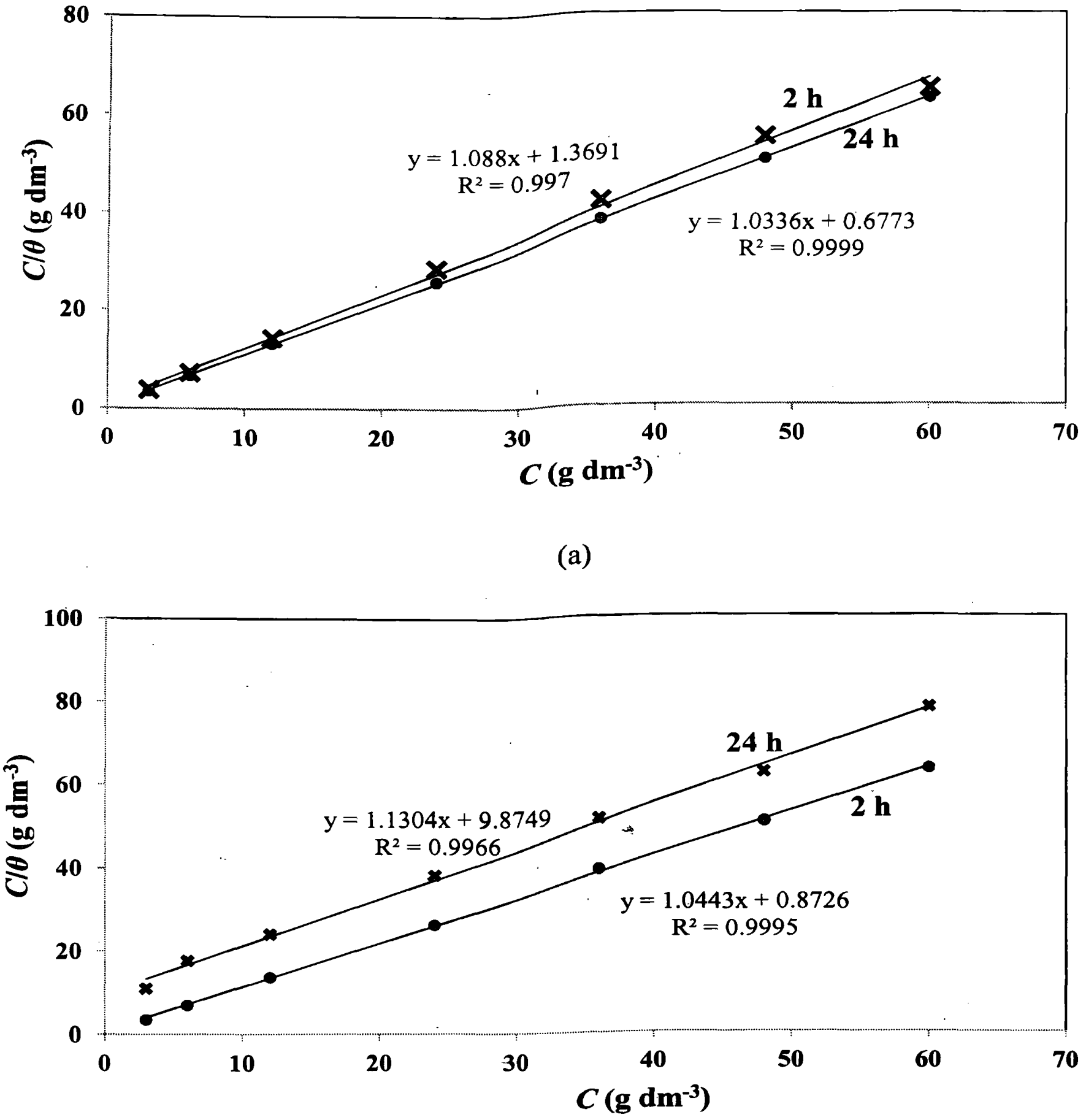

(a)

(b)

Figure 3.18: Langmuir adsorption isotherm for acidic extracts on mild steel specimen in 0.5 mol dm^{-3} HCl at (a) ambient temperature and (b) 50 °C for different immersion times (indicated in the figure).

Equations of linear regression lines and the corresponding regression coefficients are given with each line.

Table 3.7: Gibbs free energy of adsorption of components in the cinnamon leaf extract obtained from mass loss measurements.

Immersion time (h)	Adsorption free energy (kJ mol^{-1})	
	25 °C	50 °C
2	-9.17	-11.15
24	-10.92	-4.70

3.1.5 Enhancement of inhibition effect of cinnamon leaf extracts using KI

Iodide ions have been widely reported to synergistically increase the inhibition effect of organic inhibitors on corrosion of metals in acidic medium [106]. As the corrosion inhibition depends on the concentration of the extract, 3.0 g dm^{-3} and 0.1 g dm^{-3}extracts prepared in 0.5 mol dm^{-3} HCl were selected to study the synergistic effect of I^-.

Electrochemical experiments were conducted in 0.1 g dm^{-3} cinnamon leaf extract prepared in 0.5 mol dm^{-3} HCl with 0.5 and 2.5 mmol dm^{-3} KI. Increase in the charge transfer resistance with the addition of KI to the extract implies the enhanced corrosion inhibition effect of the extract. Figure 3.19 compares the Nyquist plots recorded in the presence and absence of KI. Increase in the charge transfer resistance in the presence of KI is similar to the increase observed in the presence of the extract. This suggests that the addition of KI does not change the corrosion mechanism and hence the same equivalent circuit can be used to determine the electrochemical parameters. Further, the addition of KI to the blank solution does not change the impedance of mild steel.

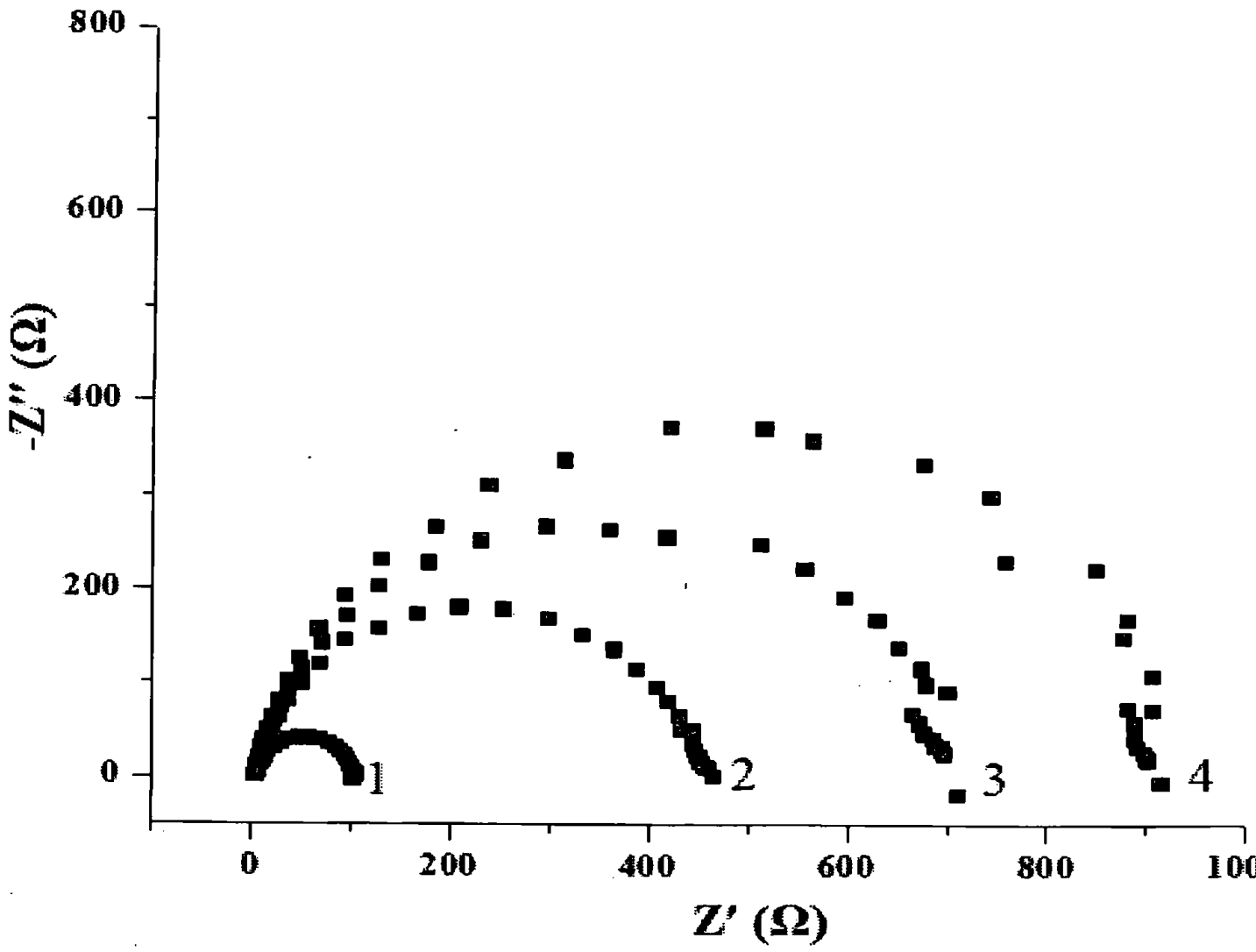

Figure 3.19: Nyquist plots of mild steel specimens in 0.5 mol dm^{-3} HCl (1) and 0.1 g dm^{-3} extracts prepared in 0.5 mol dm^{-3} HCl with KI of different concentrations of (2) 0, (3) 0.5 and (4) 2.5 mmol dm^{-3}.

Mass loss measurements conducted with the addition of iodide ions to the acidic extract of cinnamon leaves indicate higher corrosion inhibition than the corrosion inhibition obtained for the extract only. This was demonstrated by calculating the percentage inhibition efficiencies for the 3.0 g dm^{-3} extract in the presence and absence of different concentrations of KI, using Equation (3.6), and are shown in Table 3.8.

Enhancement of corrosion inhibition in the presence of iodide ions is not significant within short time durations, as shown in the table. However, allowing the specimens in the medium containing iodide ions for long time periods improves the corrosion inhibition effect. For example, the increase in corrosion inhibition efficiency of 3.0 g dm^{-3} extract in the presence of 2.5 mmol dm^{-3} iodide ion are 3.5%, 8.6% and 13.2% for 2 h, 24 h and 48 h immersion time, respectively.

Table 3.8: Percentage inhibition efficiency of 3.0 g dm^{-3} of acidic extract of cinnamon leaves prepared in 0.5 mol dm^{-3} with different concentrations of iodide ions.

Concentration of iodide (mmol dm^{-3})	% Inhibition efficiency		
	2 h	24 h	48 h
0	74.6	81.7	66.3
0.5	74.6	86.6	73.6
1.0	74.8	87.5	75.8
2.5	78.1	90.3	79.5

Similar mass losses obtained for mild steel specimens placed in 0.5 mol dm^{-3} with and without KI indicate that the presence of iodide ions alone does not have any inhibitive effect on corrosion of mild steel in HCl, and consequently iodide ions show only a synergistic effect. From the inhibition efficiencies, the synergism parameter (S_I) can be calculated using Equation 3.11,

$$S_I = \frac{1-I_{1+2}}{1-I'_{1+2}} \tag{3.11}$$

where $I_{1+2} = I_1 + I_2$; I_1 is the inhibition efficiency of KI; I_2 the inhibition efficiency of extract and I'_{1+2} is the inhibition efficiency of the extract in the presence of KI [107-108]. As the rate of corrosion of mild steel in 0.5 mol dm^{-3} HCl in the presence and absence of KI is the same, $I_{1+2} = I_2$. However, the inhibition efficiency of the extract is increased in the presence of KI for all tested iodide ion concentrations leading to $I'_{1+2} > I_{1+2}$ and hence, values of S_I greater than 1 indicate the synergetic effect of iodide ions.

The synergistic effect is further confirmed by potentiodynamic polarization studies. Decrease in the corrosion current density with the addition of KI to the extract implies the enhanced corrosion inhibition effect of the extract. Figure 3.20 compares the potentiodynamic polarization curves of mild steel specimen in the presence and absence of KI.

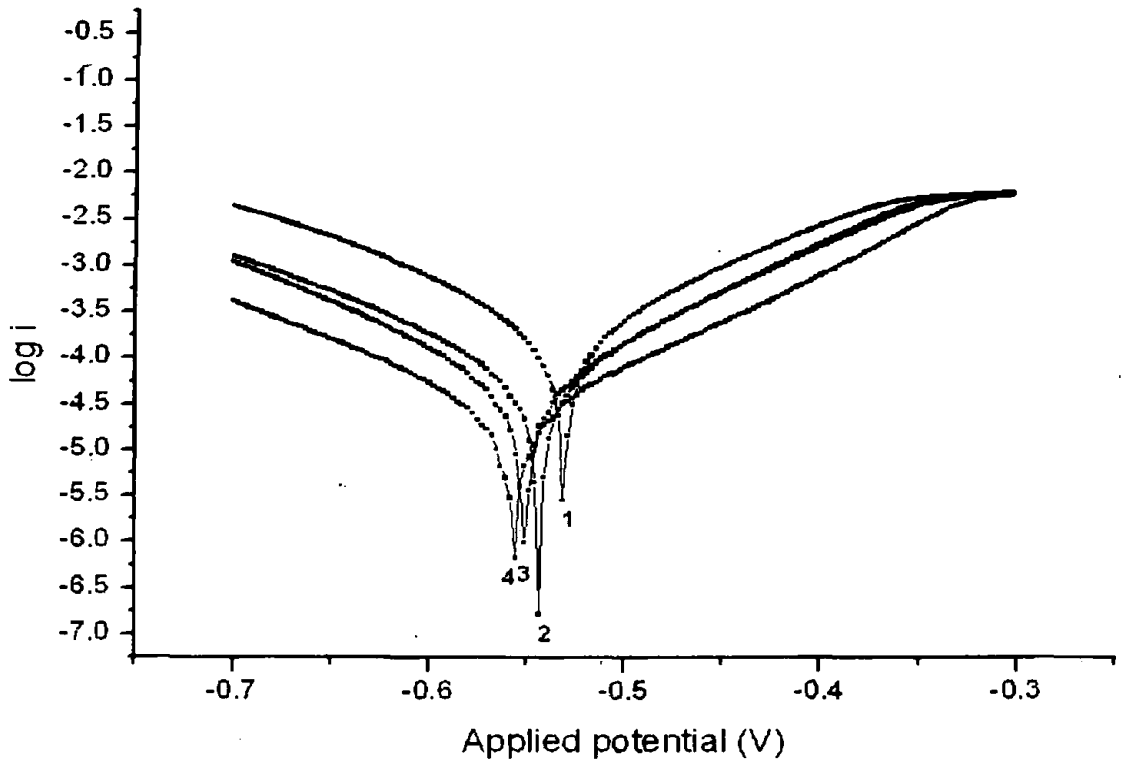

Figure 3.20: Potentiodynamic polarization curves of mild steel specimens in (1) 0.5 mol dm^{-3} HCl and 0.1 g dm^{-3} extract prepared in 0.5 mol dm^{-3} HCl with KI of different concentrations of (2) 0, (3) 0.5 and (4) 2.5 mmol dm^{-3}.

Two mechanisms have been reported for the synergistic effect of iodide ions with different corrosion inhibitors [109]. According to the reports published, iodide ions, either form an ion pair with an inhibitor cation and adsorbs on the metal surface, or they are adsorbed on the metal surface initially to recharge the electrical double layer. The inhibitor is then drawn into the double layer by the adsorbed anions to form an ion-pair on the metal surface. Both mechanisms are illustrated below.

$$I^-_{sol} + In^+_{sol} \longrightarrow (I^- - In^+)sol \quad (3.12)$$

$$(I^- - In^+)sol \longrightarrow (I^- - In^+)ads \quad (3.13)$$

OR

$$^-_{sol} \longrightarrow I^-_{ads} \quad (3.14)$$

$$^-_{ads} + In^+_{sol} \longrightarrow (I^- - In^+)ads \quad (3.15)$$

Similar mechanism may be considered to explain the synergistic effect of iodide in the presence of cinnamon leaf extracts. As chloride ion in the HCl is adsorbed on the metal surface and facilitates the physical adsorption of inhibitor cations [110], iodide ions facilitates the adsorption of inhibitor cations. It suggests that adsorption of $(I^- - In^+)$ is more than $(Cl^- - In^+)$.

3.1.6 Morphological study

The surface morphology of mild steel specimens was examined before and after immersion of mild steel specimens in HCl solution with and without the extracts prepared in 0.5 mol dm^{-3} HCl under polarizing microscope (×100). Surface of mild steel specimen placed in HCl in the absence of the extract is affected drastically after 2 h immersion. Surface morphology of mild steel specimen placed in cinnamon leaf extracts does not show any significant change even after 24 h of immersion (Figure 3.21).

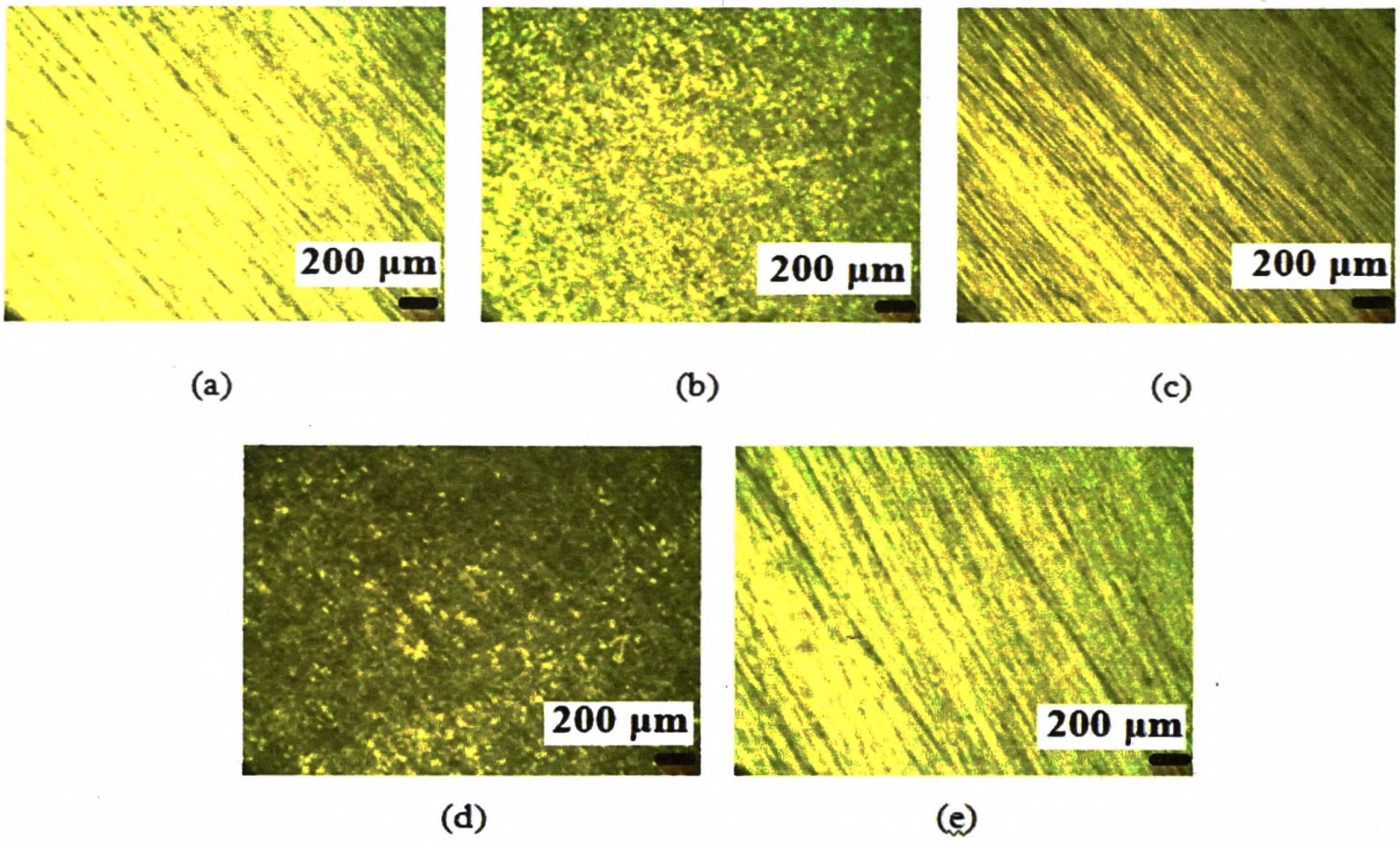

Figure 3.21: Surface morphology of mild steel specimens under polarizaing microscope (×100) (a) before immersion, (b) after 2 h immersion in 0.5 mol dm^{-3} HCl, (c) after 2 h immersion in 3.0 g dm^{-3} extract prepared in 0.5 mol dm^{-3} HCl, (d) after 24 h immersion in 0.5 mol dm^{-3} HCl and (e) after 24 h immersion in 3.0 g dm^{-3} extract prepared in 0.5 mol dm^{-3} HCl.

3.1.7 Effect of acidic extract of cinnamon leaves on removal of rust from mild steel

The purpose of adding corrosion inhibitors to pickling baths is to prevent over-pickling of mild steel. Therefore, the inhibitor added should not affect the removal of rust from the metal surface and prevent its over pickling. According to Table 3.9, almost all the rust is removed within 15 min of immersion in the presence and absence of the extracts in 0.5 mol dm^{-3} HCl indicating that the acidic extract does not decrease the extent of rust removal. However, continuous monitoring of the mass loss of mild steel specimens indicates that the mild steel surface undergoes further dissolution in the absence of the

extract and the dissolution rate becomes very low in the presence of the extract, indicating that cinnamon leaves extract acts as a good inhibitor.

It has been proven that the removal of rust from steel surface is achieved by reductive dissolution [111-112] as given in Equations 3.16 and 3.17, rather than by chemical dissolution. As chemical dissolution is slow in mineral acids, reductive dissolution is assisted by underlying metal surface by normal acid as shown in Equations 3.16 and 3.17. In this process, the reduction of the ferric components of the scale is coupled with the oxidation of the base metal, yielding ferrous species readily soluble in the acid. These processes are shown for magnetite in Equations (3.16) and (3.17).

$$Fe_3O_4(s) + 8H^+(aq) + 2e^- \rightleftharpoons 3Fe^{2+}(aq) + 4H_2O(l) \quad \text{cathodic reaction} \qquad (3.16)$$

$$Fe(s) \rightleftharpoons Fe^{2+}(aq) + 2e^- \quad \text{anodic reaction} \qquad (3.17)$$

It was observed that the rate of removal of rust from mild steel surfaces by HCl itself is faster than that of the hydrochloric acid solution of the same concentrations with cinnamon leaf extracts as the inhibitor protects the base metal from corrosion. Therefore, the removal of rust probably occurs due to the dissolution of the oxide layer in the presence of the extract.

Table 3.9: Mass loss of mild steel specimens as-received in 0.5 mol dm^{-3} HCl with and without acidic extract of cinnamon leaves.

Test medium	Trial	Mass loss (mg cm^{-2})						
		15 min	3 h	24 h	48 h	72 h	96 h	120 h
0.5 mol dm^{-3} HCl	1	5.6	6.1	11.7	24.9	35.5	43.2	51.0
	2	5.5	6.0	12.0	23.2	36.3	45.5	51.4
	3	5.8	6.1	11.3	22.0	34.2	42.3	50.6
3.0 g dm^{-3} extract prepared in 0.5 mol dm^{-3} HCl	1	5.8	6.0	7.4	9.2	11.8	13.2	15.6
	2	5.8	5.9	7.1	9.0	11.6	13.4	16.7
	3	5.6	5.9	7.2	9.4	12.1	13.9	17.3

3.2 Corrosion of Copper in HCl Solutions and Its Prevention

3.2.1 Effect of acid concentration on corrosion of copper in HCl

3.2.1.1 Mass loss measurements, pH measurements and solution analysis

In order to study the corrosion behavior of copper in HCl solutions of different concentrations, corrosion rates of copper specimens based on mass loss measurements were calculated using Equation 3.1. Corrosion rates calculated based on mass loss of copper specimens in HCl solutions after 6, 12, 18 and 24 days of immersion are reported in Table 3.10. According to mass loss measurements, corrosion rate of copper is low during the first 6 days in all tested acid concentrations, indicating that copper does not undergo quick corrosion. Then, the dissolution rate of copper increases rapidly as the exposure time increases, and as expected, copper specimens placed in high acidic environments show fast dissolution. This is probably due to the increase in the rate of the reduction of O_2 [$O_2(g) + 4H^+(aq) + 4e^- \rightleftharpoons 2H_2O(l)$] in an open environment at lower pH, which is the cathodic reaction associated with the corrosion (oxidation) of copper. However, corrosion rate of copper specimens dipped in 0.05, 0.1 and 0.2 mol dm^{-3} HCl solutions does not vary significantly with time over a period of 24 days.

Table 3.10: Corrosion rates of copper specimens in HCl solutions of different concentrations.

Concentration of HCl (mol dm^{-3})	Corrosion rate (mpy)			
	6 days	12 days	18 days	24 days
0.05	0.64	0.66	0.60	0.54
0.1	1.00	1.05	1.05	0.94
0.2	1.36	1.53	1.43	1.39
0.5	2.50	3.28	3.58	2.96
1.0	2.57	5.92	6.72	5.96

The concentration of copper ions in the corrosive medium is also a measure of the extent of corrosion. Concentration of total copper, released from a unit area of a copper specimen, to the test solution under different experimental conditions was determined by atomic absorption spectroscopy (Table 3.11). The concentration of copper in the test solution increases with immersion time. Although copper dissolution continues in lower

HCl concentrations according mass loss measurements, concentration of copper in the corrosive medium after 18 days of immersion when compared to 12 day immersion. A light green coloured substance accumulates at the top of the corrosive medium. This product may be copper carbonate formed by reacting Cu^{2+} ions with atmospheric CO_2. This process reduces the copper concentration in corrosive medium, and further, the pH of 0.05 mol dm^{-3} HCl and 0.1 mol dm^{-3} HCl starts to increase rapidly at this point. This precipitation does not appear in high HCl concentrations probably due to its solubility in high acidic medium. Therefore, the concentration of copper in highly acidic medium is continuously increased, showing similarity to mass loss measurements.

Table 3.11: Variation of total concentration of copper in HCl solutions of different concentrations, which contains copper specimen, with time.

Concentration of HCl (mol dm^{-3})	**Concentration of copper (ppm)**			
	6 days	**12 days**	**18 days**	**24 days**
0.05	8.27	18.53	12.94	14.58
0.1	12.92	28.02	27.64	30.86
0.2	20.66	43.94	57.98	66.41
0.5	33.61	99.94	159.97	174.31
1.0	35.58	169.30	295.03	351.33

As the cathodic reaction is the reaction of H_3O^+ with dissolved O_2 to produce $H_2O(l)$, the pH of the medium would increase with time. However, the pH of the medium does not change significantly during early periods of immersion, indicating the low corrosion rate of copper. However, the pH of low acidic (0.05 mol dm^{-3}) solution starts to increase after 14 days immersion and attained steady state (at pH = 4.8) indicating the saturation of corrosion. Insignificant change in pH of corrosive media of higher acid concentration indicates that still the medium is corrosive as the H_3O^+ concentration is high (Figure 3.22).

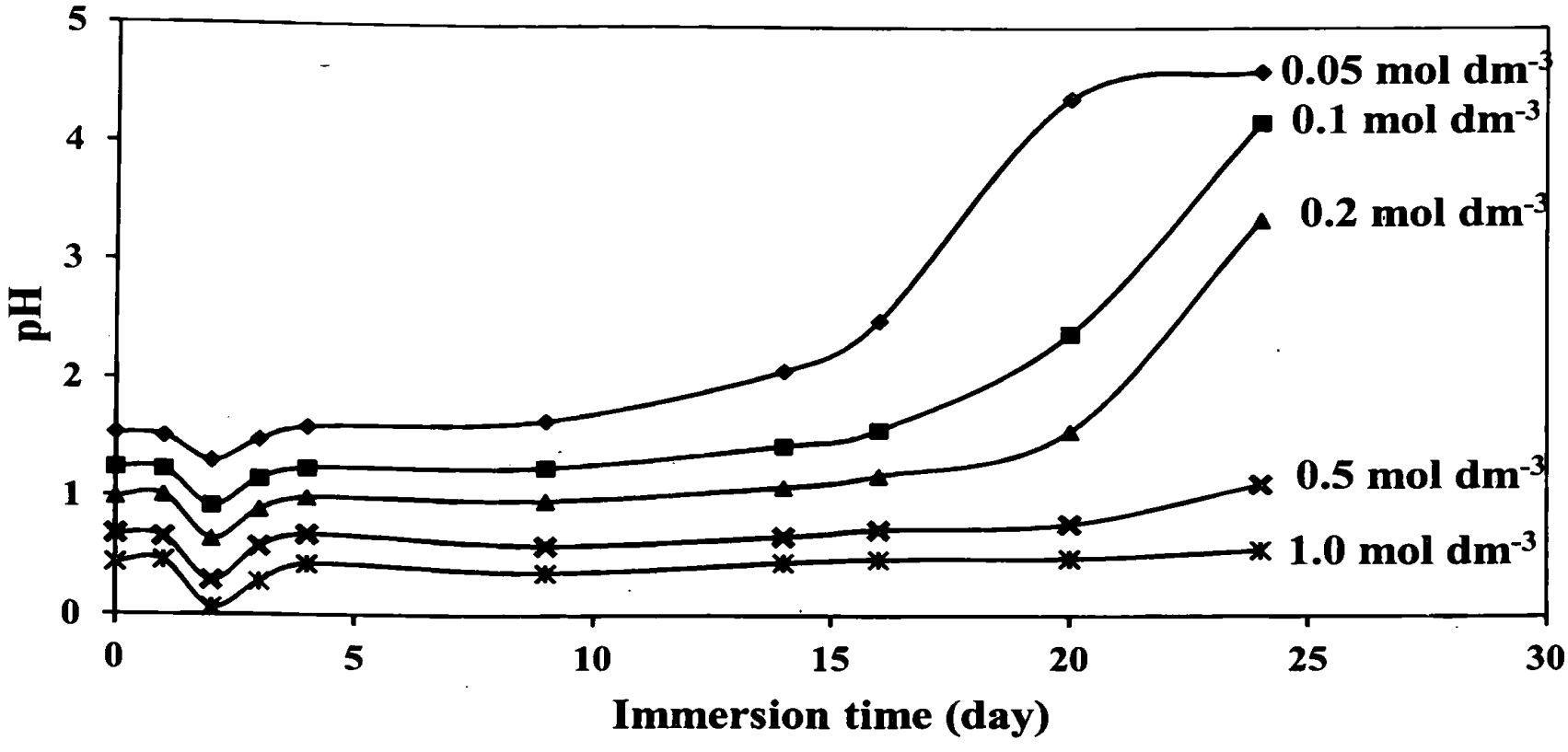

Figure 3.22: Variation of pH of HCl solutions which contains copper specimens, as a function of immersion time. Initial pH of each solution has been given in the figure.

3.2.1.2 Open circuit potential (V_{oc}) measurements

Figure 3.23 shows the variation of V_{oc} of copper specimens in HCl solutions of different concentrations. The V_{oc} measurements show exponential decay with higher rates in more concentrated HCl solutions. This is expected for metallic surfaces due to initial surface conditions followed by equilibrium. Copper surfaces in HCl solution have reached equilibrium after about 2 weeks according to V_{oc} measurements, beyond which V_{oc} values do not change because the surface composition would not change although dissolution continuously occurs.

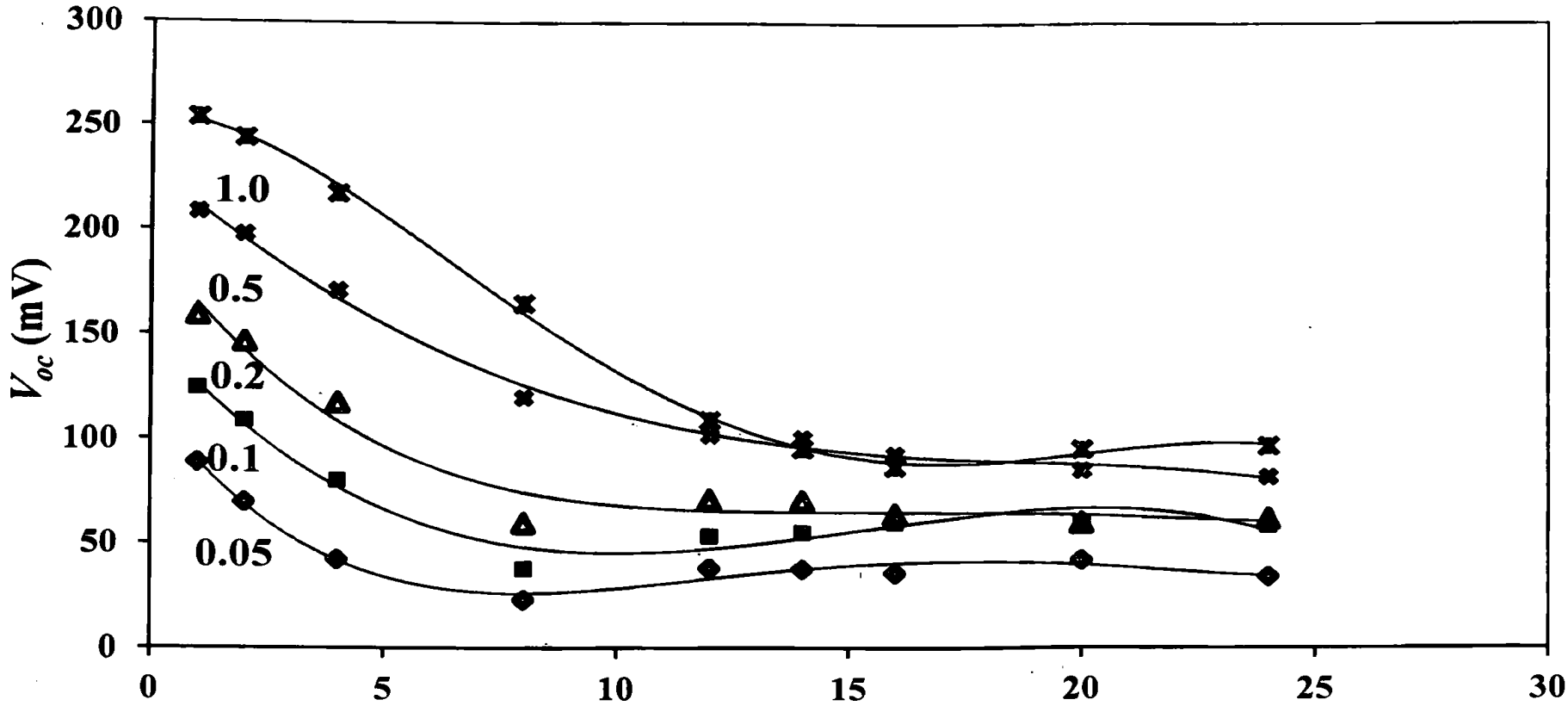

Figure 3.23: Variation of V_{oc} of copper specimens in HCl solutions of different concentrations in mol dm^{-3} with time.

3.2.2 Inhibition of copper corrosion in HCl using methanol extract of tea leaves

Although the corrosion rates calculated based on mass loss of copper in HCl solutions is comparatively low for short periods of immersion, localized corrosion attack may lead to perforation, and hence causes failure of equipments. Therefore, measures should be taken to prevent corrosion of copper in HCl. Inhibition effect of 10% (v/v) methanol extract of tea leaves in HCl solutions of different concentrations was investigated initially using mass loss measurements at ambient temperature. Corrosion rates of copper specimens in HCl solutions in the presence and absence of tea leaf extract calculated according to Equation 3.1 are reported in Table 3.12.

Table 3.12: Corrosion rate of copper specimens in HCl solutions of different concentrations with 10% (v/v) tea leaf extract.

Concentration of HCl (mol dm^{-3})	Concentration of extract (% v/v)	Average corrosion rate (mpy)				
		1 day	2 days	3 days	4 days	5 days
0.05	0	0.28	0.42	0.43	0.52	0.56
	10	0.14	0.09	0.07	0.06	0.06
0.1	0	0.35	0.44	0.62	0.78	0.89
	10	0.18	0.14	0.19	0.28	0.42
0.5	0	0.42	0.59	0.81	1.30	2.37
	10	0.36	0.44	0.54	0.80	1.36
1.0	0	0.55	0.70	0.96	1.53	2.73
	10	0.37	0.47	0.63	0.94	1.53

3.2.3 Effect of inhibitor concentration on corrosion inhibition of copper in HCl

Figures 3.24 and 3.25 compare the Nyquist plots obtained for copper specimens in 0.05 mol dm^{-3} HCl and 1.0 mol dm^{-3} HCl with and without tea leaf extracts of different concentrations after 2 h immersion. According to Figure 3.24, Nyquist plots obtained for Cu specimens in 0.05 mol dm^{-3} HCl in the presence of tea leaf extract show a small semi-circle in the higher frequency region which corresponds to the adsorbed inhibitor film on Cu surface, a large semi circle which represents the charge trasfer resistance and a diffusive contribution in the low frequency region which represents the Warburg impedance. However, Nyquist plot obtained for a Cu specimen in 0.05 mol dm^{-3} HCl does not show small semi-circle in the higher frequency region. The presence of Warburg impedance components indicate that the system is influenced by mass transfer of corrosion products from the copper surface to bulk. As observed by Nyquist plots, the charge transfer resistance of copper specimen increases with the introduction of the tea leaf extract, and further, the diameter of the small semi-circle observed in the high frequency region increases when increasing the concentration of tea leaf extract, suggesting the formation of an inhibitor film.

According to Figures 3.24 and 3.25, Nyquist plots obtained in 0.05 mol dm^{-3} HCl and 1.0 mol dm^{-3} HCl in the absence of the extract are similar, indicating that there is no effect from the acid strength within short time periods as fresh copper specimens are used in generating Nyquist plots and as the experiment requires only 2 h. In contrast to the Nyquist plots of copper specimens in 0.05 mol dm^{-3} HCl with tea leaf extract of different concentrations, effect of inhibitor-film formation is prominent in 1.0 mol dm^{-3} HCl as the diameter of the semi circle at higher frequency region increases significantly with increase in the concentration of the extract. Based on above observations, it can be concluded that inhibition mechanism of the extract at low concentration is different from that at high concentrations. Adsorption of inhibitor on copper surface may contribute to the corrosion inhibition in 1.0 mol dm^{-3} HCl.

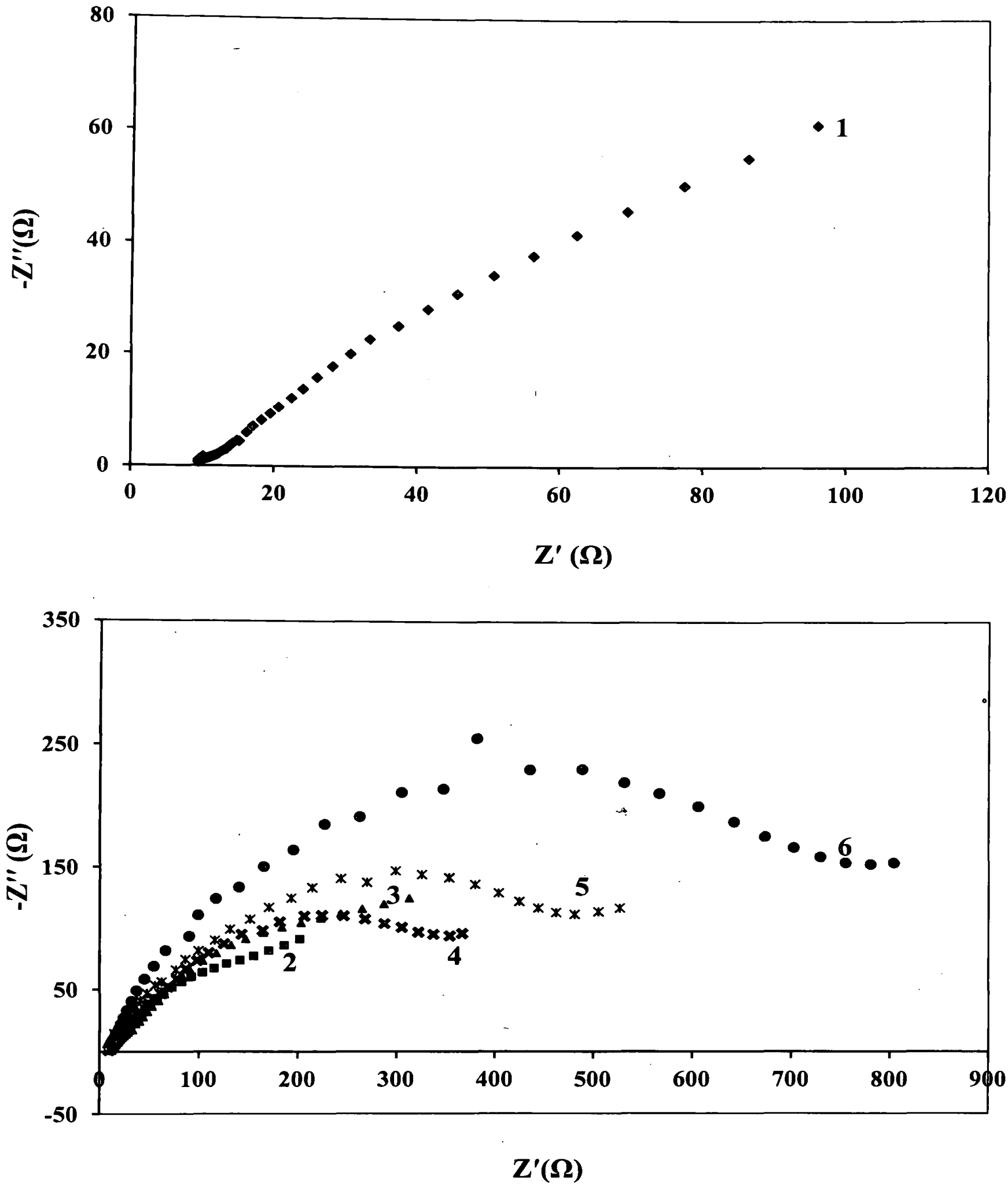

Figure 3.24: Nyquist plots of copper specimens in 0.05 mol dm^{-3} HCl with methanol extracts of tea leaves of different concentrations (1) 0%, (2) 2%, (3) 4%, (4) 6%, (5) 8% and (6) 10 % (v/v) after 2 h of immersion.

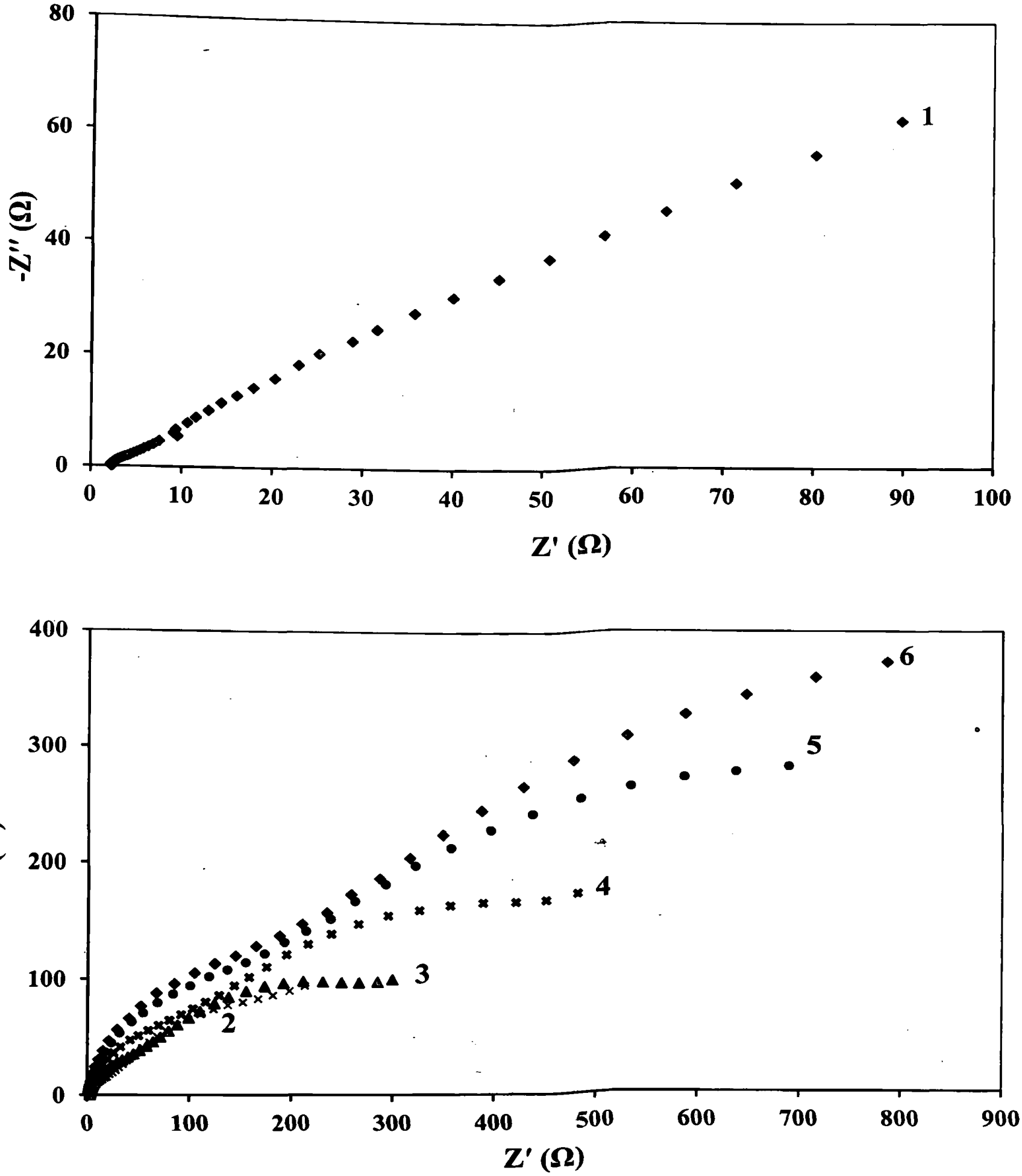

Figure 3.25: Nyquist plot of the copper specimens in 1.0 mol dm^{-3} HCl with methanol extracts of tea leaves of different concentrations (1) 0%, (2) 2%, (3) 4%, (4) 6%, (5) 8% and (6) 10 % (v/v) after 2 h of immersion.

Figure 3.26 and 3.27 show potentiodynamic polarization curves of copper specimens in HCl without and with the tea leaf extracts of different concentrations. Corrosion current density decreases with increse in the concentration of the extract at both acid concentrations, suggesting that less corrosion susceptibility of copper in the presence of tea leaf extracts. Shift in corrosion potential towards negative values and change in the cathodic Tafel slope in the presence of the extract in 0.05 mol dm^{-3} HCl indicate the

inhibition of the cathodic reaction prominently. This could be due to the scavenging of oxygen by catechins present in tea leaves. However, the presence of tea leaf extract does not affect the slope of anodic and cathodic Tafel branches in 1.0 mol dm^{-3} HCl indicating that the extract inhibits the corrosion by just blocking the active sites.

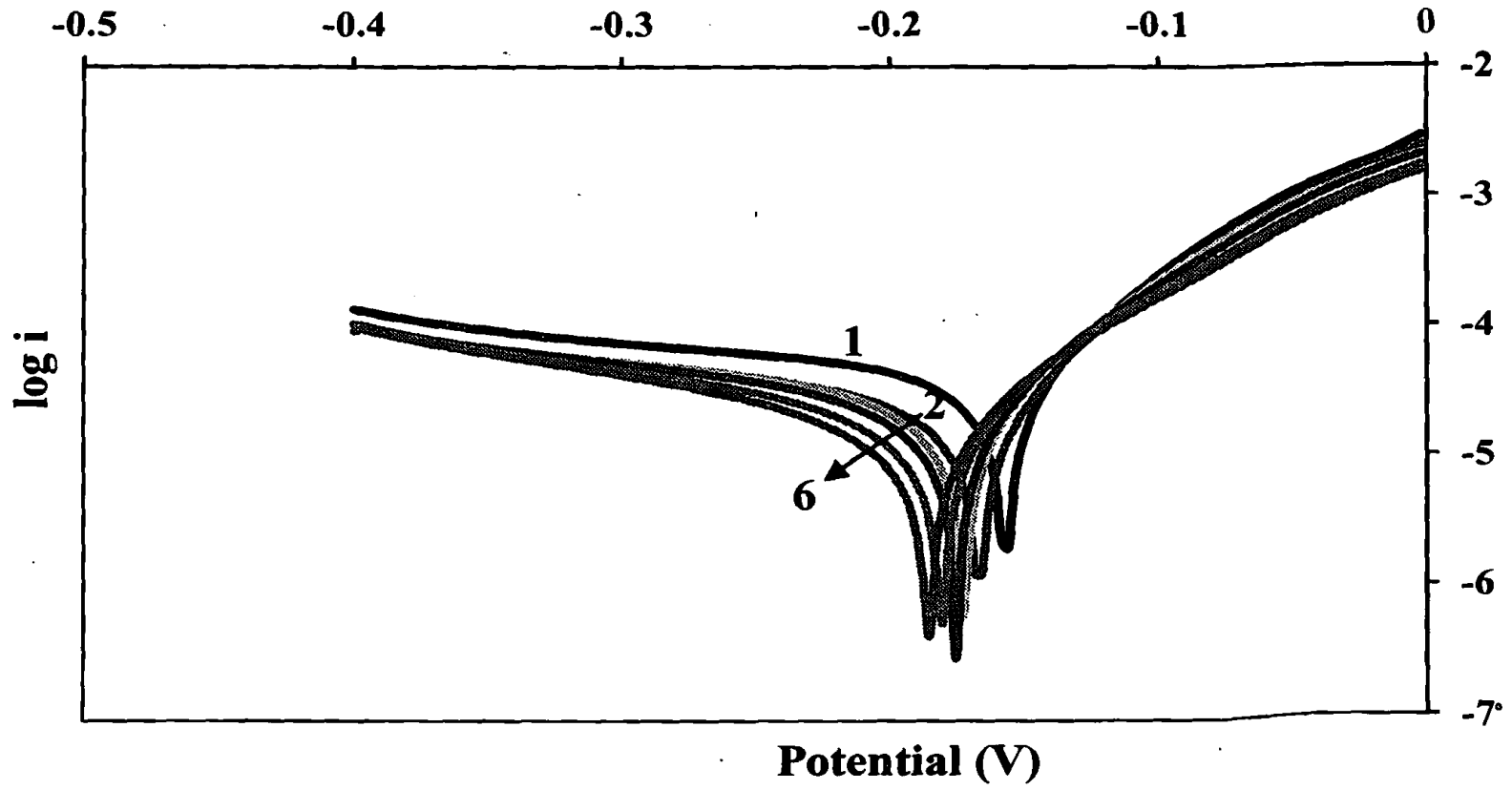

Figure 3.26 : Potentiodynamic polarization curves of copper specimens in 0.05 mol dm^{-3} HCl with methanol extracts of tea leaves of different compositions (1) 0%, (2) 2%, (3) 4%, (4) 6%, (5) 8% and (6) 10% (v/v) after 2 h immersion.

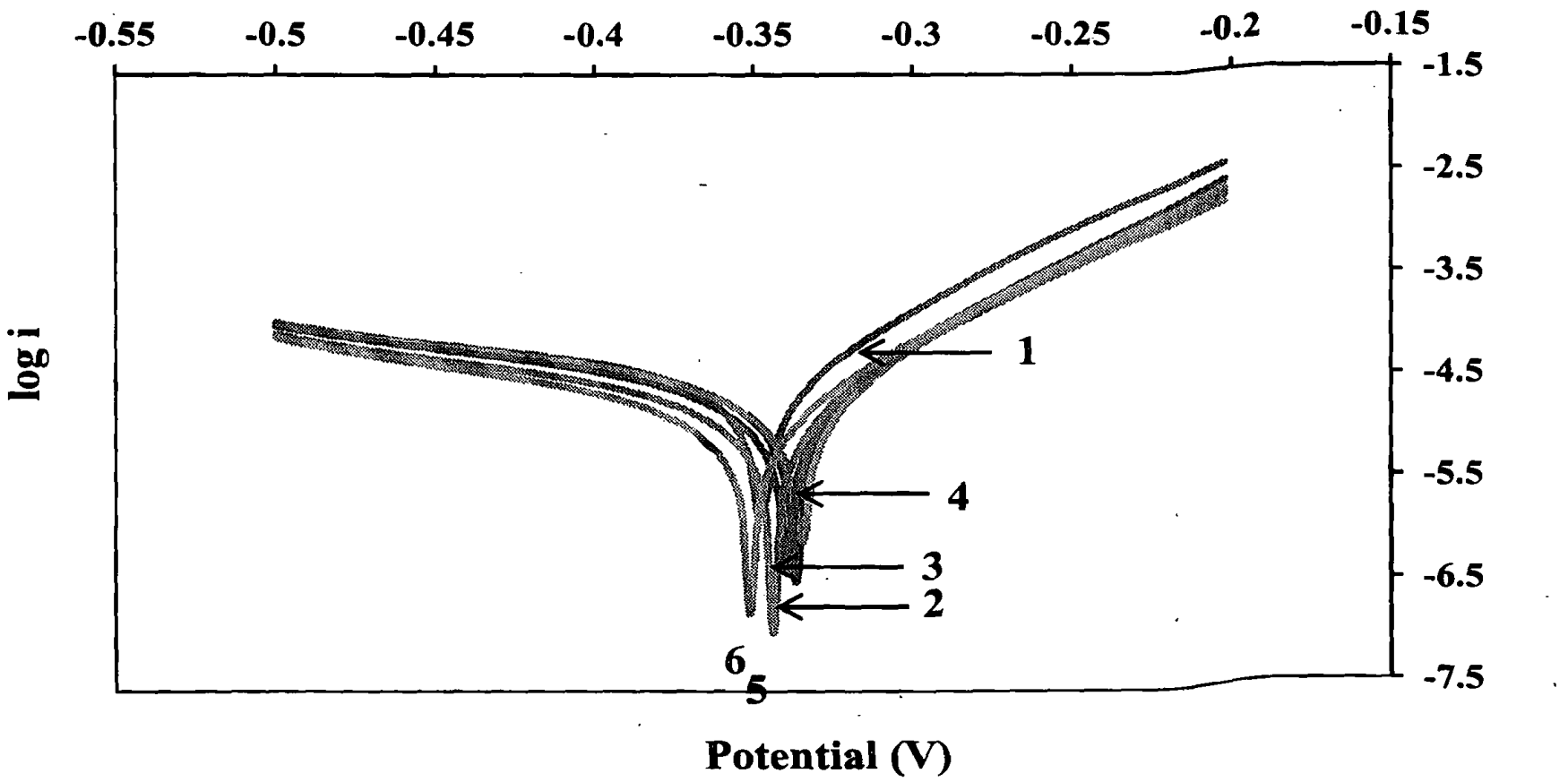

Figure 3.27 : Potentiodynamic polarization curves of copper specimens in 1.0 mol dm^{-3} HCl with methanol extracts of tea leaves of different compositions (1) 0%, (2) 2%, (3) 4%, (4) 6%, (5) 8% and (6) 10% (v/v) after 2 h immersion.

Figure 3.28 shows the Nyquist plots of copper specimens in 0.05 mol dm^{-3} HCl with and without the tea leaf extracts of different concentrations after 24 h immersion. Characteristic features of plots 1 and 2 (Figure 3.28) are the presence of difussive contribution at low frequency, the Warberg impedance. It can be attributed to the diffusion of soluble copper species from the electrode surface to the bulk solution or the diffusion of dissolved oxygen from the bulk to the electrode surface. Exposure of copper to 0.05 mol dm^{-3} HCl in the presence of the extract for 24 h increases the charge transfer resistance from the Ohm range to the kOhm, demonstrating the strong ability of corrosion inhibition which is probably due to inhibitor-film formation which would act as a barrier between the copper surface and the corrosive environment.

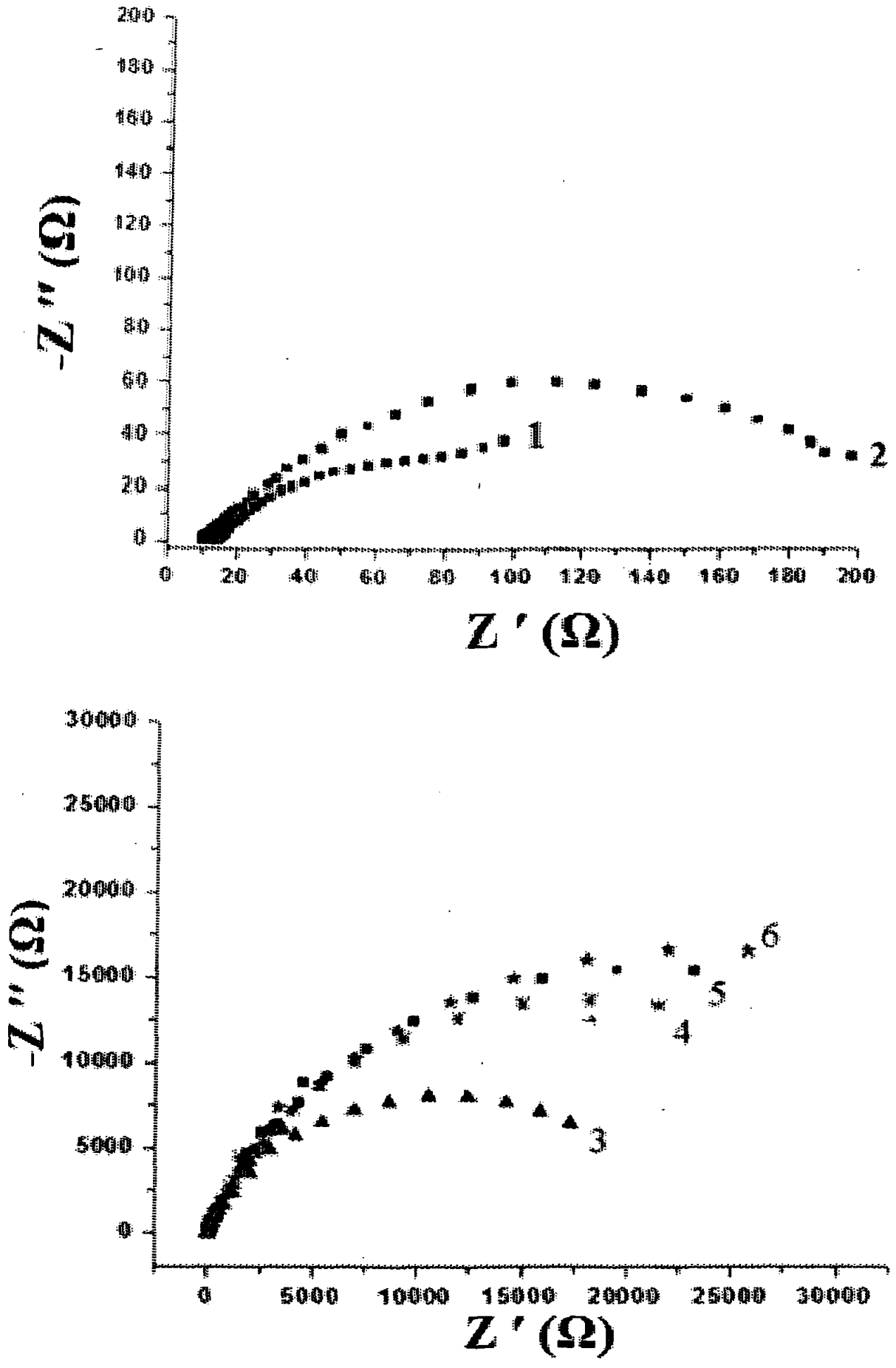

Figure 3.28: Nyuist plots of copper specimens in 0.05 mol dm^{-3} HCl with tea leaf extracts of different compositions of (1) 0%, (2) 2%, (3) 4%, (4) 6%, (5) 8% and (6) 10% (v/v) after 24 h immersion.

Electrochemical impedance spectra recorded were not complete and the recorded EIS consisted of scattered data below 10 mHz. Therfore, EIS were recorded in the frequency range of 100 kHz – 10 mHz. Although EIS were not complete, equivalent circuit can be assaigned for the recorded EIS to extract electrochemical impedance spectroscopic parameters. The electrochemical impedance spectroscopic parameters of copper specimens in HCl solutions calculated by fitting the experimental data with the equivalent circuit shown in Figure 3.29 with the help of the NOVA software are reported

in Tables 3.13 and 3.14. Equivalent circuit shown in Figure 3.29 (c) represents the copper/0.05 mol dm^{-3} HCl (for 2h and 24 h immesrsion) and copper/1.0 mol dm^{-3} HCl systems (for 2h immesrsion) in the absence of tea leaf extract. Equivalent circuit shown in Figure 3.29 (a) represents the copper/0.05 mol dm^{-3} HCl (for 2h immersion) and copper/1.0 mol dm^{-3} HCl systems (for 24 h immesrsion) in the presence of tea leaf extract. Equivalent circuit shown in Figure 3.29 (b) represents the copper/0.05 mol dm^{-3} HCl (for 24 h immesrsion) and copper/1.0 mol dm^{-3} HCl systems (for 2h immesrsion) in the presence of tea leaf extract. Electrochemical parameters used in equivalent circuit models are solution resistance (R_s), charge transfer resistance (R_f, probably due to the inhibitor film), capacitance of film (C_1), capacitance of double layer (C_2) and Warburg impedance component (W).

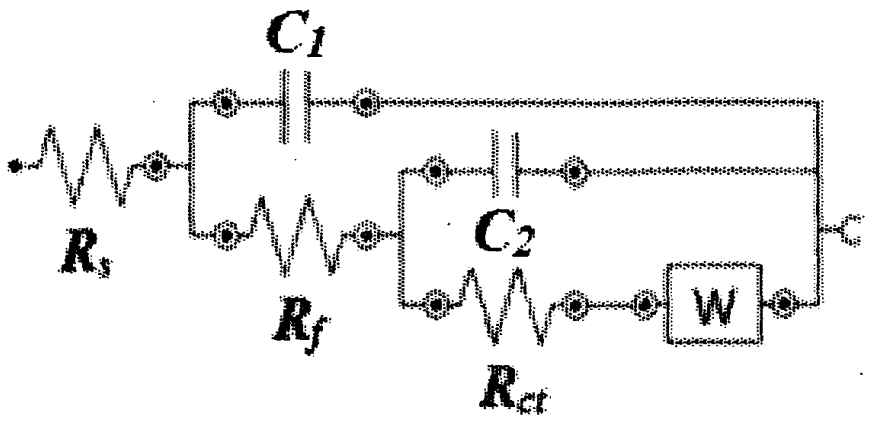

(a)

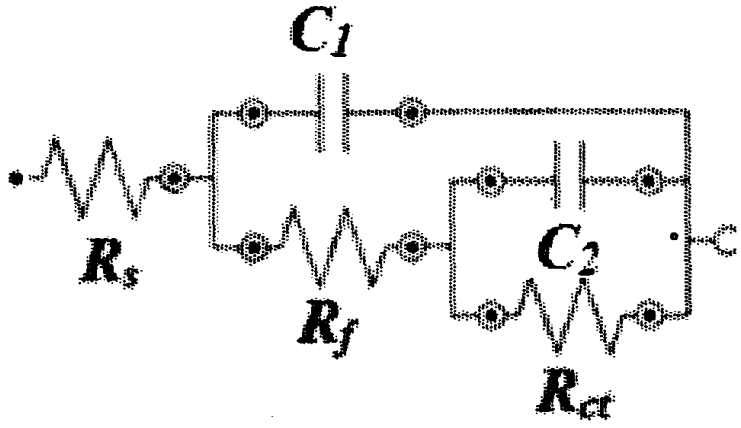

(b)

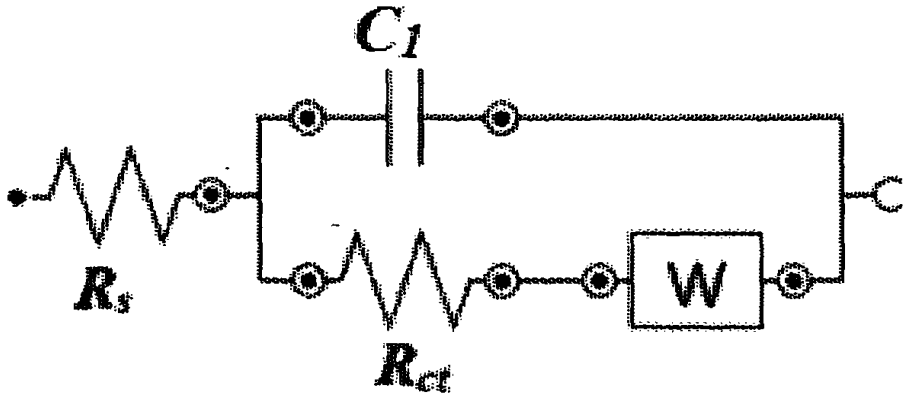

(c)

Figure 3.29: Equivalent circuits used to represent the mild steel/HCl system under different experimental conditions.

Table 3.13: Electrochemical impedance parameters (as defined on page 73) for copper specimen in 0.05 mol dm^{-3} HCl in the absence and presence of different concentrations of methanol extracts of tea leaves.

Immersion time (h)	Inhibitor concentration (% v/v)	R_s (Ω)	R_f (Ω)	C_1 (μF)	R_{ct} (Ω)	C_2 (μF)
2	0	11.4			4.4	237
	2	11.7	13.7	38.6	55.0	385
	4	11.6	23.7	25	78.9	232
	6	15.1	38.1	25.6	129	196
	8	11.9	78.6	16.3	224	87
	10	13.1	136	14.1	383	56
24	0	14.9			23.8	612
	2	11.2	26.7	47.4	109.0	253
	4	20.2	826	6.26	14800	10
	6	17.9	601	7.02	22400	14
	8	16.9	871	6.76	25300	14
	10	19.8	2320	6.06	30200	12

Table 3.14: Electrochemical impedance parameters for copper specimen in 1.0 mol dm^{-3} HCl in the absence and in the presence of different concentrations of methaol extracts of tea leaves.

Immersion time (h)	**Concentration of inhibitor (% v/v)**	R_s **(Ω)**	C_1 **(μF)**	R_f **(Ω)**	C_2 **(μF)**	R_{ct} **(Ω)**
2	0	0.82	-	-	44.9	7.14
	2	1.13	39.6	43.7	664	255.0
	4	7.19	38.9	97.3	533	328.0
	6	2.73	31.7	104.0	479	314.0
	8	2.36	31.1	169.0	465	474.0
	10	1.34	31.0	195.0	474	571.0
24	0	0.85	76.8	6.3	532	21.6
	2	0.91	43.2	14.1	405	48.6
	4	0.70	33.9	19.8	295	60.8
	6	0.80	33.6	24.2	283	70.1
	8	1.04	32.1	31.2	265	78.8
	10	1.20	26.9	49.5	158	119

The inhibitor film formation is comparable with the formation of (5-Methyl-[1,3,4]thiadiazol-2-ylsulfanyl)-acetic acid 4-dimethylamino-benzylidene)-hydrazide; (MTYDBH) film on copper surfaces in 3.5% NaCl solution as reported by Weihua Li *et al.* [113].

Figure 3.30 shows potentiodynamic polarization curves obtained for copper specimens in 0.05 mol dm^{-3} with and without methanol extracts of tea leaves of different concentration of after 24 h immersion. According to the figure, current density of the system decreases significantly with the introduction of the extract and the maximum inhibition was obtained for 6% extract, beyond which corrosion current density does not change significantly. This may be due to the completion of film formation at 6% concentration of the extract.

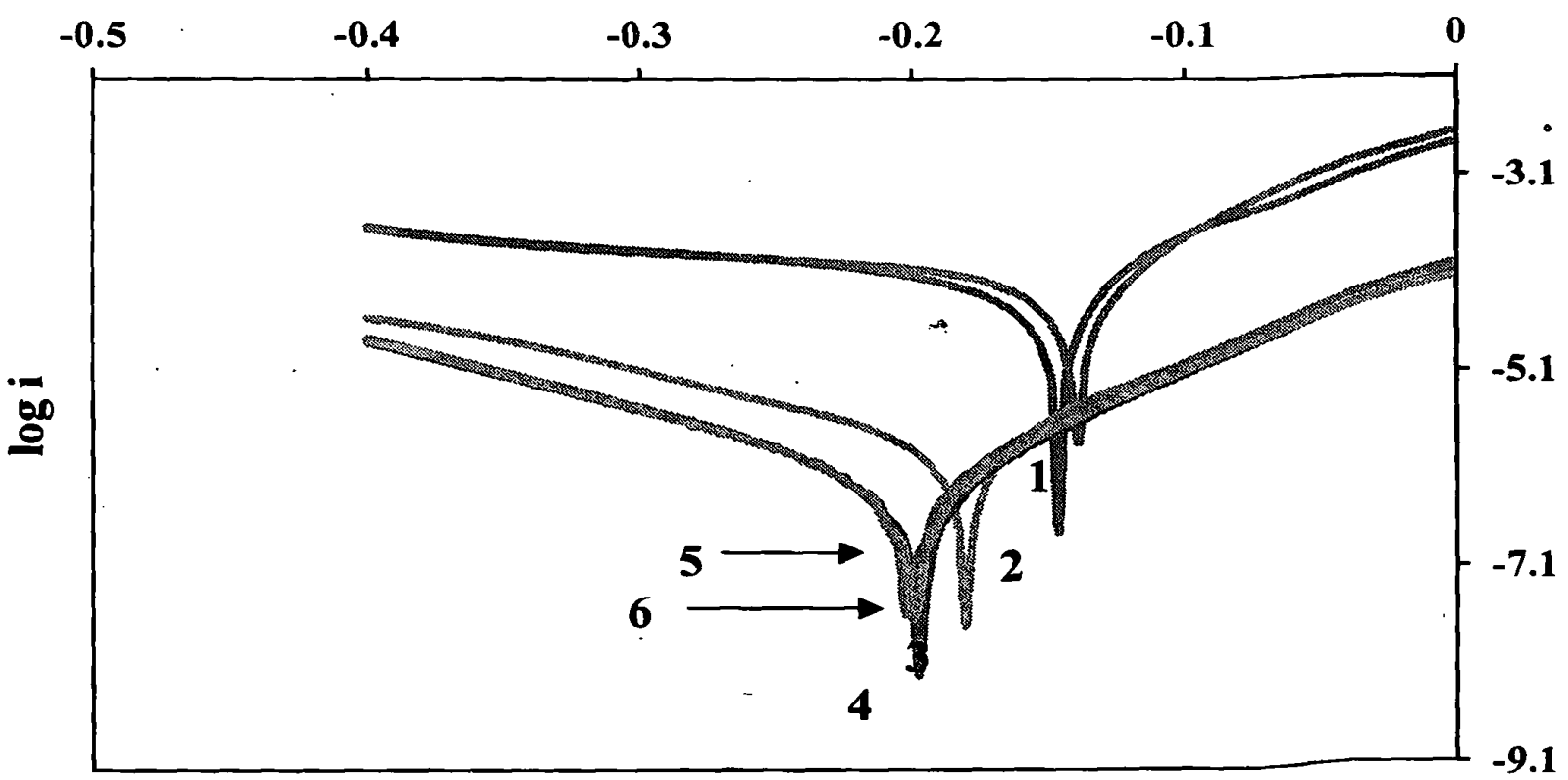

Figure 3.30: Potentiodynamic polarization curves of copper specimens in 0.05 mol dm^{-3} HCl with methanol extracts of tea leaves of different compositions (1) 0%, (2) 2%, (3) 4%, (4) 6%, (5) 8% and (6) 10% (v/v) after 24 h immersion.

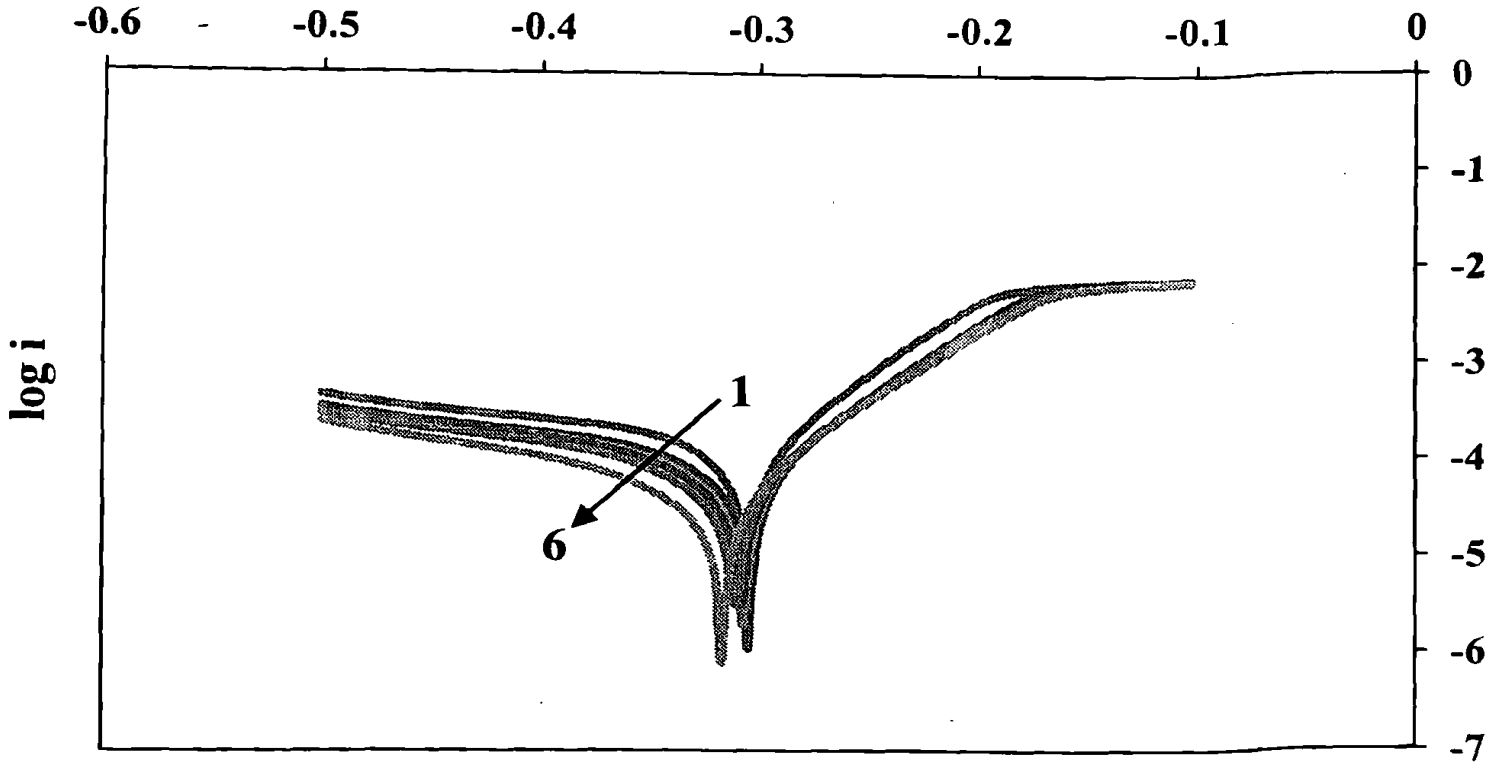

Figure 3.31: Potentiodynamic polarization curves of copper specimens in 1.0 mol dm^{-3} HCl with methanol extracts of tea leaves of different compositions (1) 0%, (2) 2%, (3) 4%, (4) 6%, (5) 8% and (6) 10% (v/v) after 24 h immersion.

Table 3.15 and 3.16 show the potentiodynamic polarization parameters, such as anodic and cathodic Tafel slopes, corrosion current density and corrosion potential. Corrosion current density and Tafel slopes of cathodic and anodic branches were determined by extrapolating the linear portions of cathodic and anodic branches to the zero over voltage with the help of the NOVA software.

Table 3.15: Polarization parameters extracted from podentiodynamic polarization curves of copper specimens in methanol extracts of tea leaves in 0.05 mol dm^{-3} HCl of different concentrations.

Immersion time (h)	[Inhibitor]	b_a ($mVdec^{-1}$)	b_c ($mVdec^{-1}$)	(-) E_{corr} (mV)	I_{corr} ($\mu A\ cm^{-2}$)	% IE
2	0	51.8	139.4	156.0	10.6	
	2	55.0	125.0	169.0	6.5	39
	4	56.8	114.5	174.7	6.3	41
	6	52.9	99.5	177.0	5.1	52
	8	50.3	98.9	181.0	4.1	62
	10	52.6	81.9	186.0	3.8	65
24	0	55.6	139.5	144.8	20.4	
	2	61.5	115.5	147.0	14.1	31
	4	62.5	77.3	181.6	0.4	98
	6	61.5	74.9	197.0	0.2	99
	8	57.3	75.3	201.1	0.2	99
	10	61.7	75.2	200.1	0.2	99

Table 3.16 : Polarization parameters extracted from potentiodynamic polarization curves of copper specimens in methanol extracts of tea leaves in 1.0 mol dm^{-3} HCl of different concentrations.

Immersion time (h)	[Inhibitor]	b_a (mV dce^{-1})	b_c (mV dce^{-1})	(-) E_{corr} (mV)	i_{corr} (μA cm^{-2})	% IE
2	0	56.4	157.8	347	22.8	
	2	54.0	167.6	333	8.6	62.3
	4	58.6	161.0	334	8.4	63.2
	6	58.0	136.9	342	6.4	71.9
	8	57.9	140.2	342	6.3	72.4
	10	51.7	108.9	364	6.1	73.2
24	0	54.0	176.0	300	43.6	
	2	58.4	167.4	300	28.2	35.3
	4	62.0	137.8	306	23.0	47.3
	6	62.8	126.2	310	21.8	50.0
	8	63.1	115.7	315	18.3	58.2
	10	61.6	102.6	323	12.3	71.8

3.2.4 Adsorption cosideration

Experiments carried out in order to investigate corrosion inhibition effect of methanol extracts of tea leaves on copper in HCl solution indicate that the dissolution of copper in HCl medium decreases in the presence of the tea leaf extracts. Mass loss mesurements conducted in 0.05 mol dm^{-3} HCl with methanol extracts of tea leaves of different concentrations show that mass loss of copper specimens is negligible upto first four days of immersion, as clearly seen in Figure 3.32. This effect may be due to the oxygen scavenging ability of catechins present in the extract. Percentage inhibition efficiency of the extract initially increases with exposure time, then decreases with long exposure time as the extarct probably starts to decay. After that, dissolution rate increases with decrease in the concentration of the extract, suggesting that adsorption of components in the extract on metal surfaces.

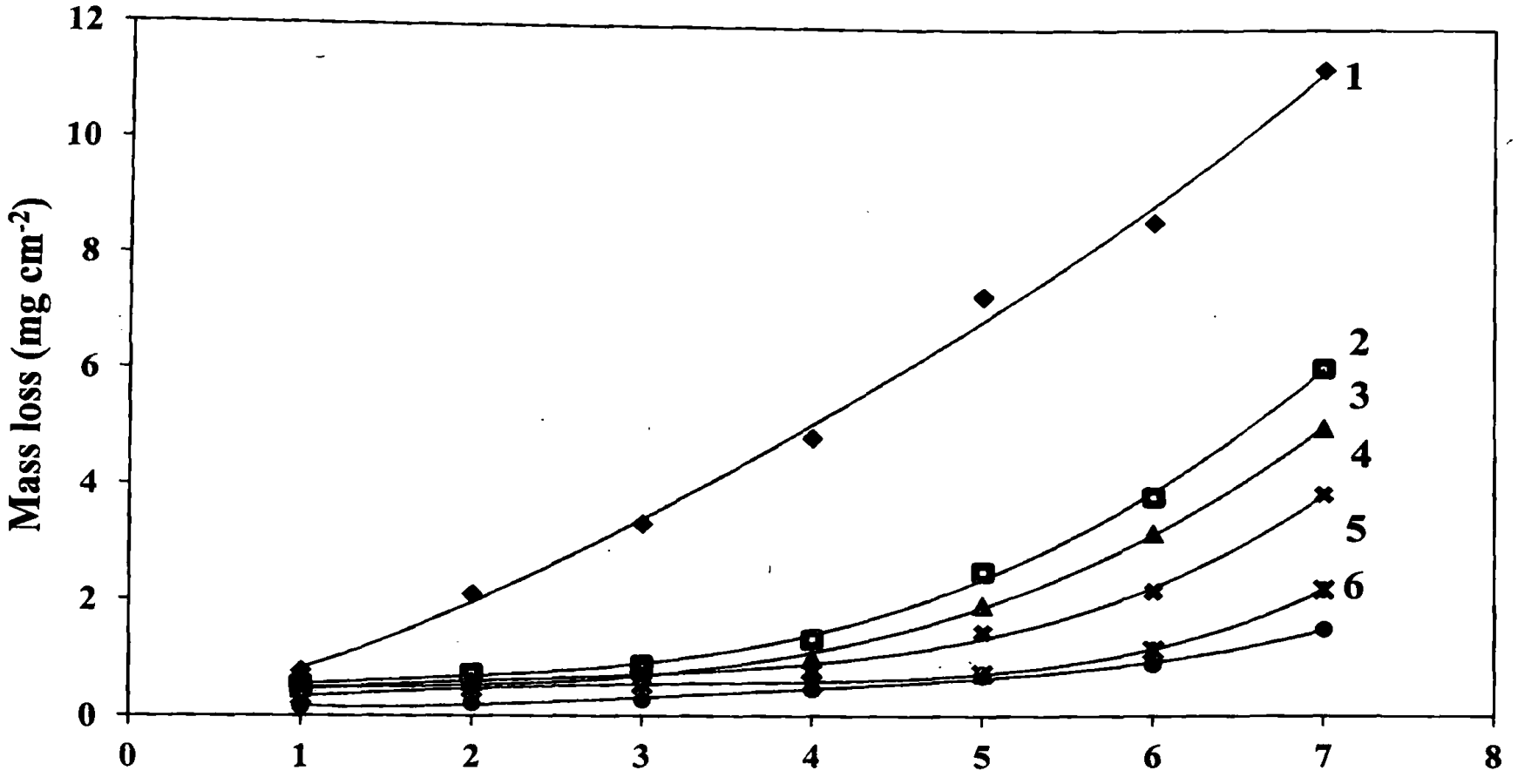

Figure 3.32: Variation of mass loss of copper specimens in 0.05 mol dm^{-3} HCl with tea leaf extracts of different compositions (1) 0% , (2) 4% , (3) 6 %, (4) 8%, (5) 10% and (6) 15% with time.

Surface coverage of tea leaf extracts on the copper surface calculated using Equation (3.7) based on the results obtained from mass loss measurements are reported in Table 3.17.

Table 3.17: Surface coverage of methanol extracts of tea leaves on copper surface in 0.05 mol dm^{-3} HCl with tea leaf extarcts of different concentrations after immersion for different time periods.

[Inhibitor]	Surface coverage (θ)						
% (v/v)	1 day	2 days	3 days	4 days	5 days	6 days	7 days
0	-	-	-	-	-	-	-
4	0.31	0.65	0.74	0.72	0.66	0.56	0.46
6	0.40	0.71	0.79	0.79	0.74	0.63	0.56
8	0.41	0.72	0.77	0.84	0.80	0.75	0.66
10	0.57	0.77	0.83	0.88	0.90	0.87	0.81
15	0.79	0.90	0.92	0.90	0.90	0.90	0.87

Results obtained from the mass loss measurements after 4 days of immersion were used to fit adsorption isotherms. Significant differences in mass loss were not observed before this time period. The plot of C vs. C/θ gives a straight line with a slope of approximately one indicating that the experimental data obtained at ambient temperature fit the Langmuir adsorption isotherm (Figure 3.33).

In order to confirm this further, percentage inhibition efficiency calculated after 2 h immersion from potentiodynamic polarization studies was also fitted with the Langmuir adsorption isotherm (Figure 3.34). Results obtained from both methods are comparable, with regression coefficients (R^2) of 0.999 and 0.946, respectively.

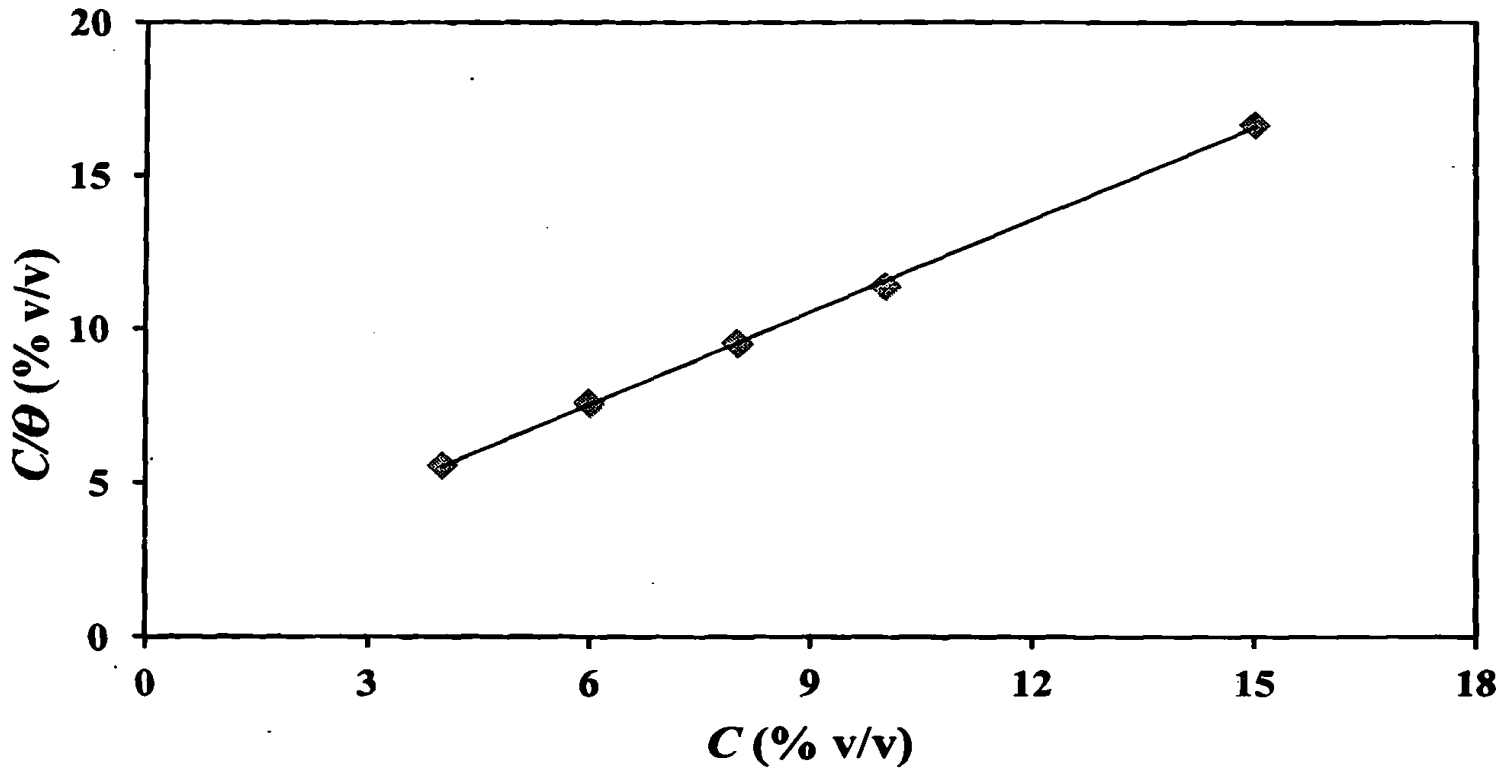

Figure 3.33: Langmuir adsorption isotherm for copper specimens in 0.05 mol dm^{-3} HCl in the presence of tea leaf extracts after 4 days of immersion at ambient temperature based on mass loss measurements.

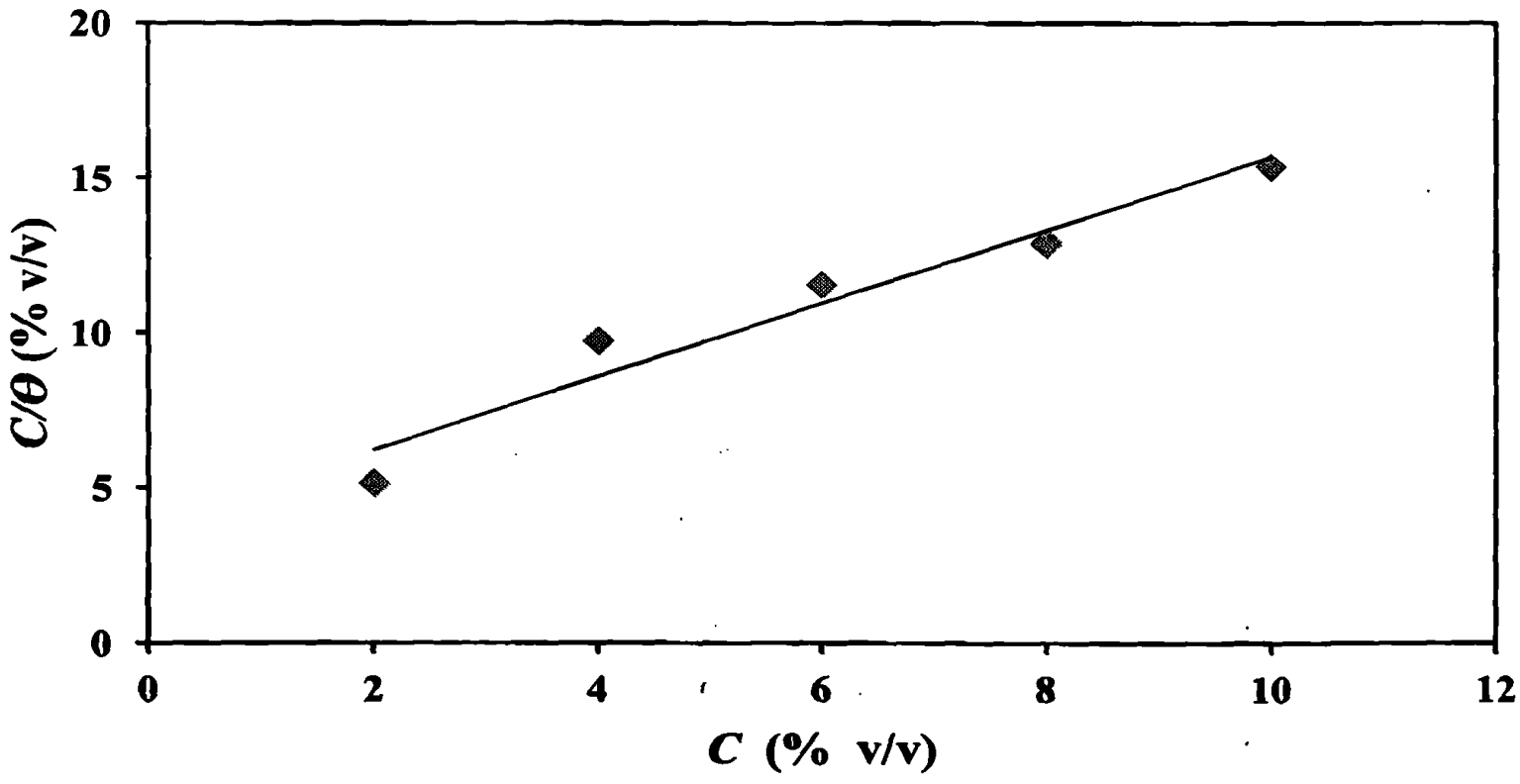

Figure 3.34: Langmuir adsorption isotherm for copper specimen in 0.05 mol dm^{-3} HCl in the presence of tea leaf extracts after 2 h immersion at ambient temperature based on potentiodynamic polarization measurements.

3.2.5 UV-Vis Spectroscopic studies

The UV-Vis spectrum of the methanol extract of tea leaves shows one sharp band in the UV region at 278 nm and 2 broad peaks in the visible region (Figure 3.35). The band at 278 nm is attributed to the presence of caffeine by comparision with the UV-Vis spectrum of pure caffein in 0.05 mol dm^{-3} HCl which shows a band at 272 nm. Bands in the visible region is due to the presence of pigments and polyphenolic compounds present in the extract. The UV-Vis spectrum of the methanolic solution obtained by dipping a copper specimen, which had been placed in 10% (v/v) tea leaf extract in 0.05 mol dm^{-3} HCl in methanol for 2h and 24 h, shows bands in the vissible region only, indicating that copper surface selectively adsorbs coloured component(s) in the tea leaf extract that show λ_{max} at 651 and (350-472) nm (Figure 3.36). Further, the band intensity of adsorbed species is higher for 24 h immersion than for 2 h immersion supporting the results obtained from potentiodynamic polarization studies carried out in 0.05 mol dm^{-3} HCl. Selective adsorption of component(s) was further supported by observing the same band pattern as observed in Figure 3.36 in the spectrum obtained for the 10% (v/v) extract in 0.05 mol dm^{-3} HCl after removal of the copper plate (Figure 3.37).

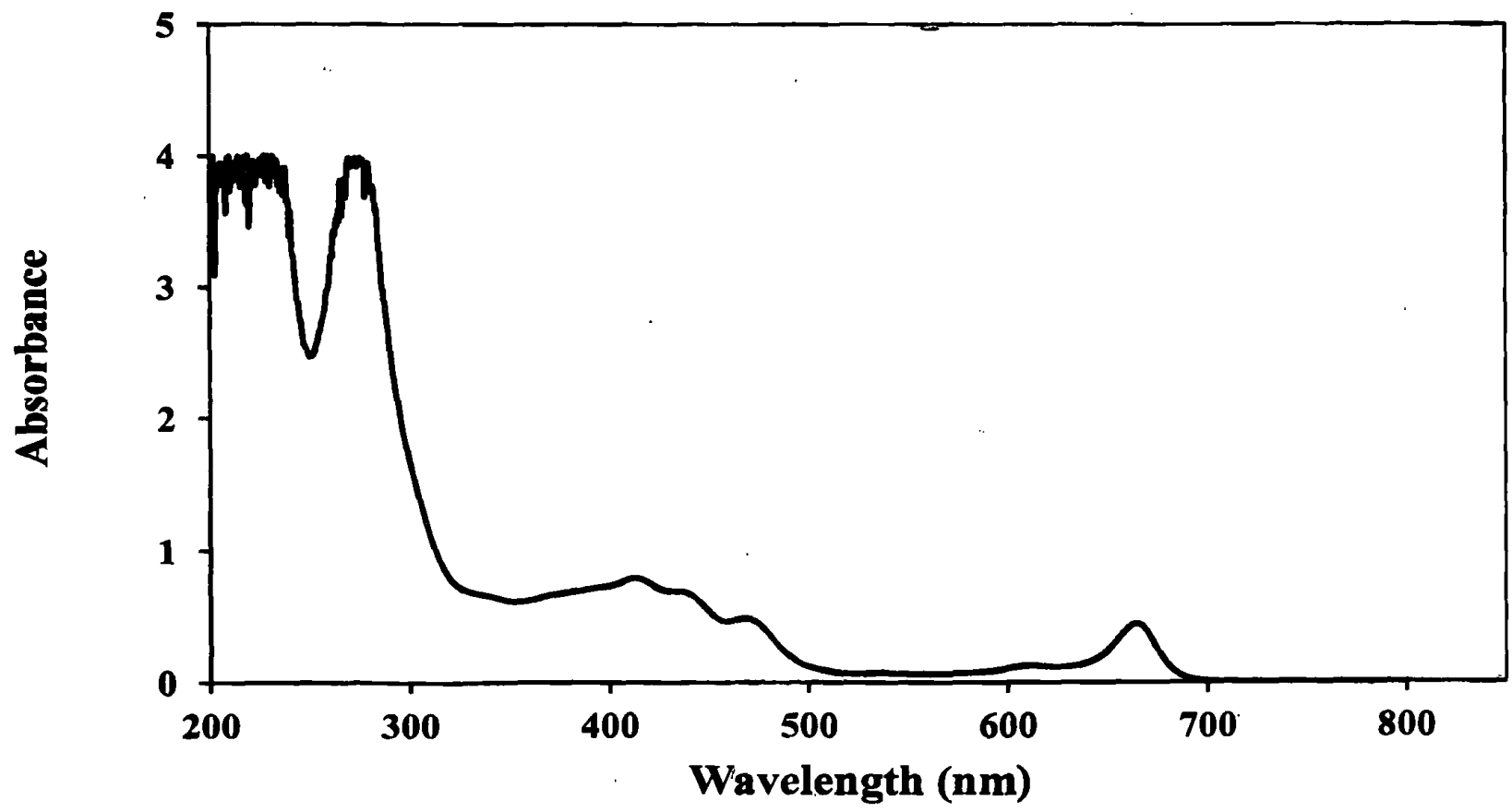

Figure 3.35: UV –Vis spectrum of 10 times diluted methanol extract of tea leaves.

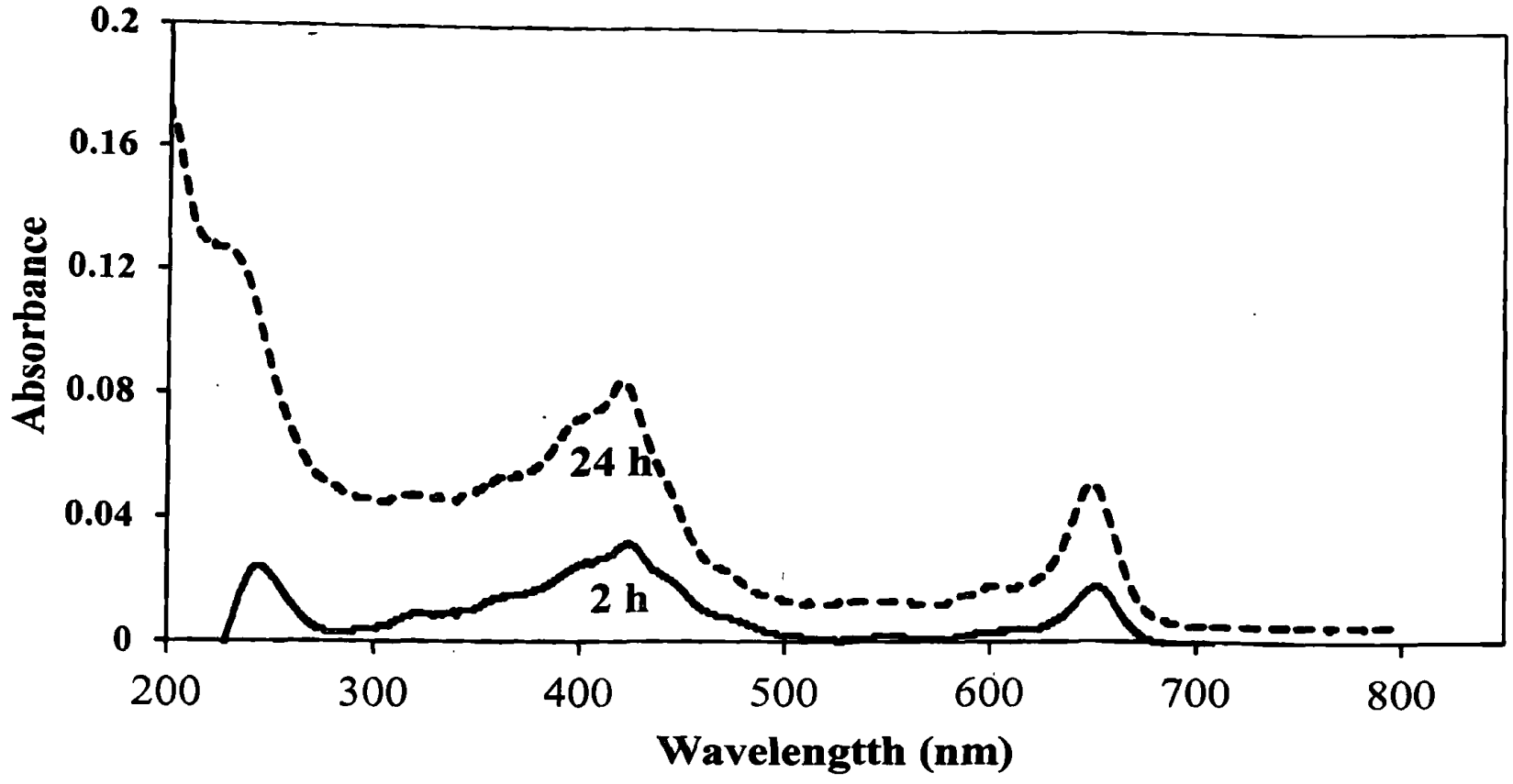

Figure 3.36: UV–Vis spectra of methanolic solution obatined by dipping the copper specimen in methanol, which had been placed in 10% (v/v) tea leaf extract in 0.05 mol dm^{-3} HCl for 2 h and 24 h.

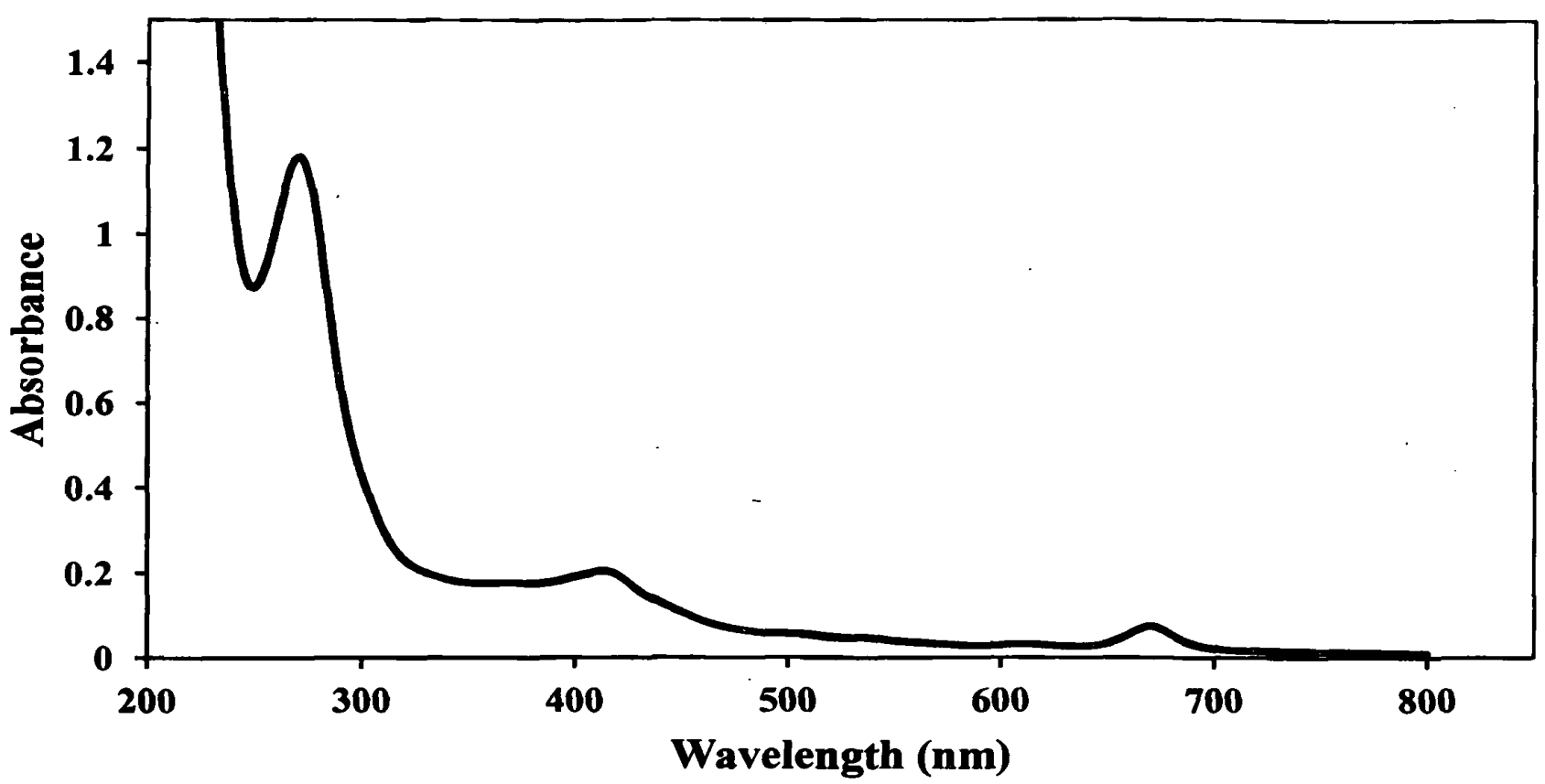

Figure 3.37: UV –Vis spectrum of 10% (v/v) tea leaf extarct in 0.05 mol dm^{-3} HCl obtained after removal of the copper specimen after 24 h immersion.

The adsorption of tea leaf components on the copper plate, that had been placed in HCl solution of much higher concentration (1.0 mol dm^{-3}) shows adsorption patterns similar to that is obtained for 0.05 mol dm^{-3} HCl solution after 2 h immersion. However,

the broad band observed at (280 nm – 340 nm) after 24 h, suggests that the reaction of caffeine with the copper surface (Figure 3.38). When a copper specimen dipped in 1.0 mol dm^{-3} HCl in the presence of 1000 ppm caffein, a white colour deposit was observed. This indicates the reaction of caffein with copper in acidic environments. This was further confimed by the UV-Vis spectrum of 10% (v/v) tea leaf extract in 1.0 mol dm^{-3} HCl after removal of the copper plate. Acording to figure 3.39, immesion of copper plate in 10% (v/v) tea leaf extarct prepared in 1.0 mol dm^{-3} HCl solution changes the band at 278 nm. It indicates that the exposure of copper plates in highly acidic medium facilitates the reaction between caffeine and copper. This may be the reason for low inhibition efficiency in acid solutions of higher concentrations.The reaction of copper with caffeine prevents the adsorption of corrosion-resistant componenets of the tea leaf extracts.

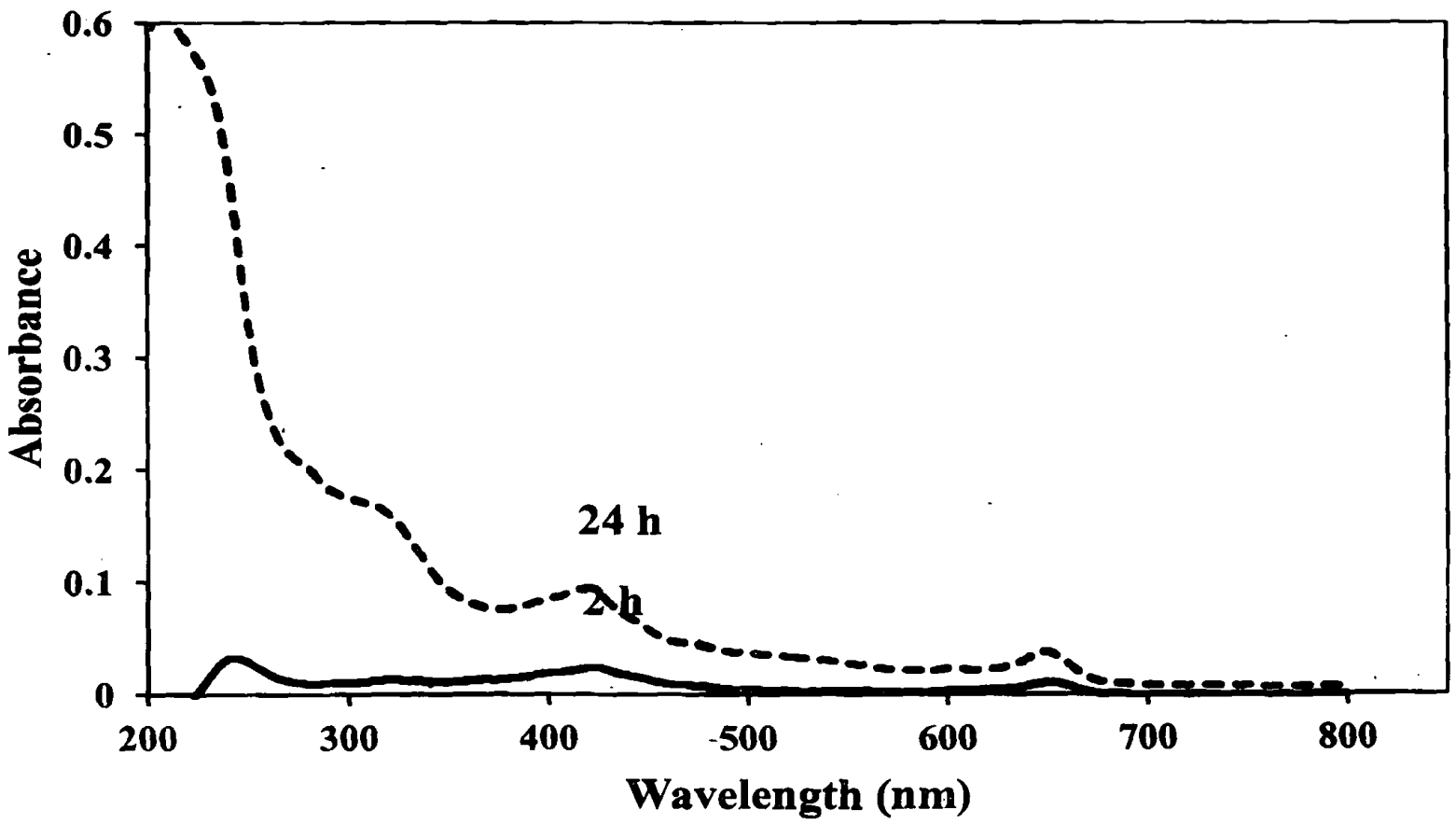

Figure 3.38: UV–Vis spectra of solution obatined by dipping two copper specimens in methanol. One had been removed from 10% (v/v) tea leaf extract in 1.0 mol dm^{-3} HCl after 2 h and the second 24 h immersion.

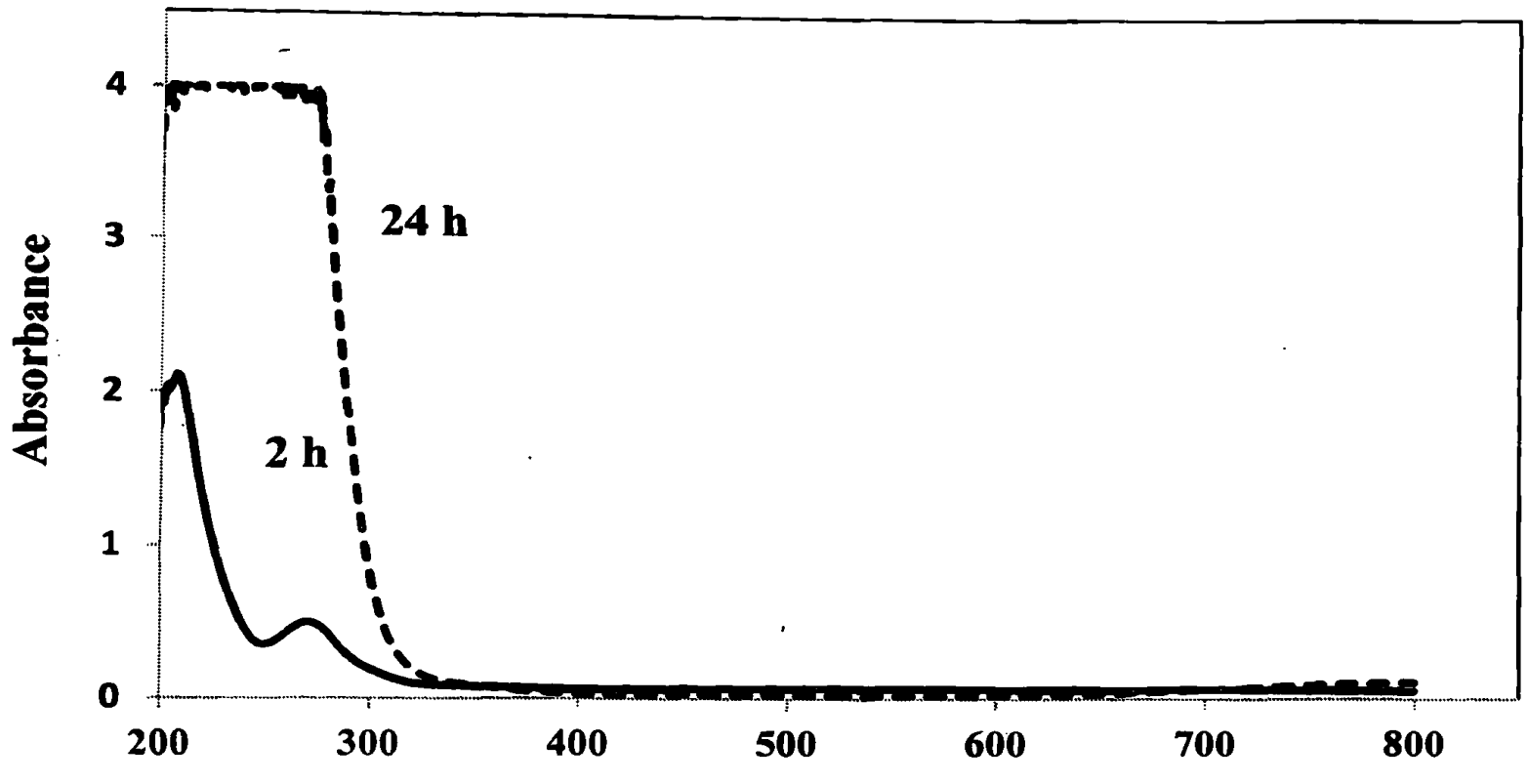

Figure 3.39: UV–Vis spectra of 10% (v/v) tea leaf extract in 1.0 mol dm^{-3} HCl obtained after 2 h immersion of a copper specimen and after 24 h immersion of a copper specimen.

3.2.6 Active components in the tea leaf extract responsible for corrosion inhibition

Tea leaves mainly contain polyphenolic compounds and caffeine. Mass loss measurements carried out with 0.05 mol dm^{-3} HCl alone, 0.05 mol dm^{-3} HCl with methanol extracts of tea leaves of different concentrations and 0.05 mol dm^{-3} HCl with synthetic caffeine solutions of different concentrations (10, 50, 100 and 1000 ppm) indicate that caffeine has no contribution towards the inhibition effect. Threfore, it can be concluded that polyphenolic compounds may be responsible for the inhibition effect. As polyphenolic compounds in tea are oxygen scavengers, they probably inhibit the corrosion of copper by scavenging oxygen from the system. According to the UV-Vis spectroscopic studies, adsorption of certain components, which give absorbance in the visible region, on copper surface also contribute to corrosion inhibition.

The anti-oxidant capacity of 10% (v/v) tea leaf extract prepared in HCl at different concentrations was determined by measuring the absorbance of the $ABTS^{\cdot+}$ in the presence and absence of 10% (v/v) tea leaf extract at 734 nm which is one of the methods used to determine the antioxidant capacity [114]. As $ABTS^{\cdot+}$ is scavenged by the antioxidants present in the tea leaf extract, blue colour intensity of $ABTS^{\cdot+}$ decreases. The colour density, and hence the absorbance of $ABTS^{\cdot+}$ decreases with the addition of 10% (v/v) extract prepared in HCl solutions of different concentrations as compared to the control indicating the anti-oxdant capacity of the tea leaf extract. However, addition of 10% (v/v)

tea leaf extract prepared in 0.05 mol dm^{-3} HCl decreases the absorbance of $ABTS^{\cdot+}$ to a great extent as compared to the decrease in absorbance of $ABTS^{\cdot+}$ in the presence of 10% (v/v) tea leaf extract prepared in 1.0 mol dm^{-3} HCl as shown in Table 3.18. Therefore, higher anti-oxidant capacity of the exract at lower acid concentration (0.05 mol dm^{-3} and 0.1 mol dm^{-3}) leeds to a higher possibility for scavenging of oxygen. This could also be a reason for higher inhibition efficiency at lower acid concentrations.

Table 3.18: Variation of absorbance of $ABTS^{\cdot+}$ with the addition of 10% (v/v) tea leaf extract prepared in HCl solutions of different concentrations at 734 nm.

Test solution	Absorbance
Control	0.927
0.05 mol dm^{-3} HCl	0.273
0.1 mol dm^{-3} HCl	0.277
0.5 mol dm^{-3} HCl	0.439
1.0 mol dm^{-3} HCl	0.477

3.2.7 Surface pictures

Surface morphology of Cu specimens examined on a polarizing microscope (×100), provides pictures shown in Figure 3.40, supporting the results obtained from other corrosion monitoring techniques. The surface of copper specimens, dipped in 10% (v/v) methanol extract of tea leaves (in 0.05 mol dm^{-3} HCl), does not show any significant change after 2 day exposure to the corrosive medium, while the surface morphology of Cu plates dipped in 0.05 mol dm^{-3} HCl changes drastically.

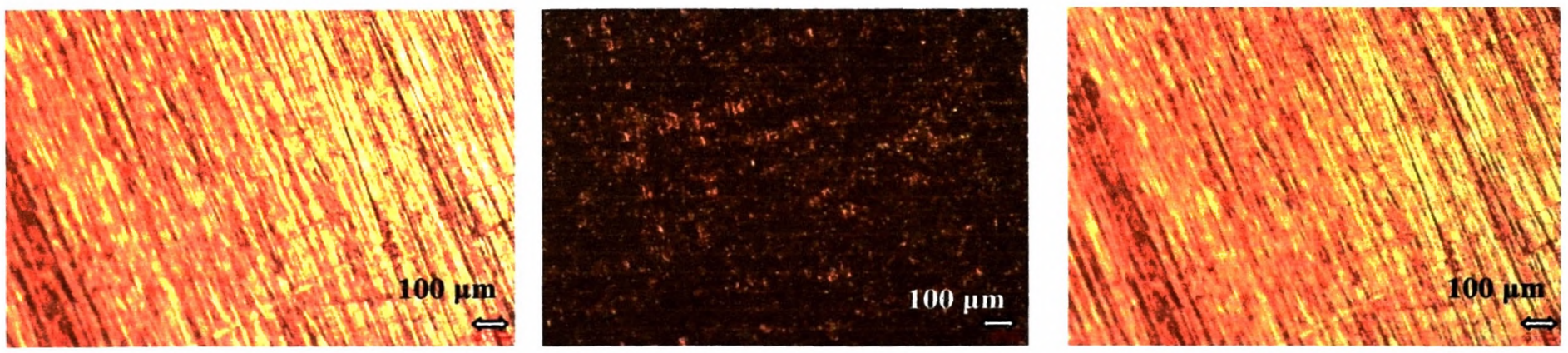

(a) (b) (c)

Figure 3.40: Surface morphology of copper specimens (a) before immersion (b) after immersion in 0.05 mol dm^{-3} HCl for 2 days and (c) after immersion in 0.05 mol dm^{-3} HCl with 10% (v/v) methanol extract of tea leaves for 2 days.

3.3 Corrosion of Galvanized Steel in NaCl Solutions and Its Prevention

3.3.1 Effect of NaCl on corrosion behavior of galvanized steel (GS) in NaCl environments

According to Figure 3.41, the V_{oc} of GS specimens placed in 0.1 mol dm^{-3} NaCl is increased from 1003 mV to 1075 mV after 24 h immersion and starts to decrease gradually and attains steady state at around 1010 mV after 10 days. Further, V_{oc} of GS placed in 1.0 mol dm^{-3} NaCl is increased from 1055 mV to 1104 mV after 48 h immersion and starts to decrease gradually and attains steady state at around 1050 mV after 10 days. In contrast, V_{oc} of GS placed in 4.0 mol dm^{-3} NaCl solutions remains almost constant with time at about 1070 mV. Rate of change in V_{oc} of GS placed in 0.1 mol dm^{-3} is higher than that in 1.0 mol dm^{-3} NaCl and insignificant changes in V_{oc} of GS placed in 4.0 mol dm^{-3} NaCl indicate that the initial corrosion rate of GS is higher in low concentrations of NaCl solutions and increase in the chloride concentration to a higher value increases the corrosion protection. After immersion of GS for 24 h in 0.1mol dm^{-3} and 1.0 mol dm^{-3} NaCl, the solutions became turbid white colour with a white deposit on GS specimens. This phenomenon is more significant in 0.1 mol dm^{-3} NaCl solution. However, only a slight white colour precipitation was observed on GS specimens placed in 4.0 mol dm^{-3} NaCl solutions even after 1 week of immersion.

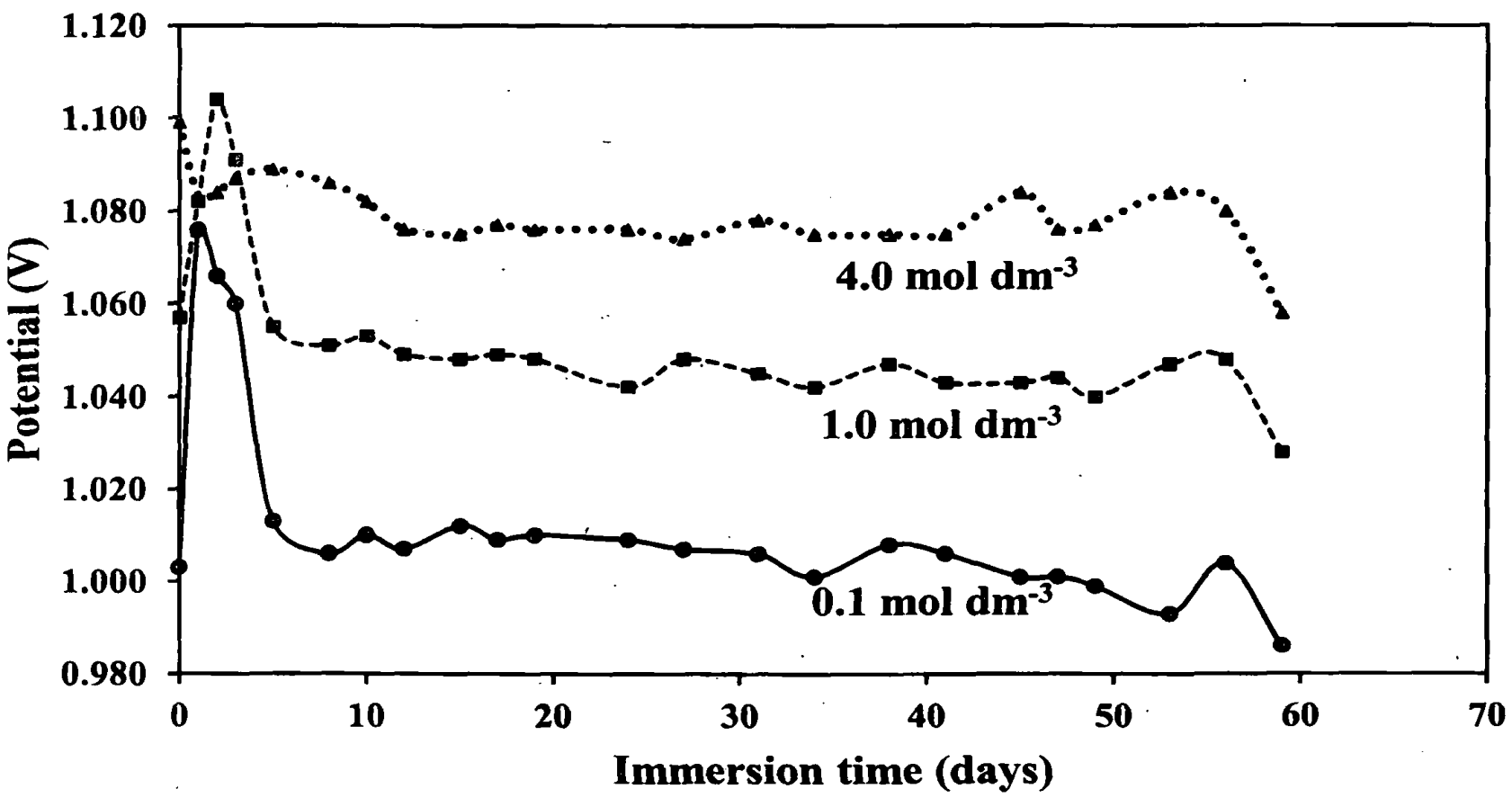

Figure 3.41: Variation of open circuit potential (V_{oc}) of GS specimens in NaCl solutions of different concentrations with time at ambient temperature.

After immersion for 10 days, V_{oc} of galvanized steel specimens was fluctuated about the steady value as shown in Figure 3.41 and the fluctuation is higher in 0.1 mol dm^{-3} NaCl. This may be due to the temperature fluctuation and deposition of white rust on the metal surface. The V_{oc} of GS specimens placed in 0.1 and 1.0 mol dm^{-3} NaCl shows higher variation because of the white rust formation to a large degree, which was confirmed by the open circuit potential measurements at elevated temperatures. As the dissolution of white rust occurs at 50 °C, V_{oc} decreases initially and attains the steady state of 650 mV after a 20 day immersion as shown in Figure 3.42. This low potential suggests that the exposure of mild steel underneath the zinc layer. This was further confirmed by monitoring the open circuit potential in 0.1 mol dm^{-3} NaCl at pH = 1. In low acidic environments, dissolution of zinc layer exposes the steel surface to the corrosive environment. Corrosion potential becomes stable at around 600 mV as shown in Figure 3.43.

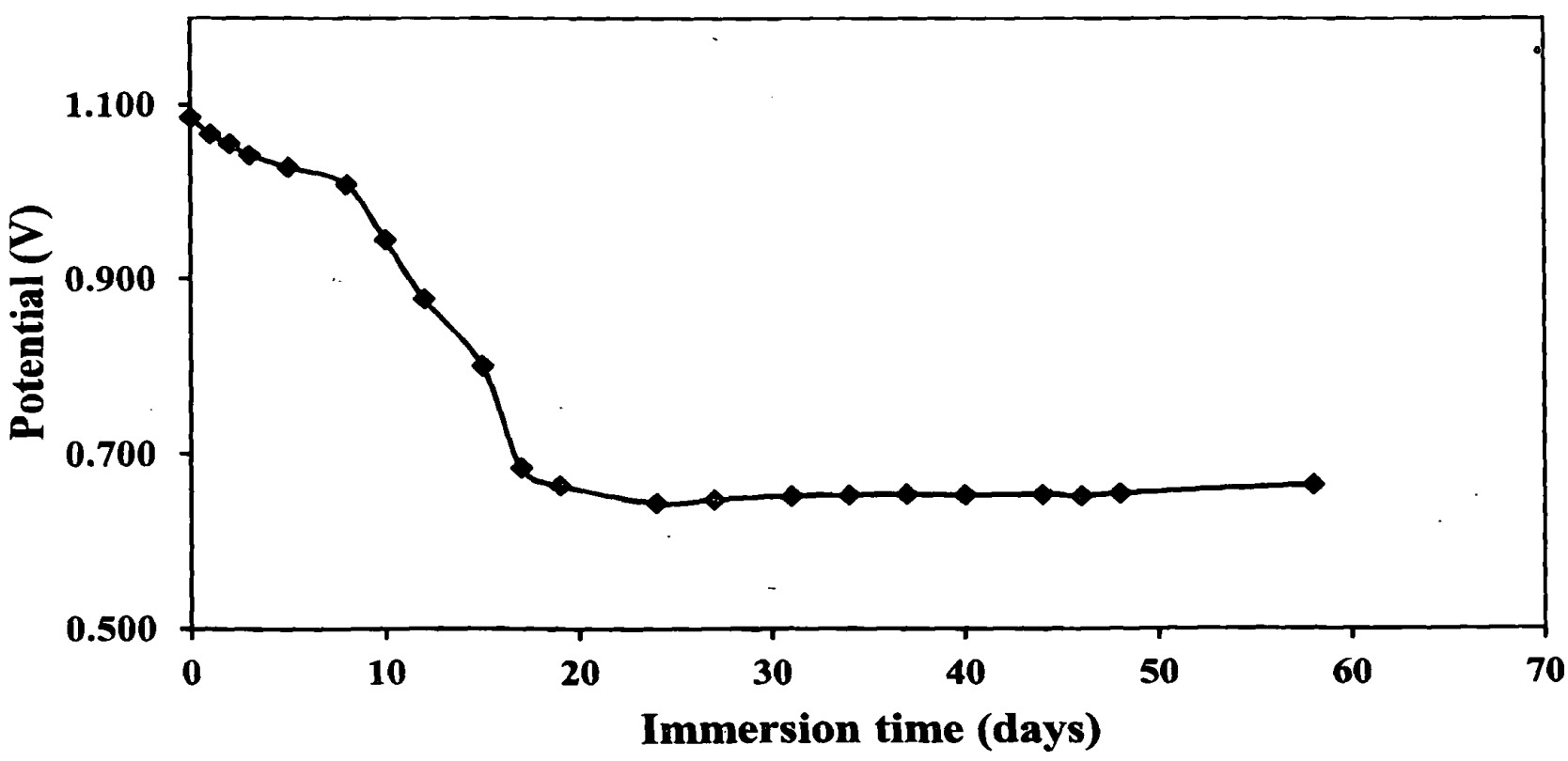

Figure 3.42: Variation of V_{oc} of GS specimen in 1.0 mol dm^{-3} NaCl with time at 50 °C.

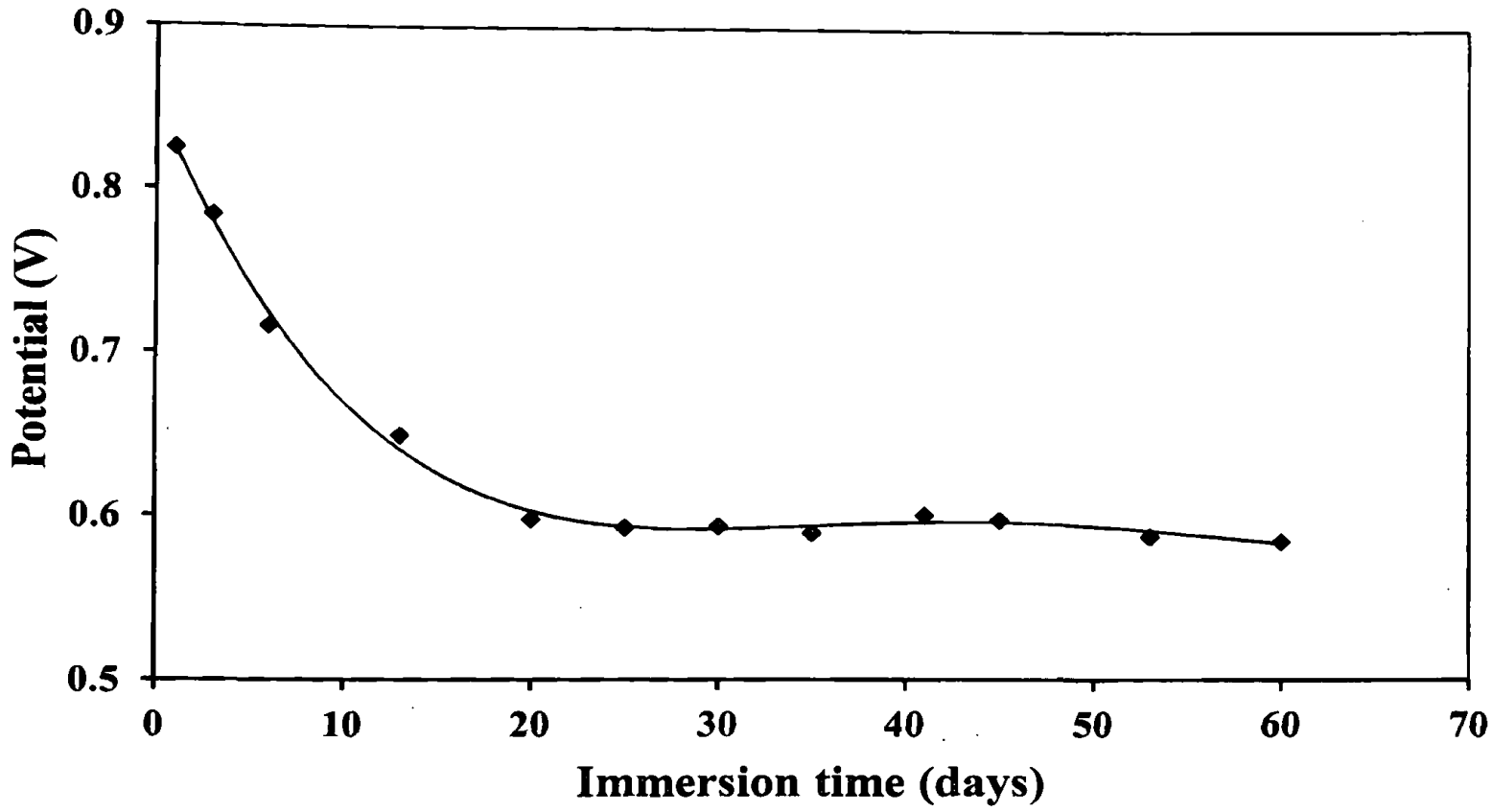

Figure 3.43: Variation of V_{oc} of GS specimen in 0.1 mol dm^{-3} NaCl acidified to pH=1.

The results obtained from V_{oc} measurements are further confirmed by EIS and potentiodynamic polarization studies. Figure 3.44 shows the potentiodynamic polarization curves of GS specimens in NaCl solutions of different concentrations. Corrosion current densities of GS specimens in 0.1, 1.0 and 4.0 mol dm^{-3} NaCl are 37.6, 28.2 and 9.0 μA cm^{-2}, respectively after 24 h immersion. Figure 3.45 shows the Nyquist plots of GS specimens in NaCl solutions of different concentrations. Nyquist plots obtained in the frequency range of 100 kHz – 10 mHz were not complete. However, recording the EIS at lower frequency (<10 mHz) did not yield satisfactory results as scattered points were observed at very low frequencies. Therefore, equivalent circuits were assigned for the recorded spectra. Nyquist plot of GS in 0.1 mol dm^{-3} NaCl was analyzed by fitting the experimental data with the equivalent circuit shown in Figure 3.46 (a) and Nyquist plots of GS in 1.0 mol dm^{-3} and 4.0 mol dm^{-3} NaCl were analyzed by fitting the experimental data with the equivalent circuit shown in Figure 3.46 (b). R_{ct} values of GS specimens in 0.1, 1.0 and 4.0 mol dm^{-3} NaCl are 215, 281 and 983 Ω, respectively, and C_{dl} of GS in 0.1, 1.0 and 4.0 mol dm^{-3} NaCl are 15.9, 6.7 and 0.5 μF cm^{-2}, respectively, after 24 h immersion. Increase in charge transfer resistance, decrease in corrosion current density and decrease in double layer capacitance with increase in the concentration of NaCl indicate that the corrosion rate and the concentration of NaCl have a reciprocal relationship. Corrosion rate of galvanized steel in NaCl depends on the formation of layer of corrosion products on the galvanized steel surface. The corrosion products of zinc in NaCl solutions could be zinc

hydroxide chloride [$Zn_5(OH)_8(Cl)_2.2H_2O$] and zinc hydroxide carbonate [$Zn_5(CO_3)_2(OH)_6$] [115]. If the layer is more compact then corrosion rate of zinc will be lower. More surface studies have to be conducted to determine the compounds of the corrosion product layer on the galvanized steel surface.

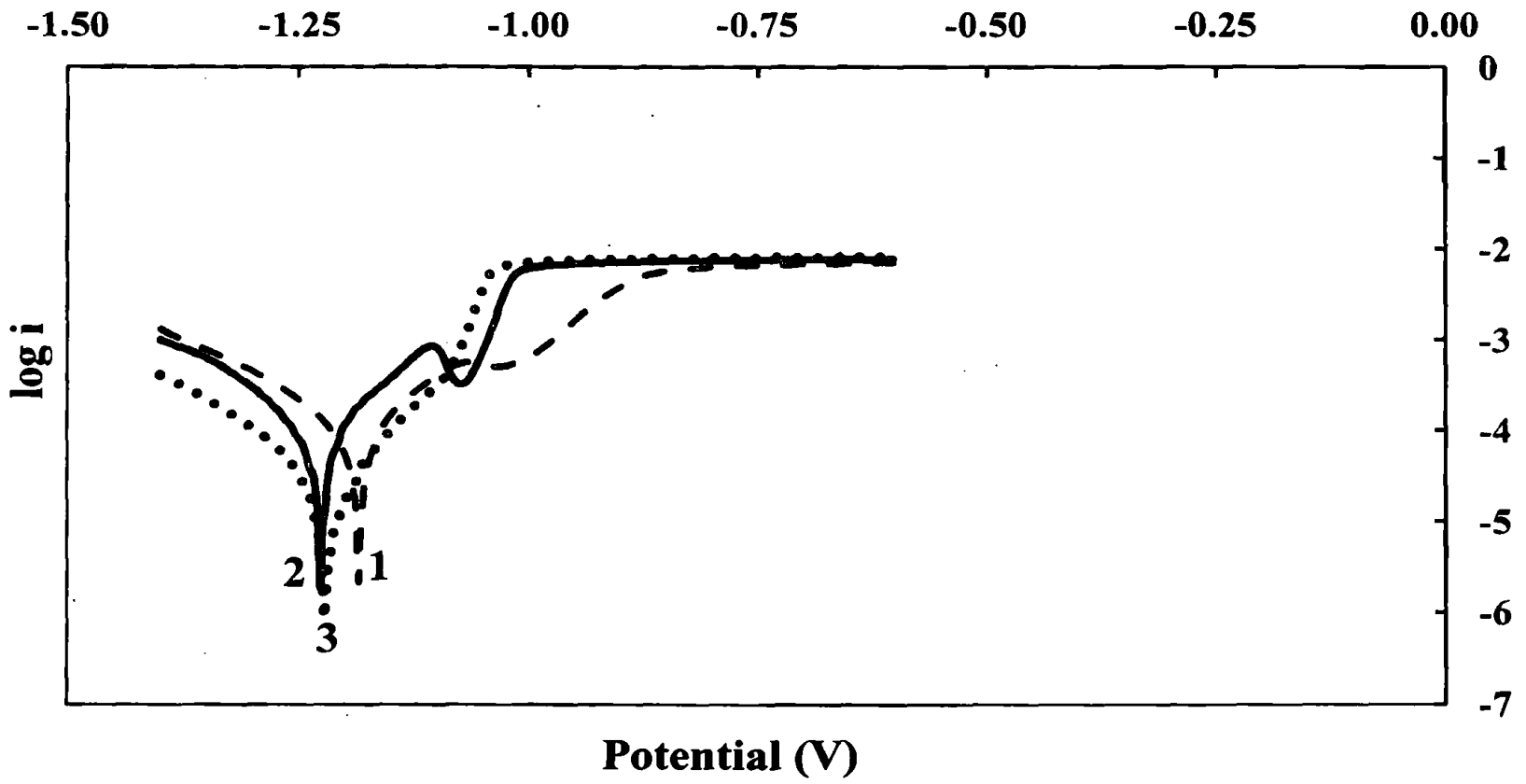

Figure 3.44: Potentiodynamic polarization curves of GS specimens in NaCl solutions of different concentrations (1) 0.1, (2) 1.0 and (3) 4.0 mol dm^{-3} after 24 h immersion.

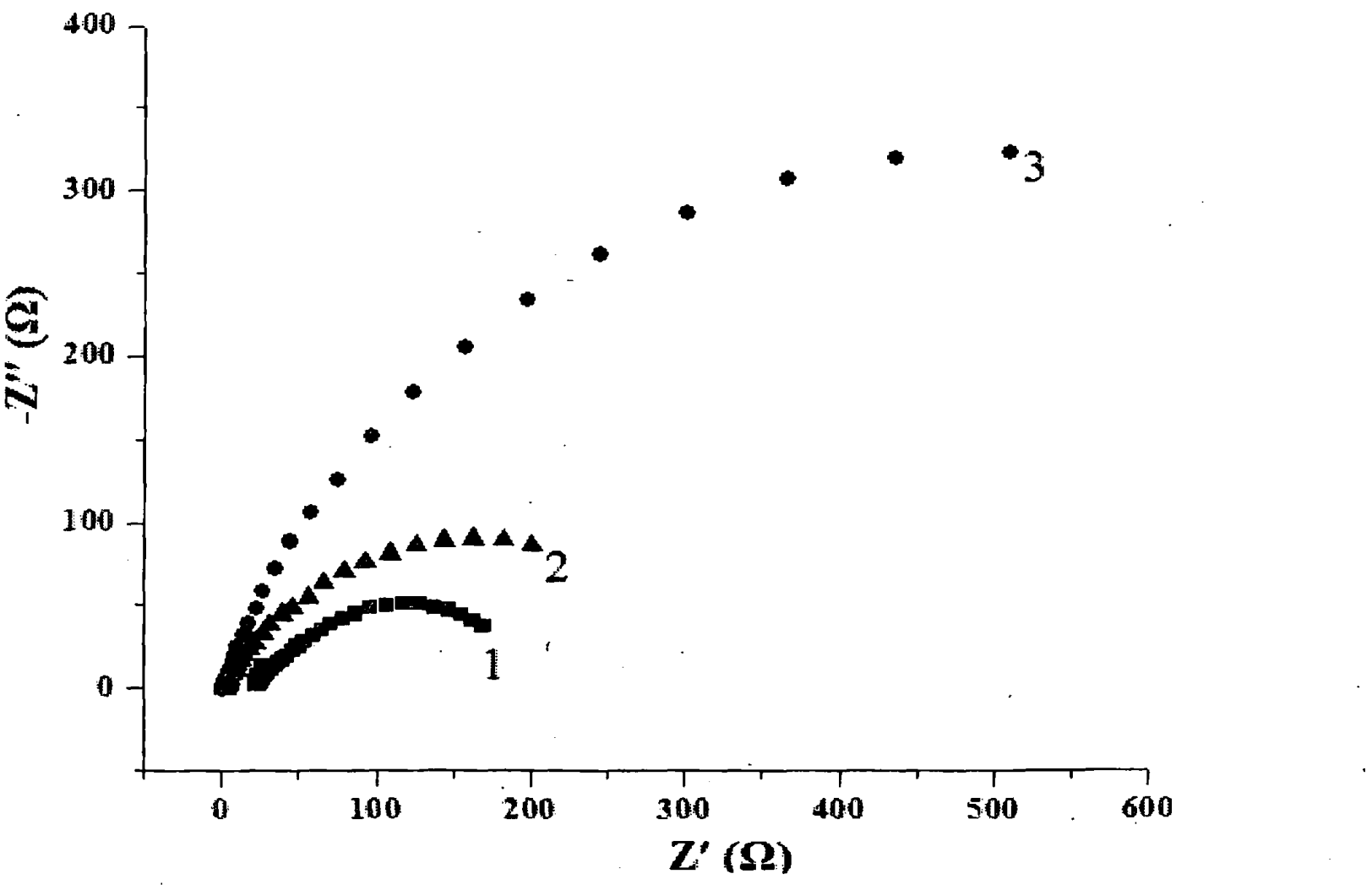

Figure 3.45: Nyquist plots of GS specimens in NaCl solutions of different concentrations (1) 0.1, (2) 1.0 and (3) 4.0 mol dm^{-3} after 24 h immersion.

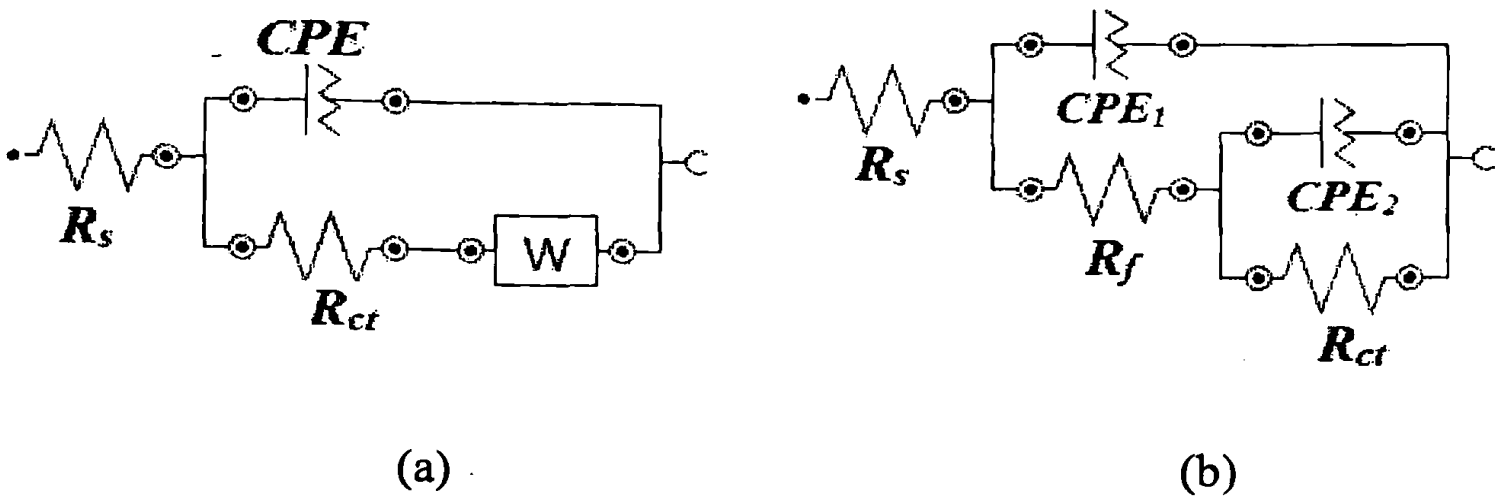

Figure 3.46: Equivalent circuits used to represent GS in NaCl solutions after 24 h immersion.

Corrosion rates of GS in 0.1 and 1.0 mol dm^{-3} NaCl calculated using mass loss measurements, as shown in Table 3.19, also confirm the higher corrosion rate in 0.1 mol dm^{-3} NaCl solutions. The total concentration of Zn in the corrosive medium is higher in 0.1 mol dm^{-3} NaCl solutions. Further, red colored spots were observed on the surface of GS specimens dipped in 0.1 mol dm^{-3} NaCl after 63 days immersion. As white rust is not a protective layer, stagnation of corrosive media would cause localized corrosion of mild steel beneath the zinc layer. Therefore, long time exposure of equipment made up of GS would cause failure in 0.1 mol dm^{-3} NaCl solutions.

Table 3.19: Parameters extracted from mass loss measurements and solution analysis.

Parameters	**After 1 week**		**After 2 weeks**	
	0.1 mol dm^{-3}	**1.0 mol dm^{-3}**	**0.1 mol dm^{-3}**	**1.0 mol dm^{-3}**
Mass loss (mg cm^{-2})	2.16	0.83	5.13	1.19
Mass of precipitate (mg cm^{-2})	3.56	4.16	12.82	7.80
Concentration of Zn (ppm)	3.40	2.95	7.58	6.60
Corrosion rate (mpy)	0.14	0.06	0.16	0.03

3.3.2 Corrosion inhibition of GS in NaCl using tea leaf extracts

Although, corrosion rate of GS is low based on mass loss measurements, white rust deposition on GS surface will facilitate the stagnation of corrosive media, and hence causing localized corrosion attack eventually. Therefore, the addition of corrosion inhibitors is essential for long term use of GS objects. Hence, the effect of tea leaf extracts on corrosion of GS in 0.1 mol dm^{-3} NaCl at different pH values was tested by monitoring the mass loss of GS specimens and change in solution pH. According to mass loss measurements, GS specimens placed in 0.1 mol dm^{-3} NaCl with 5% (v/v) extract show lower mass loss than its corresponding blank solutions and the change in pH of the corrosive medium is lower than that of blank solutions. According to Table 3.20, inhibition effect is higher at pH = 2 and 3 as compared to other pH values.

Table 3.20: Mass loss of GS specimens in 0.1 mol dm^{-3} NaCl and change in pH of corrosive media in the presence and absence of 5% (v/v) tea leaf extracts.

pH	Concentration of inhibitor (% v/v)	Mass loss (mg cm^{-2})			ΔpH		
		24 h	48 h	72 h	24 h	48 h	72 h
1	0	17.7	19.0	19.7	0.07	0.11	0.05
	5	16.3	17.2	17.9	0.03	0.06	0
2	0	1.28	2.16	3.15	0.09	0.96	2.32
	5	0.92	1.79	3.06	0.04	0.67	1.96
3	0	0.36	0.65	0.79	3.58	3.57	3.54
	5	0.33	0.42	0.57	1.22	2.92	3.49
4	0	0.24	0.43	0.53	2.84	3.26	2.95
	5	0.27	0.69	0.77	2.51	2.97	3.21
5	0	0.40	0.74	0.85	1.86	2.27	2.47
	5	0.36	0.72	0.72	1.86	2.23	2.30

3.3.3 Effect of concentration of tea leaf extract on corrosion inhibition of GS in NaCl

As tea leaf extracts show higher inhibition efficiency on the corrosion of GS in 0.1 mol dm^{-3} NaCl at pH = 2 and 3, effect of the concentration of the extract on corrosion inhibition was studied at pH = 2 by monitoring the mass loss of GS and pH of corrosive media. According to mass loss measurements, percentage inhibition efficiency increases with increase in the concentration of tea leaf extract as shown in Table 3.21.

Table 3.21: Effect of concentration of tea leaf extracts on corrosion inhibition of GS in 0.1 mol dm^{-3} NaCl solutions at pH = 2.

Concentration of inhibitor (% v/v)	Mass loss (mg cm^{-2})			ΔpH			% IE		
	24 h	48 h	72 h	24 h	48 h	72 h	24 h	48 h	72 h
0	1.28	2.16	3.15	0.09	0.96	2.28	–	–	–
2.5	1.10	1.86	3.18	0.05	0.66	1.89	14	14	-1
5.0	0.92	1.79	3.06	0.05	0.67	1.90	28	17	3
7.5	0.62	1.03	2.18	0.02	0.48	1.40	52	52	31
10.0	0.54	0.98	1.58	(-)0.05	0.04	0.32	58	55	50

The results obtained from mass loss measurements are further confirmed by electrochemical experiments. Nyquist plots and potentiodynamic polarization curves of GS specimens in the presence and absence of different concentrations of methanol extracts of tea leaves in 0.1 mol dm^{-3} NaCl at pH = 2 are shown in Figure 3.47. R_{ct} values were calculated from the difference in impedance at lower frequency and higher frequency intersections after fitting the experimental electrochemical impedance spectroscopic data to a simple semi-circle. Increase in R_{ct} in the presence of tea leaf extract demonstrates the corrosion inhibition potential of extracts. According to EIS measurements, 10% (v/v) methanol extract shows about 85% inhibition efficiency after 18 h of exposure in the corrosive medium. Percentage inhibition efficiency was calculated using Equation (3.4).

Corrosion current densities in the presence and absence of tea leaf extracts of different concentrations were calculated by extrapolating anodic and cathodic branches of polarization curves towards the corrosion potential. The presence of the extract decreases

both cathodic and anodic current densities, suggesting that the inhibitor acts as a mixed-type inhibitor. However, shift in corrosion potential of GS towards more positive direction suggesting that the retardation of anodic dissolution is more prominent during the inhibition process.

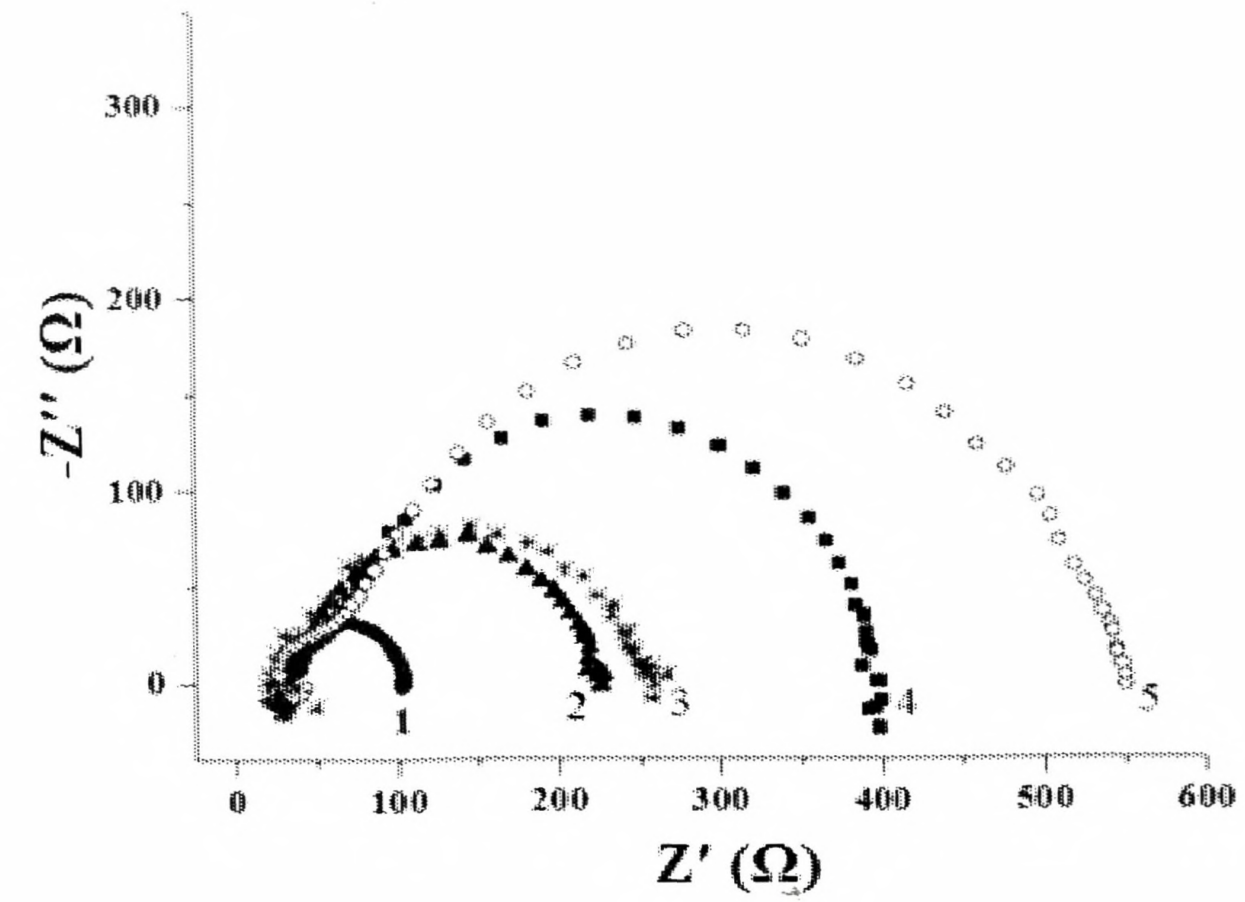

(a)

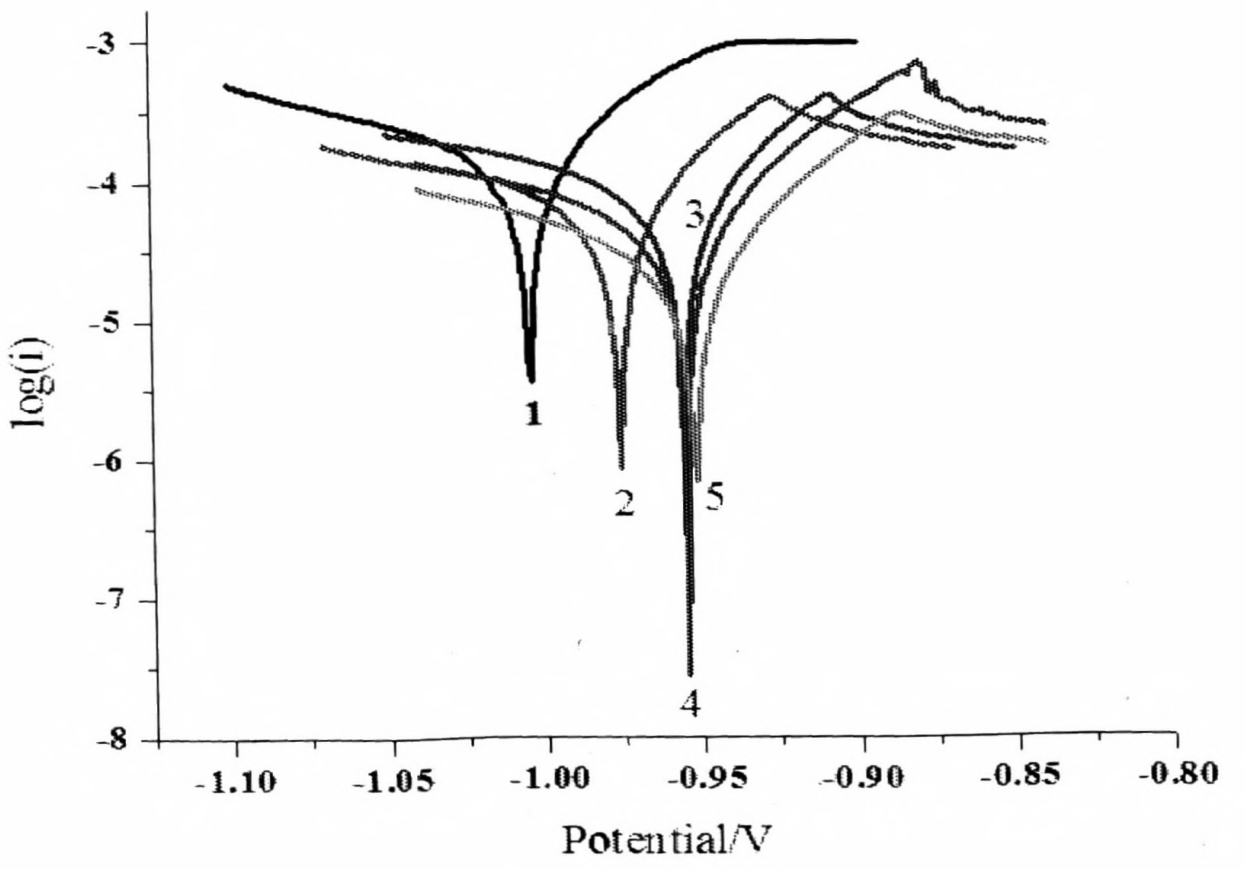

(b)

Figure 3.47: (a) Nyquist plots and (b) potentiodynamic polarization curves of GS specimens in 0.1 mol dm^{-3} NaCl at pH = 2 with tea leaf extracts of different compositions (1) 0, (2) 2.5% (v/v), (3) 5% (v/v), (4) 7.5% (v/v) and (5) 10% (v/v).

3.4 Corrosion of Copper in NaCl Solutions and Its Prevetion

3.4.1 Effect of NaCl on corrosion behavior of copper in NaCl environments

Corrosion rates of copper in NaCl solutions of different concentrations were determined using potentiodynamic polarization curves (Figure 3.48). According to potentiodynamic polarization studies, corrosion rates of Cu in 0.1 and 0.5 mol dm^{-3} NaCl are almost the same, which indicates that the increase in NaCl concentration from 0.1 to 0.5 mol dm^{-3} does not affect the corrosion rate significantly. However, increase in NaCl concentration from 0.1 to 1.0 mol dm^{-3} significantly increases the corrosion rate of copper.

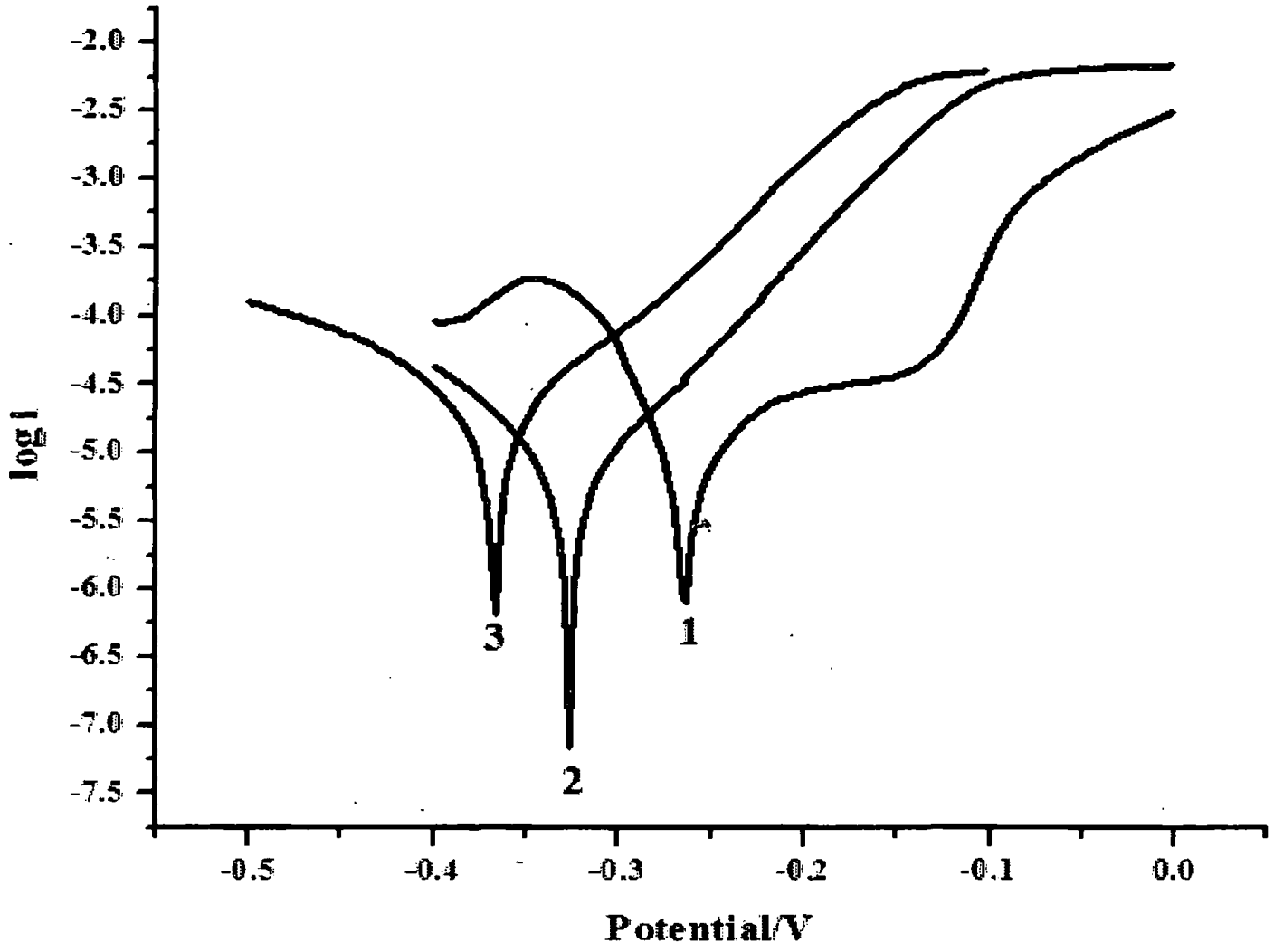

Figure 3.48: Potentiodynamic polarization curves of copper specimens in NaCl solutions of different concentrations (1) 0.1, (2) 0.5 and (3) 1.0 mol dm^{-3} after 24 h immersion.

Table 3.22 shows the potentiodynamic polarization parameters, such as anodic and cathodic Tafel slopes, corrosion potential, corrosion current density and corrosion rate. Although the corrosion rates of copper in 0.1 mol dm^{-3} and 0.5 mol dm^{-3} are similar, corrosion mechanism of copper in 0.1 mol dm^{-3} is probably different from that in 0.5 mol dm^{-3} and 1.0 mol dm^{-3} based on the values obtained for cathodic and anoidic Tafel slopes.

Table 3.22: Electrochemical parameters extracted from potentiodynamic polarization curves.

Concentration of NaCl (mol dm^{-3})	b_a (mV dec^{-1})	b_c (mV dec^{-1})	(-) E_{corr} (mV)	i_{corr} (μA cm^{-2})	CR (mpy)
0.1	61.6	34.8	263.4	2.43	0.028
0.5	68.8	80.7	321.5	2.55	0.029
1.0	77.6	86.7	367.7	5.81	0.067

3.4.2 Corrosion inhibition of copper in NaCl

The electrochemical impedance spectra of copper specimens in 0.1 mol dm^{-3} NaCl solutions without and with tea leaf extracts of different concentrations obtained at V_{oc} after 24 h immersion under air saturated conditions are shown in Figure 3.49. Although the impedance spectra were incomplete, charge transfer resistance can be estimated using the recorded data as a semi-circle observed in the intermediate frequency range. The R_{ct} values of copper specimens in the presence and absence of tea leaf extracts were determined from the difference in impedance at lower frequency and higher frequency intersections of the Nyquist plots obtained by fitting the experimental data to a simple semi-circle. The increase in R_{ct}, in the presence of tea leaf extracts indicates decreased corrosion rates. The corrosion behavior of copper in the absence of the extract is influenced by mass transport since the Warburg impedance is observed in the low frequency region. Impedance spectra obtained in the presence of tea leaf extracts contain depressed semicircles indicating the inhomogenities of the copper specimens. This may be due to the adsorption of components present in the extract on the copper surface. Percentage inhibition efficiencies were calculated using Equation 3.4 are reported in Table 3.23.

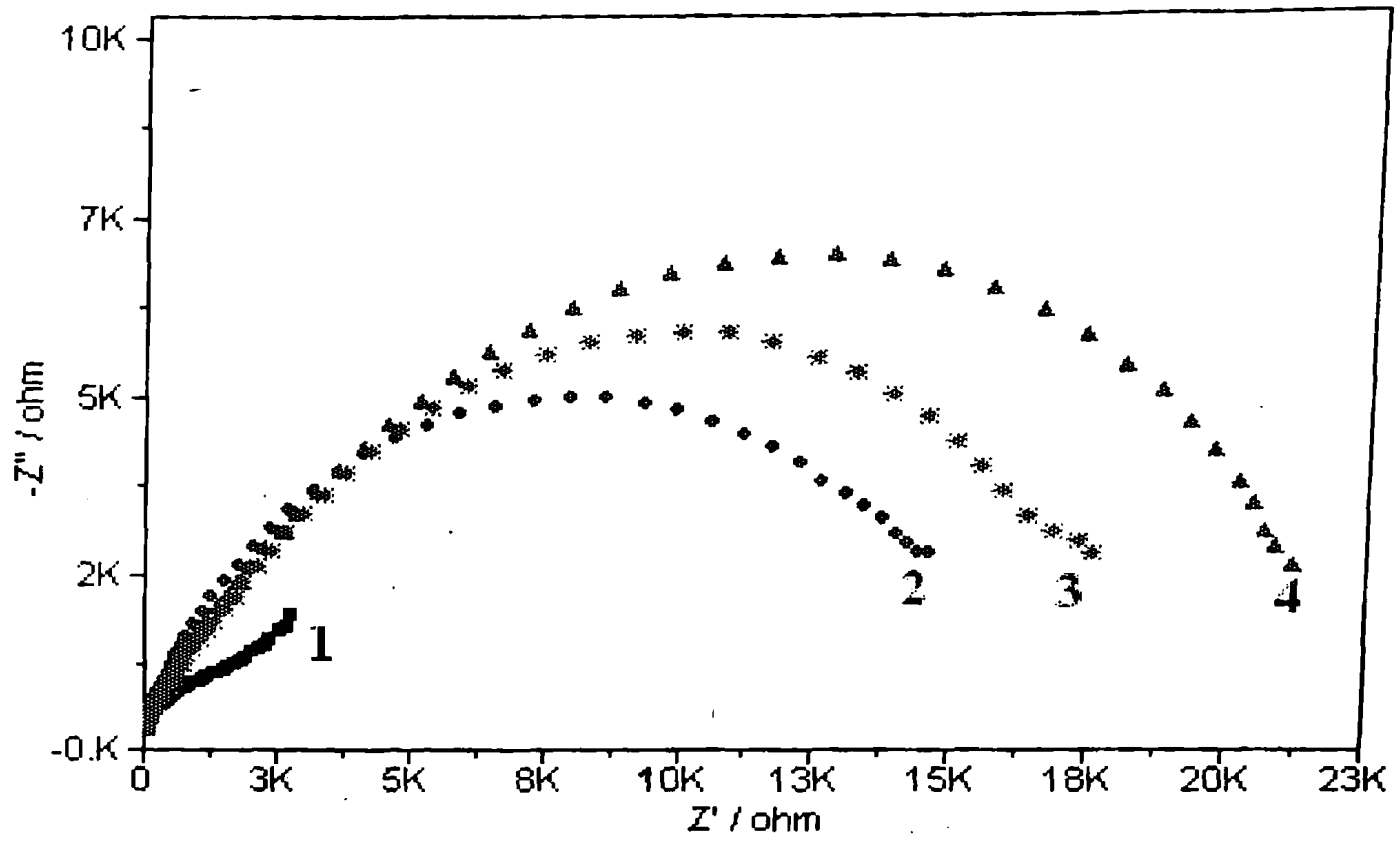

Figure 3.49: Nyquist plots for copper specimens in 0.1 mol dm^{-3} NaCl with tea leaf extracts of different compositions (1) 0, (2) 10%, (3) 15% and (4) 20% (v/v) after 24 h immersion.

Figure 3.50 shows the potentiodynamic polarization curves of copper specimens in 0.1 mol dm^{-3} NaCl solutions without and with tea leaf extracts of different concentrations. Corrosion current density decreases when the concentration of the extract is increased. The percentage inhibition efficiency calculated using Equation (3.5), are reported in Table 3.23.

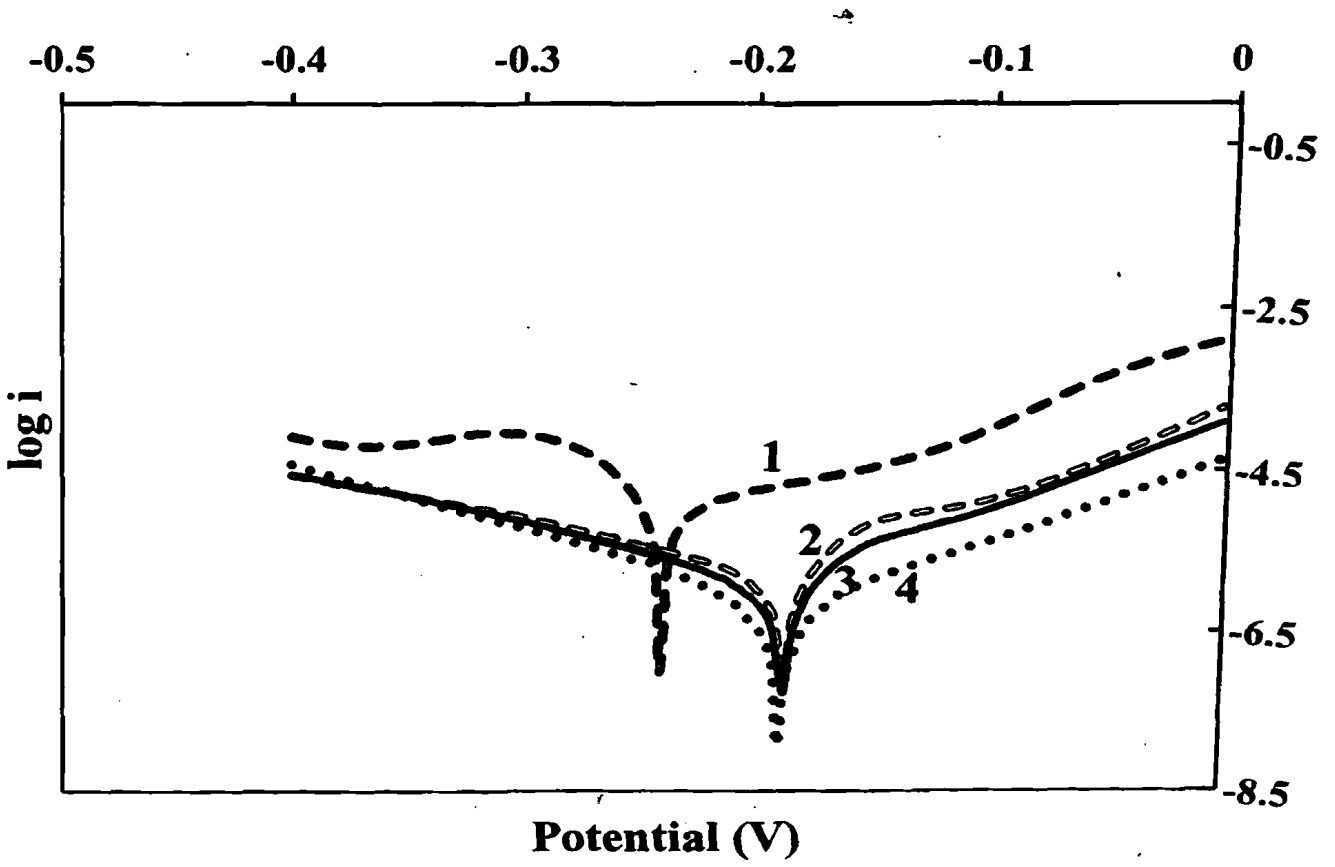

Figure 3.50: Potentiodynamic polarization curves of copper specimens in 0.1 mol dm^{-3} NaCl with (1) 0, (2) 10% (3) 15% and (4) 20% (v/v) methanol extracts of tea leaves after 24 h immersion.

Table 3.23 summarizes the percentage inhibition efficiency achieved with the tea leaf extracts of different concentrations in 0.1 mol dm^{-3} NaCl based on electrochemical measurements.

Table 3.23: Electrochemical parameters of copper specimens in 0.1 mol dm^{-3} NaCl with and without different concentrations of tea leaf extracts.

Concentration of extract (% v/v)	Tafel slope analysis					EIS	
	b_a (mV dec^{-1})	b_c (mV dec^{-1})	(-) E_{corr} (mV)	i_{corr} (μA cm^{-2})	% IE	R_{ct} (Ω)	% IE
0	62.7	35.1	236.4	3.00		3603	
10	41.1	115.3	184.8	0.54	82	15626	77
15	47.0	109.5	183.4	0.40	87	19081	81
20	48.8	95.5	184.3	0.36	88	22794	84

The mass loss of copper specimens was measured in 0.1 mol dm^{-3} in the absence and presence of 20% (v/v) tea leaf extract at pH 1, 2, 3 and 4 as a function of time. The surface coverage (θ) calculated from the mass loss data using Equation (3.7) are shown in Table 3.24. At low pH, rate of dissolution of copper specimen is high, and hence inhibition efficiency is low. At pH = 2 and 3, percentage inhibition efficiency reaches more than 90%. This condition facilitates the dissolution of corrosion products (in blank) away from the metal surface, and hence easier to monitor the mass loss. Although, the dissolution rate of copper in the presence of tea leaf extract at pH 4 is low, percentage inhibition efficiency calculated based on mass loss measurements is low because of the deposition of corrosion products on the copper surface dipped in the blank solution. Therefore, it shows less mass loss than the actual mass loss.

Table 3.24: Mass loss and surface coverage of copper surface in 0.1mol dm^{-3} NaCl with and without tea leaf extarcts at different pH values.

Initial pH	Medium	Mass loss (mg cm^{-2})			Surface coverage (θ)		
		24 h	48 h	72 h	24 h	48 h	72 h
1	Blank	0.58	2.10	5.63	-	-	-
	Extract	0.25	0.59	1.11	0.57	0.72	0.80
2	Blank	0.48	1.35	3.48	-	-	-
	Extract	0.05	0.10	0.13	0.90	0.92	0.96
3	Blank	0.28	0.56	0.86	-	-	-
	Extract	0.02	0.04	0.06	0.93	0.93	0.93
4	Blank	0.03	0.05	0.09	-	-	-
	Extract	0.02	0.02	0.05	0.33	0.60	0.44

The cathodic reaction of copper in aerated sodium chloride solution is the oxygen reduction (Equations 3.18 and 3.19). Figure 3.55 shows the variation of pH of test solutions with and without 20% (v/v) tea leaf extract at different initial pH values. As shown in Figure 3.51, the pH of the corrosive media in the absence of tea leaf extract shows a rapid increase at all initial pH values.

$$O_2(g) + 4H^+(aq) + 4e^- \rightleftharpoons 2H_2O(l) \qquad (3.18)$$

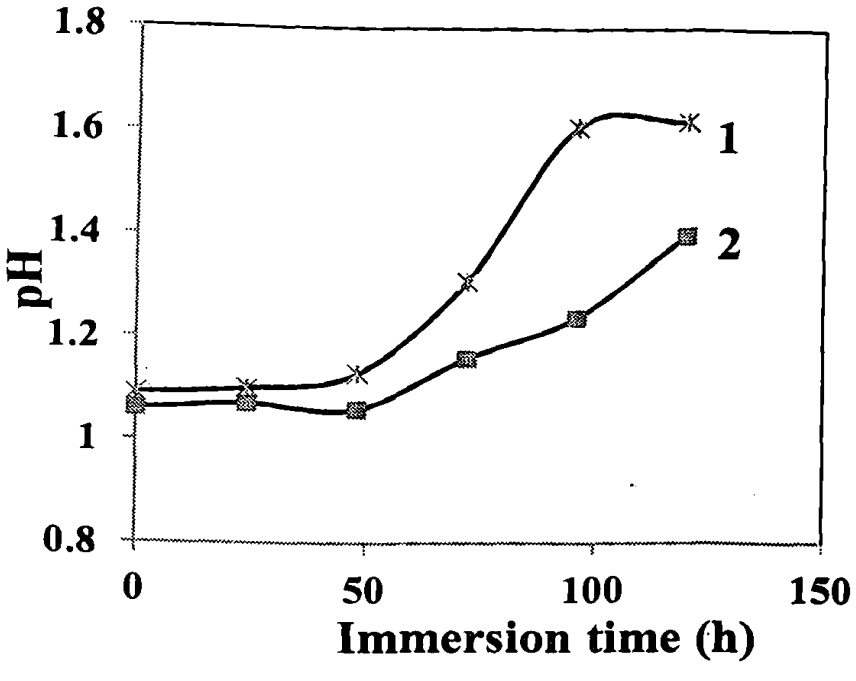

(a)

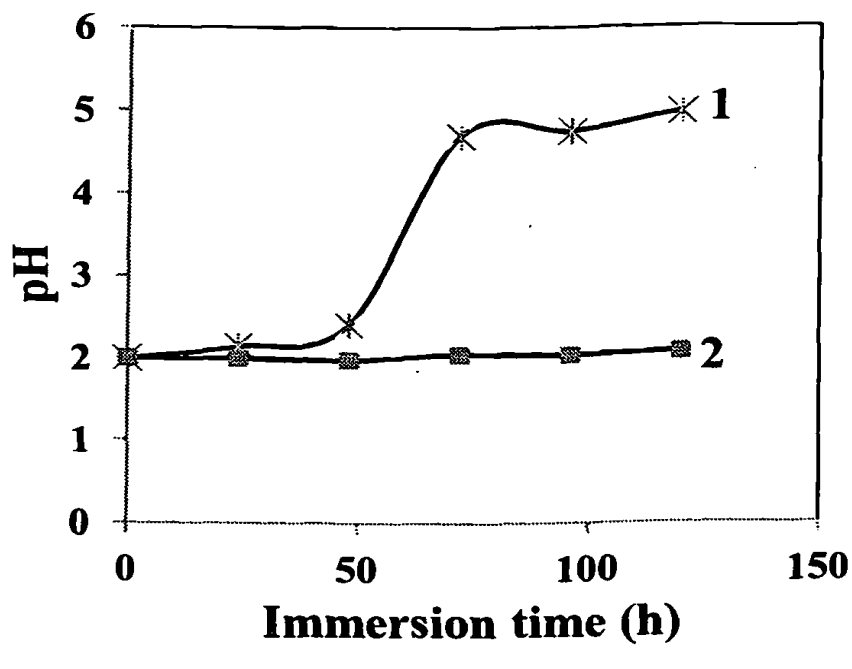

(b)

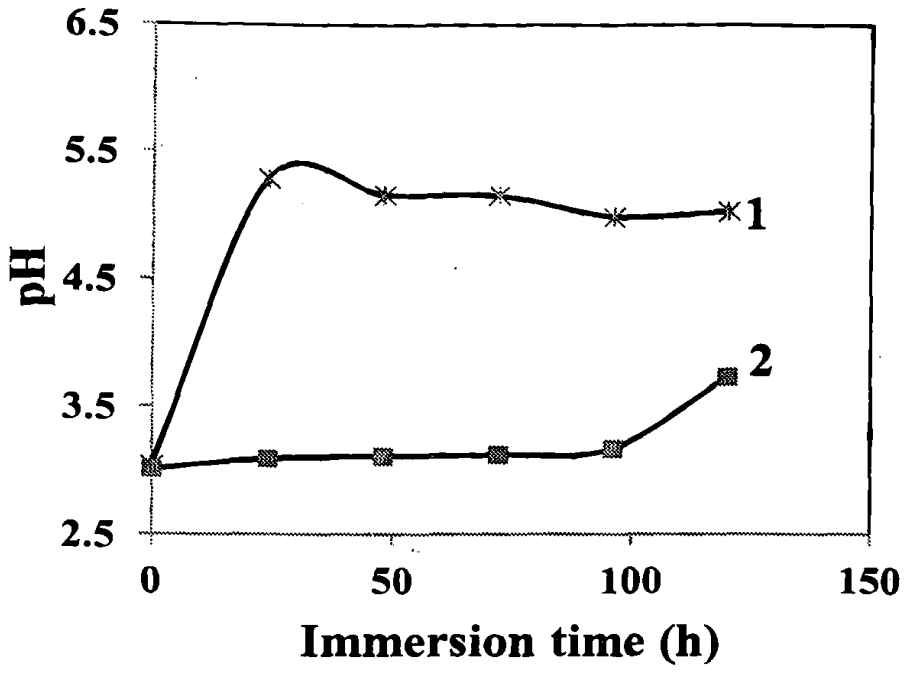

(c)

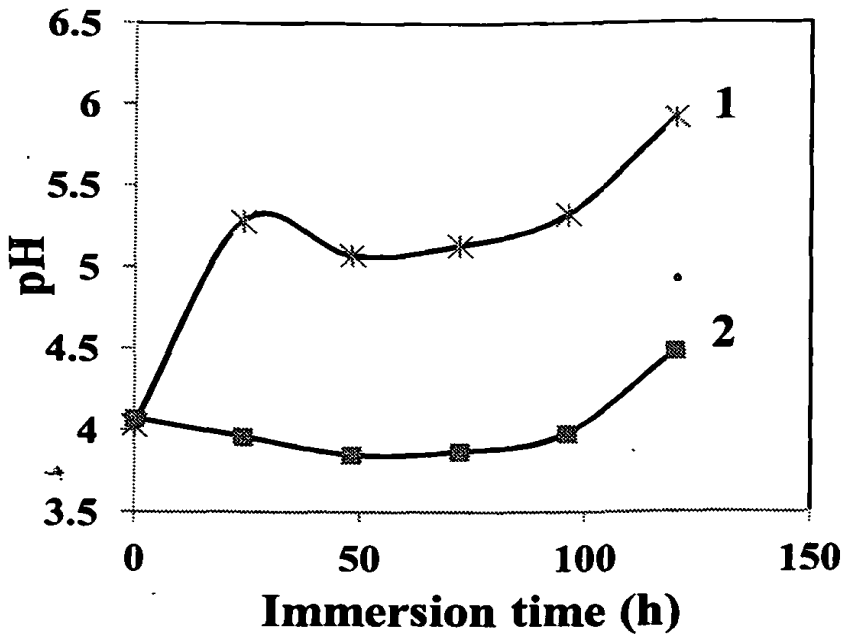

(d)

Figure 3.51: Variation of pH of corrosive media in the presence (1) and absence (2) of 20% (v/v) tea leaf extract at initial pH of (a) 1, (b) 2, (c) 3 and (d) 4.

Caffein and polyphenolic compounds are the major components in the tea leaf extract. It was confirmed that caffein has no effect on the inhibition behavior by examination of synthetic caffein. Therefore, the active components would probably be the polyphenolic compounds. Based on the all experimental results, methanol extracts of matured tea leaves can act as a good inhibitor for corrosion of copper in 0.1 mol dm^{-3} NaCl solutions. Inhibition effect is due to the adsorption of chemical components present in the tea leaf extract.

3.4.3 UV-Vis Spectroscopic studies

Copper specimens dipped in 20% (v/v) extract in 0.1 mol dm^{-3} NaCl adsorbs components of tea leaf selectively. It was confirmed by retrieving the copper specimen after 24 h, washed well with distilled water and then immersed completely in methanol and UV-Vis spectrum was recorded using this methanolic solution (Figure 3.52). According to UV-Vis spectroscopic studies, selective adsorption of certain compounds on the copper surface was confirmed. Therefore, adsorption of certain species found in the tea leaf extracts is responsible for the inhibition effect.

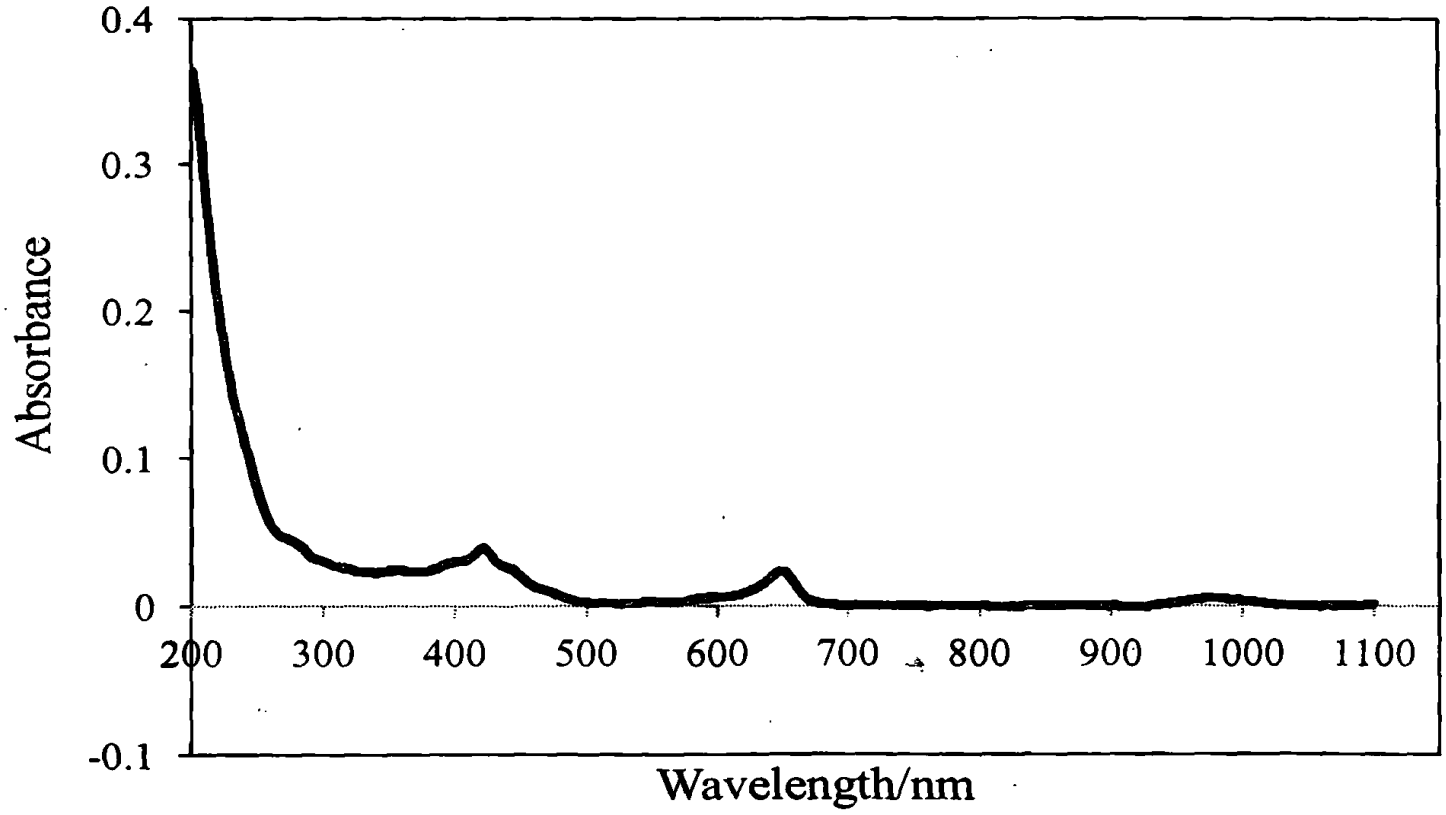

Figure 3.52: UV-Vis spectrum of methanolic solution obtained by dipping the copper specimens in methanol, which had been placed in 20% (v/v) tea leaf extract in 0.1 mol dm^{-3} NaCl.

CHAPTER 4

CONCLUSIONS AND FUTURE DIRECTIONS

The extract of cinnamon leaves (*Cinnamomum zeylanicum*) is found to be an effective corrosion inhibitor for mild steel surfaces in HCl solutions of different concentrations ranging from 0.1 mol dm^{-3} to 2.0 mol dm^{-3}. The data obtained from mass loss measurements and electrochemical measurements are in reasonably good agreement. According to mass loss measurements, more than 90% inhibition efficiency is achieved in the presence of 60.0 g dm^{-3} extract after 24 h immersion in all tested acid concentrations. Inhibition efficiency increases with increase in the concentration of the extract over the range from 3.0 g dm^{-3} to 60.0 g dm^{-3} prepared in 0.5 mol dm^{-3} HCl to reach the maximum efficiency of 96% after 24 h immersion. Cinnamon leaf extracts act as a mixed-type inhibitor based on potentiodynamic polarization studies. The data obtained from all experimental techniques reveal that adsorption of components of the cinnamon leaf extract contributes to corrosion inhibition, which follows the Langmuir isotherm model.

Methanol extracts of matured tea (*Camellia sinensis*) leaves show inhibition effect on corrosion of copper in HCl solutions. The results obtained from all experimental techniques show that methanol extracts show high corrosion inhibition ability in solutions of low acidic concentrations (below 0.05 mol dm^{-3}). Based on all experimental techniques, it can be concluded that the inhibition of corrosion of copper is due to the anti-oxidant capacity of polyphenols present in tea leaves and adsorption of certain components (plant pigments) present in the extract. As antioxidant capacity is higher in hydrochloric acid of low concentrations, cathodic reaction is controlled preferentially in dilute acid solutions. Further, completion of adsorption of tea leaf extract takes place in low acidic medium. As the antioxidant capacity of tea leaf extracts decreases with the increase in the concentration of acid, inhibition process highly depends on adsorption of components in the extract on the copper surface. However, long term exposure of copper plates leads to the interaction with the caffeine present in the extract and leads to less inhibition. Therefore, removal of caffeine in the extract improves the corrosion inhibition property of the extract in highly acidic medium.

Corrosion behavior of GS in 0.1 mol dm^{-3} NaCl in the presence and absence of the methanol extract of tea leaves was studied at ambient temperature at different pH levels. Results obtained from all experimental techniques reveal that the corrosion inhibition

ability of tea leaf extracts on GS corrosion in 0.1 mol dm^{-3} NaCl is higher at pH = 2 and 3. According to EIS results, about 85% inhibition is achieved with the introduction of 10% (v/v) tea leaf extract to 0.1 mol dm^{-3} NaCl at pH = 2. Inhibition efficiency can be improved by increasing the concentration of the extract and by concentrating the active component in the extract.

Inhibition effect of methanol extracts of tea leaves on the corrosion of copper in 0.1 mol dm^{-3} NaCl was investigated using electrochemical techniques. Based on EIS results, presence of 20% (v/v) methanol extract shows 84% inhibition efficiency after 24 h immersion. According to mass loss measurements, the maximum inhibition efficiency of 93% is achieved with the introduction of 20% (v/v) extract at pH = 3 after 24 h immersion. Rapid change in the pH of the corrosive medium in the absence of the extract at all pH values demonstrates the inhibition ability of tea leaf extracts and corrosion inhibition due to adsorption of components in the tea leaf extract.

According to this study, it is concluded that cinnamon leaf extracts are considered as a source of relatively cheap, eco-friendly and effective corrosion inhibitor for mild steel in HCl. Tea leaf extracts can be considered as a corrosion inhibitor for copper in 0.05 mol dm^{-3} HCl and 0.1 mol dm^{-3} NaCl. Corrosion inhibition of galvanized steel by using tea leaves extract can be achieved at pH = 2. Therefore, it is proposed that research should be continued to,

- Develop methods to extract the active component in cinnamon leaves and optimize experimental conditions for industrial applications.
- Increase the inhibition efficiency by concentrating the active components in tea leaf extracts in HCl solutions of higher concentrations.
- Identify the corrosion inhibition mechanism of tea leaf extract on corrosion of GS.

CHAPTER 5

REFRENCES

1. Shreir, L.L., Jarman, R.A., Burstein, G.T., (Ed), *Corrosion Metal/Environment Reactions*, Third edition, Vol. 1, Butterworth, **1994**, 1:4 - 4:50.
2. Levine, I., *Physical Chemistry*, Fifth edition, Tata McGraw Hill Publishing Company Limited, New Delhi, **2002**, 413.
3. Perez, N., *Electrochemistry and Corrosion Science*, Kluwer Academic Publishers, Boston, **2004**, 3-22.
4. Bardal, E., Drugli, J.M., *Materials Science and Engineering Corrosion Detection and Diagnosis,* Encyclopedia of Life Support Systems, Eolss Publishers, Oxford, **2004**, 1-23.
5. Craig, B.D., Lane, R.A., Rose, D.H., *Corrosion Prevention and Control: A Program Management Guide for Selecting Materials,* Alion Science and Technology, Virginia,**2006**, 74-77.
6. El Abedin, S.Z., *J. Appl. Electrochem.* **2001**, *31*, 711-718.
7. Scully, J.C., *The Fundamentals of Corrosion,* Tergamon Press Ltd., Oxford, **1968,** 85-90.
8. Kadry, S., *Eur. J. of Sci. Res.* **2008**, *22*(4), 508-516.
9. Virtanen, S., Milosev, I., Gomez-Barrena, E., Trebse, R., Salo, J., Konttinen, Y.T., *Acta Biomater.* **2008**, *4*, 468–476.
10. Abdulsalam, M.I., *Corros. Sci.* **2005**, *47*, 1336-1351.
11. Rihan, R.O., Nesic, S., *Corros. Sci.* **2006**, *48*, 2633-2659.
12. Logan, H.L., *J. Res. Natl. Bureau Stand.* **1952**, *48*, 99-105.
13. Office of Environmental Information, *Report on the Corrosion of Certain Alloys*, United States Environmental Protection Agency, Washington, **2001**, 4-64.
14. Hamdy, A., Farag, A.B., El-Bassoussi, A.A., Salah, B.A., Ibrahim, O.M., *World. Appl. Sci. J.* **2010**, *8*, 565-571.
15. Li, L., Qu, Q., Bai, W., Chen,Y., Zhang, S., Gao, G., Ding, Z., *Int. J. Electrochem. Sci.* **2012**, *7*, 3773-3786.
16. Li, Y., *Bull. Mater. Sci.* **2001**, *24*(4), 355-360.
17. Hamah-Ali, B., Ali,B.S., Yusoff, R., Aroua, M.K., *Int. J. Electrochem. Sci.* **2011**, *6* 181-198.

18. Abelev, E., Sellberg, J., Ramanarayanan, T.A., *J. Mater. Sci.* **2009**, *44*, 6167-6181.
19. Guiamet, P.S., Saravia, S.G.G.D., *Lat. Am. Appl.Res.* **2005**, *35*, 295-300.
20. Gonzalez, J.E.G., Santana, F.J.H., Mirza-Rosca, J.C., *Corros. Sci.* **1998**, *40*(12), 2141-2154.
21. Beech, I.B., *Microbiology Today*, **2003**, *30*,115-117.
22. Osarolube, E., Owate, I.O., Oforka, N.C., *Sci. Res. Essays* **2008**, *3*(6), 224-228.
23. Escriva-cerdan, C., Blasco-Tamarit, E., Garcia-Garcia, .M., Garcia-Anton, J., Ben-Bachir, A., *Int. J. Electrochem. Sci.* **2012**, *7*, 5754-5764.
24. Umoren, S.A., *Open Corros. J.* **2009**, *2*, 175-188.
25. Kumar, K.P.V., Pillai, S.N., M., Thusnavis, G.R., *J. Mater. Environ. Sci.* **2010**, (2), 119-128.
26. Idenyi, N. E., Ekuma, C. E., Owate, I. O., Okeke, C. E., *Chalcogenide Lett.* **2009**, *6*, 367 – 376.
27. Frankel, G.S., *J. ASTM Int.* **2008**, *5*(2), 1-27.
28. Ramesh, S., Rajeswari, S., Maruthamuthu, S., *Appl. Surf. Sci.* **2004**, *229*, 214-225.
29. Noor, E.A., Al-Moubaraki, A.H., *Int. J. Electrochem. Sci.* **2008**, *3*, 806-818.
30. Luca, P., *Electrochemical Impedance Spectroscopy*, Basic theory, instrumental considerations and applications work shop, Metrohm, Postgraduate Institute of Science, **2011**.
31. Walter, G.W., *Corros. Sci.* **1986**, *26*(9), 681-703.
32. Song, H. W., Saraswathy, V., *Int. J. Electrochem. Sci.* **2007**, *2*,1- 28.
33. Gopi, D., Manimozhi, S., Kovindaraju, K.M., Manisankar, P., Rajeswari, S., *J. Appl. Electrochem.* **2007**, *37*, 439–449.
34. Rajappa, S.K., Venkatesha, T.V., Praveen, B.M., *Bull. Mater. Sci.* **2008**, *31*(1), 37–41.
35. Shreir, L.L., (Ed), *Corrosion Metal/Environment Reactions*, Third edition, Vol. 2, Butterworth, **1994**, 17:3-10.
36. Shibli, S.M.A., Saji, V.S., *Chem. Ind.Dig.* **2002**, *1*, 74-80.
37. Saji, V. S., *Recent Patents on Corros. Sci.* **2010**, *2*, 6-12.
38. Zin, I.M., *Mater. Sci.* **1999**, *35*(6), 874-878.
39. Durnie, W.H., Kinsella, B.J., De Marko, R., Jefferson, A., *J. Appl. Electrochem.* **2001**, *31*, 1221-1226.
40. Rubim, J., Guts, I.G.R., Sala, A., Orville Thomas, W.J., *J. Mol. Struct.* **1983**, *100*, 571- 583.

41. Bastidas, J.M., Pinilla, P., Cano, E., Polo, J.L., Miguel, S., *Corros. Sci.* **2003**, *45*, 427-449.

42. Zin, I. M., Lyon, S.B., Pokhmorskii, V.I., *Corros. Sci.* **2003**, *45*, 777-788.

43. Hosseini, S.M.A., Azimi, A., Sheikhshoaei, I., Salari, M., *J. Iran. Chem. Soc.* **2010**, *7*, 799-806.

44. Arab, S.T., Al--Turkustani, A.M., *Port. Electrochim. Acta* **2006**, *24*, 53-69.

45. Prabhu, R.A., Venkatesha, T.V., Shanbhag, A.V., Kulkarni, G.M., Kalkhambkar, R.G., *Corros. Sci.* **2008**, *50*, 3356–3362.

46. Cao, K., Li, W., Yu, L., *Int. J. Electrochem. Sci.* **2008**, *7*, 806-818.

47. Musa, A.Y, Kadhum, A.A.H, Takriff, M. S., Daud, A.R., Kamarudin, S.K., *Aust. J. Basic Appl. Sci.* **2008**, *2*(4), 956-960.

48. Chaieb, E., Bouyanzer, A., Hammouti, B., Benkaddour, M., *Appl.Surf. Sci.***2005**, *246*, 199–206.

49. Wahdan, M.H., Hermas, A.A., Morad, M.S., *Mater. Chem. Phys.* **2002**, *76*, 111–118.

50. Bentiss, F., Lagrenée, M., *J. Mater. Environ. Sci.* **2011**, *2*(1), 13-17.

51. Dubey, A.K., Singh, G., *Port. Electrochim. Acta* **2007**, *25*, 221-235.

52. Kumar, S.H., Karthikeyan,S., *J. Mater. Environ Sci.* **2012**, *3*(5), 925-934.

53. Lopez-Sesenes, R., Gonzalez-Rodriguez, J.G., Casales, M., Martinez, L., Sanchez-Ghenno, J.C., *Int. J. Electrochem. Sci.* **2011**, *6*, 1772-1784.

54. Singh, A.K., Shukla, S.K., Quraishi, M.A., *Int. J. Electrochem. Sci.* **2011**, *6*, 5802-5814.

55. Zhang, Q.B., Hua, Y.X., *Electrochim. Acta* **2009**, *54*, 1881–1887.

56. Sherif, E.M., Park, S.M., *Electrochim. Acta* **2006**, *51*, 4665–4673.

57. Zhang, D., Gao, L., Zhou, G., *Corros. Sci.* **2004**, *46*, 3031-3040.

58. Zhang, D., Gao, L., Zhou, G., Zhou, G.D., *J. Appl. Electrochem.* **2005**, *35*, 1081–1085.

59. Sherif, E.M., Erasmus, R.M., Comins, J.D., *J. Colloid Interface Sci.* **2007**, *311*, 144–151.

60. Quartaron, G., Bellomi, T., Zingales, A., *Corros. Sci.* **2003**, *45*, 715–733.

61. Ma, H., Chen,S., Yin, B., Zhao, S., Liu, X., *Corros. Sci.* **2003**, *45*, 867–882.

62. Raj, X.J., Rajendran, N., *Int. J. Electrochem. Sci.* **2001**, *6*, 348-366.

63. Sherif, E.M., Park, S.M., *Corros. Sci.* **2006**, *48*, 4065–4079.

64. Al-Mobarak, N.A., Khaled, K.F., Elhabib, O.A., Abdel-Azim, K.M., *J. Mater. Environ. Sci.* **2010**, *1*(1), 9-19.

65. Kesavan, D., Gopiraman, M., Sulochana, N., *Chem. Sci. Rev. Lett.* **2012**, *1*(1), 1-8.

66. Rafeequee, M.Z.A., Khan, S., Saxena, N., Quraishi, M.A., *J. appl. Electrochem.* **2009** *39*, 1409–1417.

67. Nofrizal, S., Rahim, A.A., Saad, B., Bothiraja, P., Affaizza, Shah, M., Yahya, S., *Metall. Mater. Trans.* **2012**, *43* A, 1382-1393.

68. Khaled, K. F., *J.Solid State Electrochem.* **2009**, *13*, 1743–1756.

69. Raja, P.B., Sethuraman, M.G., *Mater. Lett.* **2008**, *62*, 113-116.

70. Oguzie, E. E., *Corros. Sci.* **2008**, *50*, 2993–2998.

71. Hussin, M.H., Kassim, M.J., *J. Phys. Sci.* **2010**, *21*(1), 1-13.

72. Quraishi, M.A., Singh, A., Singh, V.K., Yadav, D.K., Singh, A.K., *Mater. Chem. Phys.* **2010**, *122*, 114-122.

73. Al-Turkustani, A.M., Arab, S. T., Al- Reheli, A.A., *Int. J. Chem.* **2010**, *2*(2), 54-76.

74. Ashassi-Sorkhabi, H., Seifzadeh, D., *Int. J. Electrochem. Sci.* **2006**, *1*, 92-98.

75. Orubite-Okorosaye, K., Jack, I.R., Ochei, M. and Akaranta A. O., *J. Appl. Sci. Environ. Manage.* **2007**, *11*(2), 27-31.

76. Okafor1, P.C., Ebenso, E.E., Ekpe, U.J., *Int. J. Electrochem. Sci.* **2010**, *5*, 978 – 993.

77. Noor, *E.A., Int. J. Electrochem. Sci.* **2007**, *2*, 996 – 1017.

78. El-Etre, A.Y., Abdallah, M., El-Tantawy, Z.E., *Corros. Sci.* **2005**, *47*, 385–395.

79. Saratha, R., Priya, S.V., Thilagavathy, P., *E-J. Chem.* **2009**, *6*(3), 785-795.

80. El-Etre, A.Y., Abdallah, M., *Corros. Sci.* **2000**, *42*, 731-738.

81. Benabdellah, M., Benkaddour, M., Hammouti, B., Bendahhou, M., Aouniti, A., *Appl. Surf. Sci.* **2006**, *252*, 6212–6217.

82. Bouyanze, A., Hammouti, B., Majidi, L., *Mater. Lett.* **2006**, *60*, 2840–2843.

83. Loto, C.A., *J. Mater. Environ. Sci.* **2011**, *2* (4), 335-344.

84. Okafor, P.C., Ikpi, M.E., Uwaha, I.E., Ebenso, E.E., Ekpe, U.J., Umoren, S.A., *Corros. Sci.* **2008**, *50*, 2310–2317.

85. Lebrini, M., Robert, F., Roos, C., *Int. J. Electrochem. Sci.* **2011**, *6*, 857-859.

86. Saratha, R., Vasudha, V.G., *E-J. Chem.* **2009**, *6*(4), 1003-1008.

87. Gunasekaran, G., Chauhan, L.R., *Electrochim. Acta* **2004**, *49*, 4387–4395.

88. Rani, P. D., Selvaraj, S., *Arch. Appl. Sci. Res.* **2010**, *2* (6), 140-150.

89. Rani, P. D., Selvaraj, S., *J. Phytol.* **2010**, *2*, 58–64.

90. Osarolube, E., Owate, I. O. and Oforka, N. C., *Sci. Res. Essays* **2008**, *3* (6), 224-228.

91. Colla, V., Matarese, N., Nastasi, G., *Int. J. Soft Comput. Software Eng.* **2001**, *1*(1), 9-17.

92. Davis, J.R., ASM Speciality handbook: Copper and Copper alloys, ASM international, **2001**, Available from: books.google.lk/books?isbn=0871707268 (accessed on 02.03.2013).

93. Sherif, E.M. and Park, S., *Electrochim. Acta*, **2006**, *51*, 4665-4673.

94. Paranagama, P.A., Wimalasena, S., Jeyatilake, G.S., Jayawardena, A.L., Senanayake, U.M., Mubarak, A.M., *J. Nat. Sci. Found. Sri Lanka* **2001**, *29*(3-4), 147-153.

95. Saliyan, V.R., Adhikari, A.V., *Bull. Mater. Sci.* **2008**, *31*(4), 699–711.

96. Bentiss, F., Gassama, F., Barbry, D., Gengembre, L., Vezin, H., lagrenee, M., Treisnel, M., *Appl. Surf. Sci.* **2006**, *252*, 2684–2691.

97. Hampson, N.A., Karunathilaka, S.A.G.R., Leek, R., *J. Appl. Electrochem.* **1980**, *10*, 3-11.

98. Quraishi, M.A., Sudheer, Ebenso, E.E., *Int. J. Electrochem. Sci.* **2012**, *7*, 9920-9932.

99. Quraishi, M.A., Sardar, R., *J. Appl. Electrochem.* **2003**, *33*, 1163-1168.

100. Sankar, A., Kumaravel, M., Rameshkumar, S., Vijayan, M., *Int. J. Chem. Appl.* **2012**, *4*(2), 137-148.

101. Martinez, S., Stern, I., *J. Appl. Electrochem.* **2001**, *31*, 973-978.

102. Khaled, K.F., Babic-Samardzija, K., Hakerman, N., *J. Appl. Electrochem.* **2004**, 34, 697-704.

103. Metikos-Hukovica, M., Babic, R., Grubac, Z., *J. Appl. Electrochem.* **1998**, *28*, 433-439.

104. Satar, M.Z.M, Noor, M.F.M, Samsudin, M.W., Oathman, M.R., *Int. J. Electrochem. Sci.* **2012**, *7*, 1958-1967.

105. Singh, A.K., Ebenso, E.E., Quraishi, M.A., *Int. J. Electrochem. Sci.* **2012**, *7*, 2320-2333.

106. Ridhwan, A.M., Rahim, A.A., Shah, A.M., *Int. J. Electrochem. Sci.* **2012**, *7*, 8091-8104.

107. Umoren, S.A., Eduok, U.M., Oguzie, E.E., *Port. Electrochim. Acta* **2008**, *26*(6), 533-546.

108. Umoren, S.A., Li, Y., Wang, F.H., *Corros. Sci.* **2010**, *52*, 2422–2429.

109. Oguzie, E.E., Li, Y., Wang, F.H., *J.Colloid Interface Sci.* **2007**, *310*, 90-98.

110. Akalezi, C.O., Enenebaku, C.K., Oguzie, E.E., *Int. J. Ind. Chem.* **2012**, 3:13.

111. Avdeev, Y.G., Gorichev, I.G., Luchkin, A.Y., *Int. J. corros. Scale Inhib.* **2012**, *1*(1), 26–37.

112. Al-Mobarak, N.A., *Int. J. Electrochem. Sci.* **2008**, *3*, 666 – 675.

113. Li, W., Bai,X., Yang, F., Hou, B., *Int. J. Electrochem. Sci.* **2012**, *7*, 2680-2694.

114. Apetrei, C.L., Tuchilus, C., Aprotosoaie, A. C., Oprea, A., Malterud, K.E., Miron, A., *Mol.* **2011**, *16*, 7773-7788.

115. Mounga, M., Bercot, P., Rauch, J.Y., *Corros. Sci.* **2010**, *52*(12), 3986-3992.

116. Bard, A.J., Electrochemical Methods Fundamentals and Applications, Second Edition, New York, **1994**, 87-103, 368-388.

117. Wang, J., Analytical Electrochemistry, Second Edition, A John Wiley & Sons, INC., Publication, New York, **2001**. 11-15.

ANNEXURE

Table A.1: List of synthetic compounds reported for the inhibition of different metals in different corrosive media.

Metal	Medium	Method used	compound	Optimum concentration of inhibitor (mol dm^{-3})	Temperature (°C)	Maximum inhibition efficiency (%)	Ref. No
302 stainless steel	0.5 mol dm^{-3} H_2SO_4	ML	2,2′-[bis-N(4-chlorobenzaldimin)]-1,1′-dithio	1.62×10^{-4}	20 ± 1	92.5	[43]
		PDP				92.5	
		ML	bis-(2-aminophenyl) disulphide	3.2×10^{-4}		72	
		PDP				72	
Mild steel	2.0 mol dm^{-3} H_3PO_4	HE	Phenacyl dimethyl sulphonium bromide	5×10^{-3}	30	68.32	[44]
			4-Methylphenacyl dimethyl sulphonium bromide			84.25	
			4-Chlorophenacyl dimethyl sulphonium bromide			68.76	
			4-Bromophenacyl dimethyl sulphonium bromide			45.58	
			4-Nitrophenacyl dimethyl sulphonium bromide			84.78	
			4-Methoxyphenacyl dimethyl sulphonium bromide			68.14	
		ML	Phenacyl dimethyl sulphonium bromide			68.76	
			4-Methylphenacyl dimethyl sulphonium bromide			84.82	
			4-Chlorophenacyl dimethyl sulphonium			68.05	

			bromide				
			4-Bromophenacyl dimethyl sulphonium bromide			46.46	
			4-Nitrophenacyl dimethyl sulphonium bromide			84.69	
			4-Methoxyphenacyl dimethyl sulphonium bromide			66.77	
			Phenacyl dimethyl sulphonium bromide			66.39	
			4-Methylphenacyl dimethyl sulphonium bromide			84.71	
			4-Chlorophenacyl dimethyl sulphonium bromide			69.41	
		PDP	4-Bromophenacyl dimethyl sulphonium bromide			74.96	
			4-Nitrophenacyl dimethyl sulphonium bromide			79.83	
			4-Methoxyphenacyl dimethyl sulphonium bromide			67.9	
			Phenacyl dimethyl sulphonium bromide			54.77	
			4-Methylphenacyl dimethyl sulphonium bromide			59.72	
		EIS	4-Chlorophenacyl dimethyl sulphonium bromide	1×10^{-3}		57.96	
			4-Bromophenacyl dimethyl sulphonium bromide			39.67	
			4-Methoxyphenacyl dimethyl sulphonium bromide			62.46	
Mild steel	1.0 mol dm^{-3}	Ml	4-{[(1E)-(2-chloroquinoline-3-yl]	3×10^{-4}	27	96	[45]

	HCl	PDP	methylene]amino}phenol			97	
		EIS				97	
		Ml				92	
		PDP	N-[(1E)-(2-chloroquinolin-3-yl)methylene] -N-(4-methoxyphenyl)amine			92	
		EIS				93	
		Ml				85	
		PDP	N-[(1E)-(2-chloroquinolin-3-yl)methylene] -N-(4-nitrophenyl)amine			86	
		EIS				85	
		ML				93	
Mild steel	1.0 mol dm^{-3} HCl	EIS	1-phenyl-3-methyl-5-pyrazolone	1×10^{-3}	25	97	[46]
		PDP				91.3	
		ML				17.2	
		EIS	EDTA disodium salt	4.29×10^{-4}		17.07	
		PDP				17.99	
Mild steel	1.0 mol dm^{-3} HCl				30		[47]
		ML				63.75	
		EIS	Thiourea	2.1×10^{-3}		61.95	
		PDP				61.8	
		ML				80	
		EIS	Euginol	1.5×10^{-3}		74	
Steel	1.0 mol dm^{-3} HCl	PDP			25	64	[48]
		ML				91	
		EIS	Acetyleuginol	8.388×10^{-4}		80.5	

		PDP				75	
Pure iron						86	
0.1% C-steel	Deaerated					90	
0.5% C-steel	1 mol dm^{-3} H_2SO_4	PDP	Propargyltriphenylphosphonium bromide	1×10^{-3}	30	89	[49]
1.0% C-steel						85	
			2,5-bis(4-dimethyl aminophenyl)-1,3,4-oxadiazole			89.8	
			2,5-bis(4-dimethyl aminophenyl)-1,3,4-thiadiazole			93.9	
			2,5-bis(4-nitrophenyl)-1,3,4-oxadiazole			7.4	
Mild steel	1 mol dm^{-3} HCl	EIS	2,5-bis(4-aminophenyl)-1,3,4-oxadiazole	1×10^{-4}	30 ± 1	97.9	[50]
			3,5-diphenyl-4H-1,2,4-triazole			92.5	
			3,5-di(4-chloro)phenyl-4H-1,2,4-triazole			10.6	
			3,5-di(4-pyridyl)phenyl-4H-1,2,4-triazole			95.2	
			3,5-di(4-methylthiophenyl)-4H-1,2,4-triazole			99.1	
					25	84.2	
Mild steel	0.5 mol dm^{-3} H_2SO_4	PDP	Polyethylene glycol methyl ether	1×10^{-3}	35	90	[51]
					45	86	
					55	87.5	
		Ml				81.19	
Mild steel	1 mol dm^{-3} HCl	PDP	Cloxacillin	1.5×10^{-3}		77.55	[52]
		EIS				80.45	

1018 C-steel	0.5 mol dm^{-3} HCl	PDP	monopropianate	2.544×10^{-4}	25 40 60	85.4 66.7 23.3	[53]
Mild steel	0.5 mol dm^{-3} H_2SO_4	Ml PDP EIS	Ceftazidime	4.573×10^{-4}	35 ± 1	87.5 90.2 87.5	[54]
Mild steel	1 mol dm^{-3} HCl	Ml PDP EIS	1-butyl-3-methylimidazolium chlorides	1×10^{-2}	30	86.5 87.5 85.9	[55]
		Ml PDP EIS	1-butyl-3-methylimidazolium hydrogen sulfate			92.5 93.7 93.6	
	Deaerated 0.5 mol dm^{-3} HCl	PDP EIS				81.7 79.8	
Copper	Aerated 0.5 mol dm^{-3} HCl	PDP EIS	N-phenyl-1,4-phenylenediamine	1 × 10-2		83.75 73.6	[56]
	Oxygenated 0.5 mol dm^{-3} HCl	PDP EIS ML				70 68.42 83	

		Ml		1×10^{-3}	40	26.2	
		EIS	benzotriazole	5×10^{-3}		38.63	
		PDP				20.33	
		Ml		1×10^{-3}	40	35	
Copper	0.5 mol dm^{-3} HCl	EIS	2-mercaptobenzoxazole	5×10^{-3}		56.91	[57]
		PDP				34.16	
		Ml		1×10^{-3}	40	91.6	
		EIS	2-mercaptobenzimidazole	5×10^{-3}		68.23	
		PDP				74.9	
		Ml			40	42.7	
		EIS	DL-alanine			60.64	
Copper	0.5 mol dm^{-3} HCl			1×10^{-5}			[58]
		Ml			40	58.7	
		EIS	DL-cystein			64.11	
Copper		ML				71	
		PDP	3-amino-1,2,4-triazole	5×10^{-3}		61	[59]
					25	45.45	
					35	44.33	
		Ml			45	42.42	
					55	43.82	
Copper	0.5 mol dm^{-3} H_2SO_4		Isatin	7.5×10^{-3}			[60]
					25	94	
		PDP			35	94	
					45	92	

					55	94	
Copper	0.5 mol dm^{-3} H_2SO_4	EIS	Cetyltrimethylammonium bromide	1×10^{-4}	22	97.6	[61]
			Sodium dodecyl sulphate			95.3	
			Sodium oleate			93.8	
			Polyoxyethylene sorbitan monooleate			93.2	
		PDP	Cetyltrimethylammonium bromide			90.1	
			Polyoxyethylene sorbitan monooleate			84.5	
		PDP	2-amino-5-ethyl-1,3,4-thiadiazole			89	
		EIS				89	
Brass	Natural sea water	PDP	2-amino-5-ethylthio-1,3,4-thiadiazole	1×10^{-2}		95	[62]
		EIS				95	
		PDP	2-amino-5-tert-butyl-1,3,4-thiadiazole			91	
		EIS				90	
Copper	3.0% NaCl de-aerated	ML	2-amino-5-ethyl-1,3,4-thiadiazole	5×10^{-3}		100	[63]
						41.7	
	aerated	PDP				71.4	
						87.4	
Copper	3.5% NaCl	PDP	2-hydrazino-4-(p-methoxyphenyl) -6-oxo-1,6-dihydropyrimidine-5-carbonitrile	1×10^{-3}	25 ± 1	89.65	[64]
		EIS				91.3	

Table A.2: List of natural products reported for the inhibition of different metals in different corrosive media.

Metal	Medium	Method used	Natural product	optimum concentration	Temperature (°C)	Maximum Inhibition efficiency (%)	Ref. No
Mild steel	1mol dm^{-3} H_2SO_4	HE	Ocimum viridis (leaves)	50% (v/v) (acidic extract)	30	70.2	[70]
			Telferia occidentalis (leaves)			97.3	
			Azadiracta indica (leaves)			93.8	
			Hibiscus sabdariffa (leaves)			93.0	
			Garcinia kola (seeds)			91.0	
	2 mol dm^{-3} HCl		Ocimum viridis (leaves)			71.1	
			Telferia occidentalis (leaves)			94.8	
			Azadiracta indica (leaves)			95.6	
			Hibiscus sabdariffa (leaves)			90.4	
			Garcinia kola (seeds)			93.1	
Mild steel	Aqueous solution pH=5	ML PDP EIS	Uncaria gambir	150 ppm (ethyl acetate extract)	25	67.88 91.79 41.02	[71]
Mild steel	1 mol dm^{-3} HCl	ML PDP	Murraya koenigii (leaves)	600 ppm (aqueous	35	96.66 97.02	[72]

		EIS		extract)		97.54	
	0.5 mol dm^{-3}	ML				94.66	
	H_2SO_4	PDP				96.6	
		EIS				96.44	
		HE				92.62	
		ML		20% (v/v)		91.24	
		EIS		Aqueous	30	80.51	
		PDP		extract)		64.04	
	1.0 mol dm^{-3}	HE		5% (v/v)		92.78	
Mild steel	H_2SO_4	ML	Zyziphus Spina- Christi	(Ethanol		95.07	[73]
	containing		(leaves)	extract)			
	10% ethanol			7% (v/v)			
		EIS		(Ethanol	30	92.94	
				extract)			
		PDP		5% (v/v)		87.11	
				(Ethanol			
				extract)			
					25	94.1	
					35	92.5	
		LP			45	93.01	
					55	96.69	
St-37 steel	1 mol dm^{-3}				65	96.44	
1 cm^2	HCl		Prunus cerasus	4% (V/V)	85	81.02	[74]
			(fully rippened fruit)	(Fruit juice)			
					25	92.69	
		EIS			35	92.37	
					45	94.39	

					55	95.51	
					65	94.15	
					85	84.29	
Mild steel	0.1 mol dm^{-3} HCl	ML	Nypa *fruticans'wurmb*	360 ppm	30	77.31	[75]
	0.5 mol dm^{-3} HCl					74.23	
			Azadiracta indica (leaves)			60.4	
	2 mol dm^{-3} H_2SO_4	ML	Azadiracta indica (root)		30	66.8	
			Azadiracta indica (seeds)	4000 ppm		81.8	
Mild steel			Azadiracta indica (leaves)	(acidic extract)		36.1	[76]
	5 mol dm^{-3} H_2SO_4	HE	Azadiracta indica (root)		30	50.1	
			Azadiracta indica (seeds)			57.0	
					30	90.6	
	2 mol dm^{-3} HCl				40	88.89	
					50	91.25	
					60	91.21	
				10% (v/v)	70	92.27	
Mild steel		ML	Fenugreek (leaves)	(aqueous extract)	30	53.27	[77]
	2 mol dm^{-3} H_2SO_4				40	62.44	
					50	72.64	
					60	73.64	
					70	88.33	

Carbon steel	0.1 mol dm^{-3} HCl					95.78	
	3.5% NaCl					91.01	
	0.1 mol dm^{-3} NaOH					69.56	
Nickel	0.1 mol dm^{-3} HCl	PDP	Lawsonia (leaves)	800 ppm (aqueous extract)	30	88.77	[78]
	3.5% NaCl					82.88	
	0.1 mol dm^{-3} NaOH					73.91	
Zinc	0.1 mol dm^{-3} HCl					76.19	
	3.5% NaCl					93.44	
	0.1 mol dm^{-3} NaOH					76.92	
Mild steel	1 mol dm^{-3} HCl	ML	Citrus aurantiifolia (leaves)	2.5% (v/v) (acidic extract)	30	73.65	[79]
					40	60.99	
					50	73.93	
					60	70.59	
					70	86.61	
		PDP				97.41	
		EIS				95.34	
C-steel	high saline water	ML	Natural honey	400 ppm		91.23	[80]
						87.84	
						43.42	
		PDP				86.8	

Steel	2 mol dm^{-3} H_3PO_4	ML	Artemisia oil	6000 ppm (hydrodistillation)	25 35 45 55 65 75	74 69.1 67.1 60.5 56.3 54.4	[81]
		PDP EIS			25	79.4 744.4	
Steel	1 mol dm^{-3} HCl	ML	Pennyroyal oil from Mentha pulegium	2760 ppm	25 30 40 50 60	80 72 75 77 78	[82]
		PDP EIS			25	78 72	
Mild steel	0.2 mol dm^{-3} H_2SO_4	ML	Tea extract	100% (ethanol extract)		99	[83]
	0.5 mol dm^{-3} H_2SO_4					97.5	
Mild steel	2 mol dm^{-3} HCl	ML	Phylanthus amaus (leaves)	4000 ppm (acidic extract)	30	94.1	[84]
			Phylanthus amaus (seeds)			80.1	
			Phylanthus amaus (lea + seed)			87.2	
	5 mol dm^{-3} HCl	HE	Phylanthus amaus (leaves)		30	58.9	
			Phylanthus amaus (seeds)			29.5	

			Phylanthus amaus (lea + seed)			48.8	
	2 mol dm^{-3} H_2SO_4	ML	Phylanthus amaus (leaves)		30	88.6	
			Phylanthus amaus (seeds)			64.6	
			Phylanthus amaus (lea + seed)			76.1	
	5 mol dm^{-3} H_2SO_4	HE	Phylanthus amaus (leaves)		30	84.1	
			Phylanthus amaus (seeds)			24.4	
			Phylanthus amaus (lea + seed)			39.6	
C38 steel	1 mol dm^{-3} HCl	PDP EIS	Palicourea guianensis (leaves)	100 ppm	25	90 89	[85]
Mild steel	0.5 mol dm^{-3} H_2SO_4	ML PDP EIS	Nyctanthes arbortristis (leaves)	1% (v/v) (acidic extract)		90 98.3 72.3	[86]
Mild steel	20% (v/v) H_3PO_4	ML EIS	zenthoxylum alatum (fruits)	2400 ppm	30	88 78	[87]
	50% (v/v) H_3PO_4	ML EIS		3200 ppm		88 94	
	88% (v/v) H_3PO_4	ML PDP EIS		3200 ppm		95 98 98	

Copper			Emblica Officinalis (leaves)			88.09	
Copper alloy (Cu-27 Zn)	Natural sea water	ML		1000 ppm (ethanol extarct)		92.6	[88]
Brass	1 mol dm^{-3} HCl	ML	Punica granatum (fruit peel)	1000 ppm (ethanol extract)	30 60	90 60	[89]

* ML: Mass loss
* PDP: Potentiodynamic polarization
* HE: Hydrogen evolution
*EIS: Electrochemical impedance spectroscopy
*LP: Linear polarization

APPENDIX

Principle of the EIS technique

EIS is one of the widely used corrosion monitoring techniques which is used to extract information about the electrode surface and the electrode/electrolyte interfacial properties in order to understand the corrosion mechanism of a metal in a corrosive environment. It is based on the Ohm's law which is given by the following equation,

$$R = {}^{E}/_{I} \tag{A1}$$

where, R is the resistance, I is the current and E is the potential difference.

The resistance value of an ideal resistor is independent of frequency at all current and voltage values. Impedance is similar to resistance, which is used where complex behavior of one or more electrical circuit elements exist. In EIS, a small AC voltage (1-10 mV) is applied to the electrochemical system over a wide range of frequencies and the current response is measured. Consider an AC sinusoidal potential signal as the input to an electrochemical system. The magnitude of this signal can be given as,

$$E = E_o sin(\omega t) \tag{A2}$$

where, E is the potential at time t, E_o is the amplitude of the signal, and ω and t are radial frequency and time, respectively.

The response to the above sinusoidal potential signal will be a sinusoidal current signal which has the same frequency with different amplitude and a phase shift, as given by,

$$I = I_o sin(\omega t + \phi) \tag{A3}$$

where, I_o is the amplitude and I is the current response at time t with a phase change ϕ. Impedance of the above electrochemical system can be calculated by applying Ohm's law as below given below.

$$Z = \frac{E}{I} \tag{A4}$$

$$Z = \frac{E_o sin(\omega t)}{I_o sin(\omega t + \phi)} \tag{A5}$$

$$Z = Z_o \frac{sin(\omega t)}{sin(\omega t + \phi)} \tag{A6}$$

where $Z_o = E_o/I_o$ is the amplitude of the impedance.

By applying Euler's rule of complex functions for the above relationship, it is possible to express impedance in the form of a complex function with both real and imaginary parts as given below:

$$Z = Z_o\,(cos\phi + jsin\phi) \tag{A7}$$

The complex function is expressed in graphical representations such as Bode and Nyquist plots. Nyquist plot, which represents a series of vector points reflecting the impedance of the circuit at particular frequencies, is obtained by plotting the real part of the impedance against the imaginary part on abscissa and ordinate axes, respectively. Bode plot is plotted with frequency on the abscissa axis and the absolute value of impedance and the phase angle on the ordinate axes.

For a pure resistor, impedance is independent of the frequency and, hence, the Nyquist plot appears as a single point on the real axis.

$$Z = R \tag{A8}$$

For a pure capacitor, impedance is entirely imaginary and negative.

$$Z = \frac{1}{j\omega C_{dl}} \tag{A9}$$

where ω the is the radial frequency, C_{dl} is the double layer capacitance and $j = \sqrt{-1}$

From the Bode plot, it is possible to read impedance with respect to frequency and also the involvement of capacitance and resistance in the electrochemical reaction from the phase angle and frequency. Electrochemical parameters, such as solution resistance, polarization resistance or charge transfer resistance, and total resistance, can be extracted from the Nyquist plot with the help of equivalent circuits. An equivalent circuit consists of common electrical circuit elements, such as resistors, capacitors and inductors, which are arranged in a way that represents the actual electrochemical process taking place. The shape of the Nyquist plot may indicate how they are combined together. Figure A.1 shows the Nyquist plot of a system, which consists of a resistor and a capacitor in series. For example, an undamaged coating on a metal exhibits this behavior.

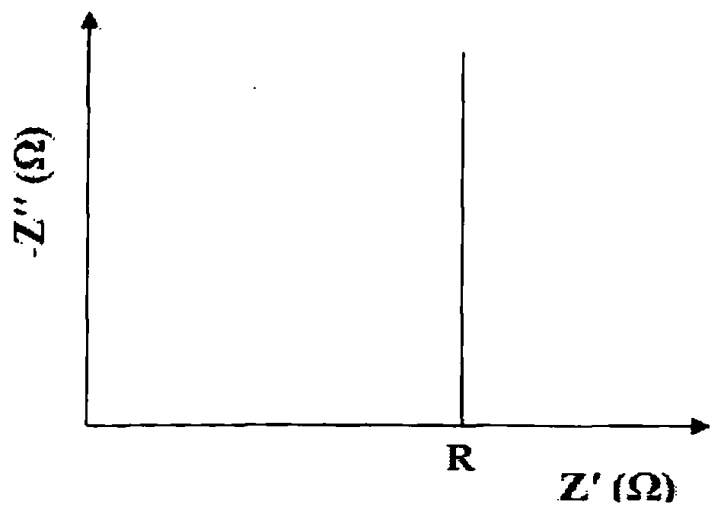

Figure A.1: Nyquist plot of a system consisting of a resistor and a capacitor in series.

The most simple common circuit model is the simplified Randles cell (Figure A.2) which represents a simple electrochemical system with solution resistance (R_s), a double layer capacitance (C_{dl}) and charge transfer resistance (R_{ct}).

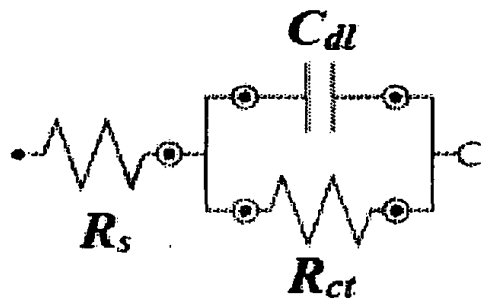

Figure A.2: Equivalent circuit for simple Randles cell [116].

Figure A.3 shows the Niquist plot for a simplified Randles cell. The solution resistance and the sum of solution resistance and the charge transfer resistance are determined from the point where the impedance curve meets the real axis in the high frequency region and the low frequency region, respectively. Therefore, the diameter of the impedance curve in the Nyquist plot gives the charge transfer resistance.

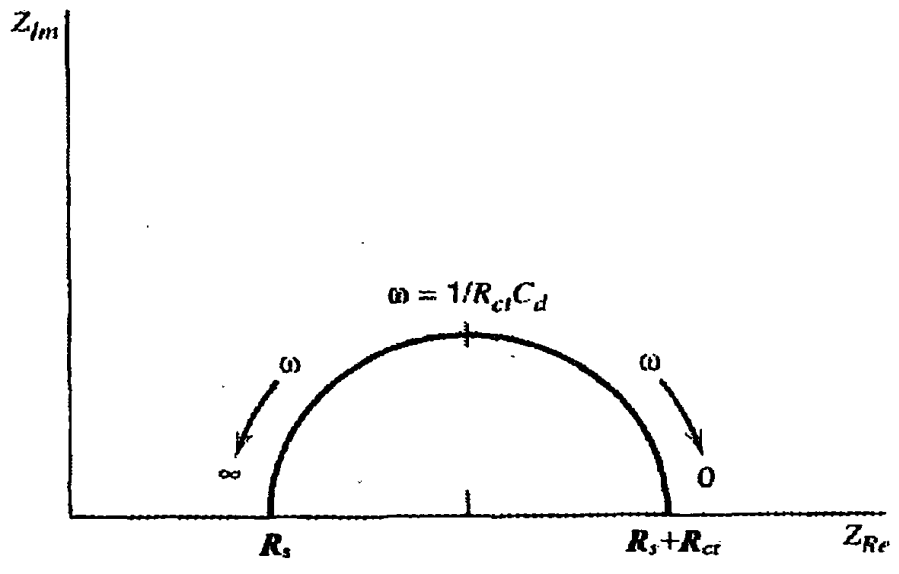

Figure A.3: Nyquist plot for simple Randles cell [116].

The impedance spectra is useful in determining the mechanism of a corrosion reaction "whether it is kinetic control or mass transfer control?". If the rate determining step of a corrosion reaction is the movement of reactants and products from and towards the electrode surface, the corrosion process is said to be in mass transfer control. The impedance created by a diffusion process is usually represented by Warburg impedance. Therefore, by looking at the shape of the Nyquist plot, it is possible to predict whether the corrosion reaction is under kinetic control or mass transfer control as shown in Figure A.4.

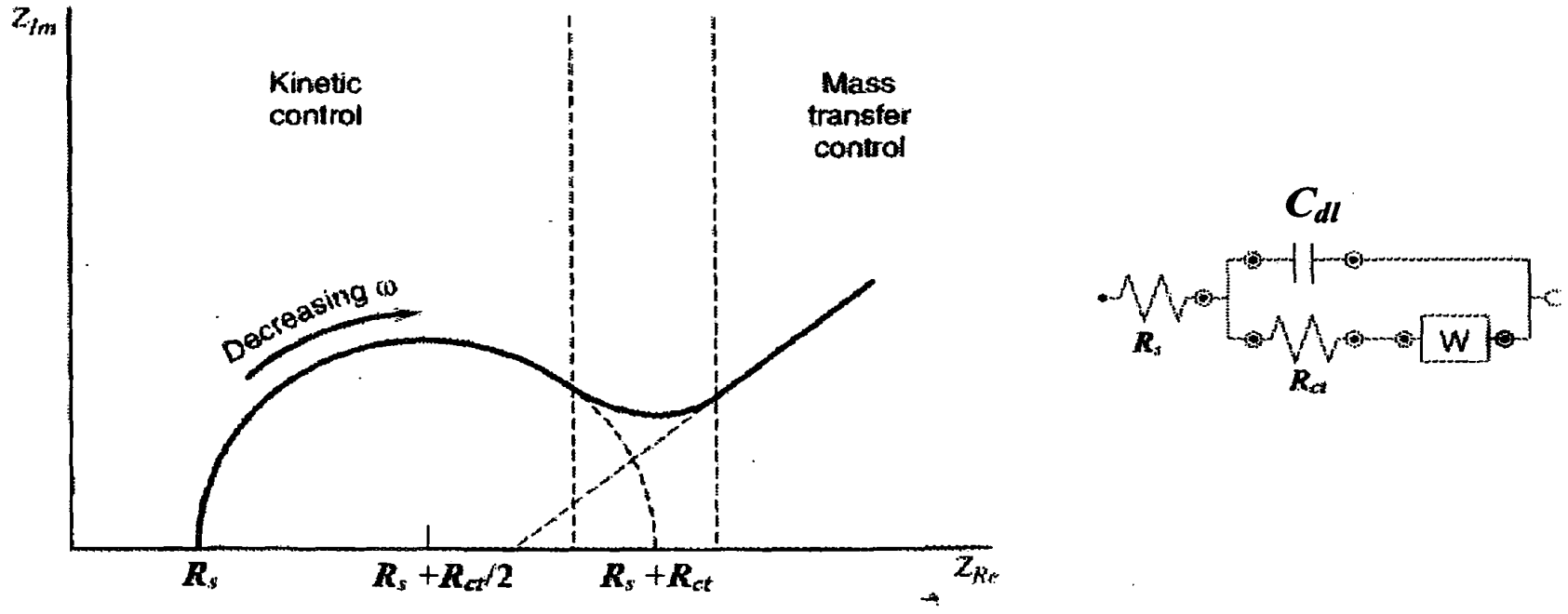

Figure A.4: Electrochemical impedance spectrum of an electrochemical system with regions of kinetic control and mass transfer control and its equivalent circuit [116].

Figure A.5 shows another sample impedance spectra of a painted metal/solution interface and its equivalent cell [31].

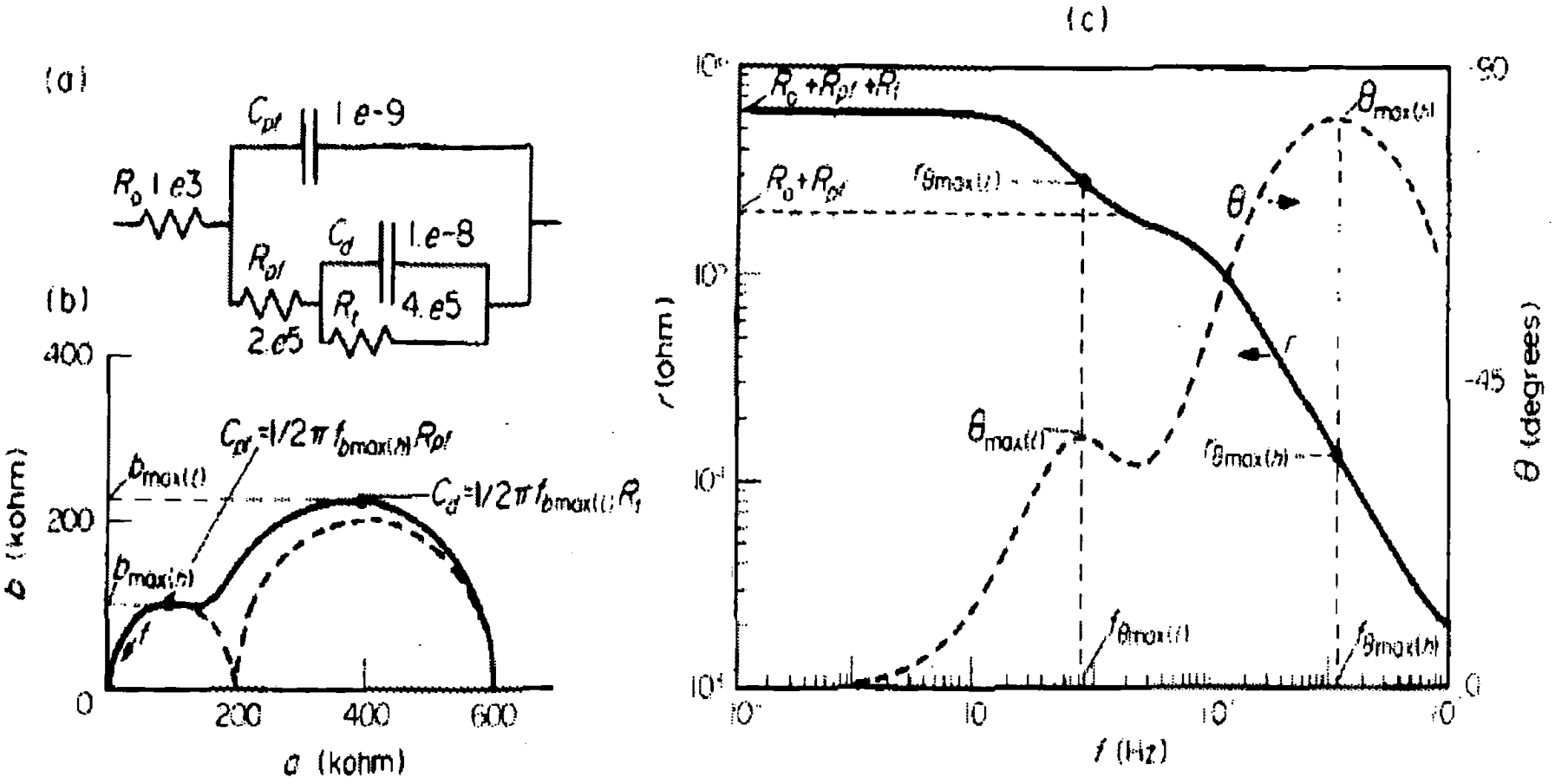

Figure A.5: Painted metal/solution interface equivalent electrical circuit model in the absence of diffusion (a) and its Nyquist (b) and Bode (c) impedance plots.

Advantage of AC impedance:

1. Use of very small signals which do not disturb the electrode properties to be measured.
2. Possibility of studying corrosion reactions and measuring corrosion rates in low conductivity media where traditional DC methods fail
3. Polarisation resistance as well as double layer capacitance data can be obtained in the same measurements

Principle of Tafel slope analysis

Consider the electrode process,

$$O + ne^- \rightleftharpoons R \qquad \text{(A10)}$$

The overall current of this reaction,

$$i_{net} = i_{cathodic} - i_{anodic} \qquad \text{(A11)}$$

At equilibrium, net current flow is zero ($i_a = i_c$). The absolute magnitude of these components at equilibrium is the exchange current density (i_o).

$$i_o = i_a = i_c \qquad \text{(A12)}$$

The exchange current density cannot be measured directly and can be calculated using Butler-Volmer equation (A13).

$$i = i_o \{\exp(-\alpha nF\ /RT) - \exp[(1-\alpha)nF\ /RT]\} \qquad \text{(A13)}$$

where i is the applied or measured current density, α is the charge transfer coefficient of the cathodic reaction, F is the Faraday constant, n is the number of electrons involved, η is overpotential ($\eta = E\text{-}E_{eq}$), R is the universal gas constant and T is the absolute temperature.

For sufficiently large over-potential, one of the exponential term in equation A13 will be negligible compare to other. For instance, at large negative over-potentials, $i_c >> i_a$ and Equation (A13) becomes,

$$i = i_o \exp(-\alpha nF\ /RT)$$

$$ln\ i = ln\ i_o - \alpha nF\ /RT$$

$$\eta = \frac{2.303RT}{\alpha nF} \log i_0 - \frac{2.303RT}{\alpha nF}\ logi_c$$

$$\eta = a - blogi_c \qquad \text{(A14)}$$

Equation (A14) is known as the Tafel equation. Tafel plots are obtained by plotting log i vs. η, and Tafel plots are linear only at high values of over-potentials and severe deviation from linearity are observed as η approaches zero as shown in Figure A.6. Extrapolation of linear portions of these plots to the zero over voltage gives an intercept. Exchange current density can be calculated from the intercept and the slope can be used to obtain the value of the transfer coefficient [117].

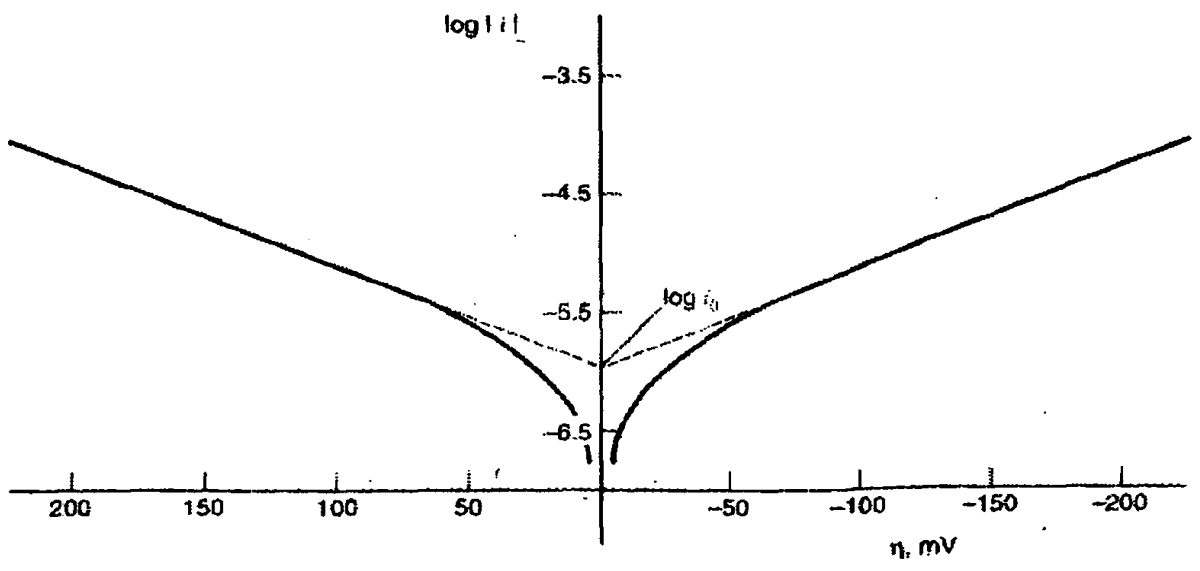

Figure A.6: Tafel plots for the cathodic and anodic branches with $\alpha = 0.5$. [116].

Effect of cathodic and anodic inhibitors on polarization curves

As anodic and cathodic inhibitors affect anodic and cathodic processes and hence shift the corrosion potential to more positive and more negative directions, respectively and cathodic and anodic inhibitors slow down cathodic and anodic current, respectively as shown in Figure A.7, changes in corrosion potential after the addition of the inhibitor are indicative of whether the anodic or cathodic reaction is retarded.

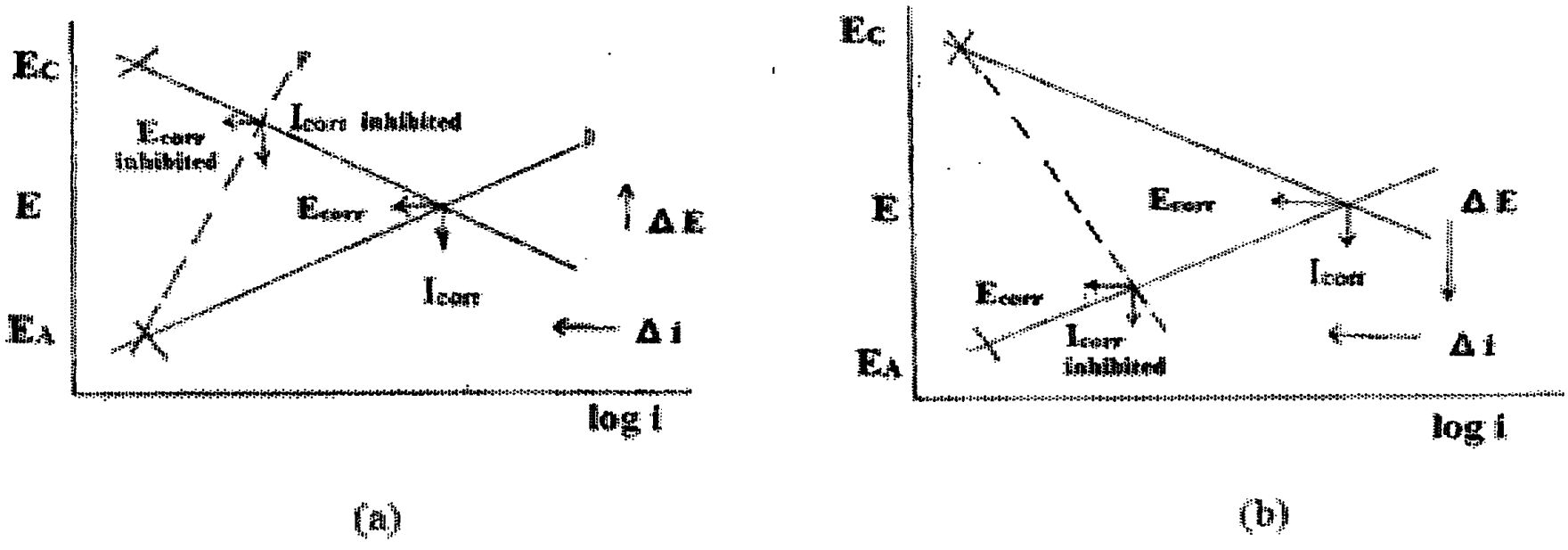

Figure A.7: Effect of anodic (a) and cathodic (b) inhibitors on polarization curves.

Mixed type of inhibitor controls both anodic and cathodic reactions, as illustrated in the Evans diagram, Figure A.8. Both anodic and cathodic current densities decrease without causing a significant shift in the corrosion potential. Mixed type inhibitors protect the metal in three possible ways: Physical adsorption, chemisorptions and film formation.

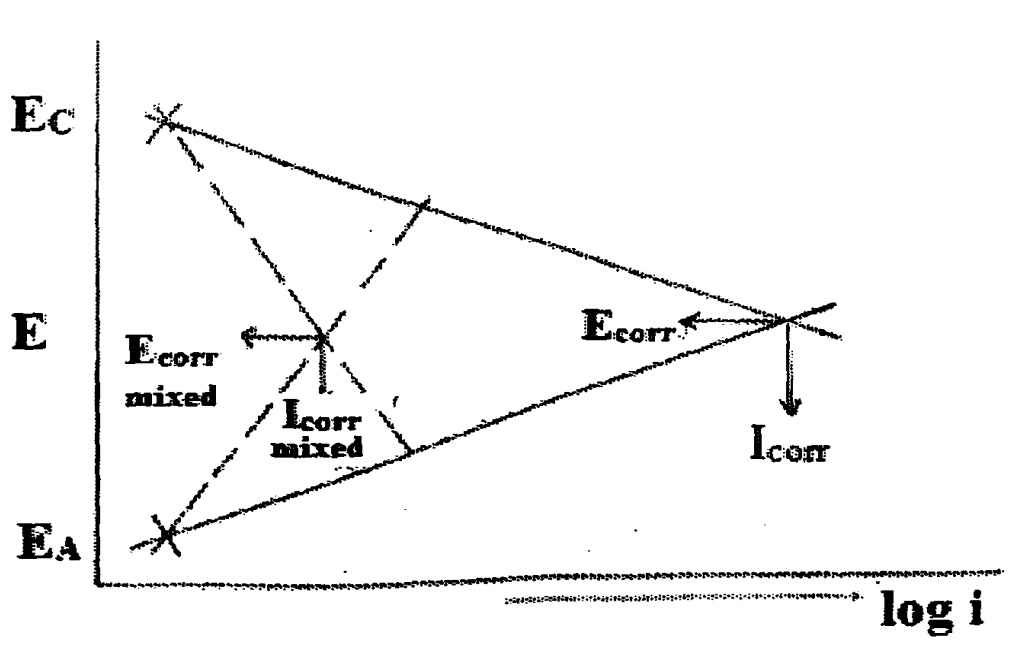

Figure A.8: Evans diagram – showing corrosion kinetics for mixed inhibition.

National Digitization Project

National Science Foundation

Institute : National Science Foundation

1. Place of Scanning : Sanje (Private) Ltd, Hokandara
2. Date Scanned : 02/06/2017
3. Name of Digitizing Company : Sanje (Private) Ltd, No 435/16, Kottawa Rd, Hokandara North, Arangala, Hokandara
4. Scanning Officer

Name : Angelo Melvin Luwis

Signature : A. M. Luwis

Certification of Scanning

I hereby certify that the scanning of this document was carried out under my supervision, according to the norms and standards of digital scanning accurately, also keeping with the originality of the original document to be accepted in a court of law.

Certifying Officer

Designation : Information Officer

Name : Renuka Sugathadasa

Signature : R. P. Sugathadasa

Date : 02/06/2017

"This document/publication was digitized under National Digitization Project of the National Science Foundation, Sri Lanka"